2017

Measurement and Modeling of Pentane-Diluted Bitumen Phase Behaviour

Johnston, Kimberly

UNIVERSITY OF CALGARY

Measurement and Modeling of Pentane-Diluted Bitumen Phase Behaviour

by

Kimberly Adriane Johnston

A THESIS

SUBMITTED TO THE FACULTY OF GRADUATE STUDIES

IN PARTIAL FULFILMENT OF THE REQUIREMENTS FOR THE

DEGREE OF DOCTOR OF PHILOSOPHY

GRADUATE PROGRAM IN CHEMICAL AND PETROLEUM ENGINEERING

CALGARY, ALBERTA

APRIL, 2017

Abstract

The phase behavior of mixtures of bitumens and *n*-alkanes is a key factor in the design and optimization of solvent-assisted heavy oil recovery processes and solvent deasphalting processes. However, data and comprehensive models are lacking for these mixtures. Crude oil phase behavior is typically modeled using cubic equations of state (CEoS). While CEoS have successfully fit saturation pressures and asphaltene onset points for bitumen-solvent systems using simple quadratic mixing rules; they do not accurately predict asphaltene precipitation yields. This thesis focuses on data collection and CEoS modeling with asymmetric mixing rules for mixtures of bitumen and *n*-pentane.

Phase behavior data were collected for *n*-pentane diluted bitumen up to 14 MPa and 280°C. Saturation pressures were measured using both a PVT cell and a blind cell apparatus. The composition at which asphaltenes precipitate was measured using a high pressure microscope apparatus and was extrapolated from asphaltene yield data. A new experimental procedure was developed to measure the phase compositions of both the light phase and the asphaltene rich heavy phase at high temperature where two liquid phases are observed. A blind cell apparatus was designed to measure asphaltene yields for multiple samples simultaneously. Binary and ternary phase diagrams were generated from the data.

The Advanced Peng Robinson (APR) CEoS with several sets of asymmetric and compositionally dependent mixing rules was evaluated using the aforementioned dataset. The use of asymmetric mixing rules significantly improved the match to asphaltene yield data; however, the yields were still under-predicted at high solvent contents and the tuning parameters that gave the best match for asphaltene yield data were not predictive or easily correlated for other solvents. The use of compositionally dependent solvent/asphaltene binary interaction parameters allowed the model to fit asphaltene yield data over the entire composition range. A set of interaction parameters was recommended that fits both asphaltene yield and saturation pressure data. While successful at fitting the data, this approach is not practical for many simulation applications and the overall conclusion is that CEoS are not well suited for the full range of bitumen-solvent phase behavior.

Acknowledgements

First and foremost I would like to express my sincere gratitude to my supervisor Dr. Harvey Yarranton for what seemed an inexhaustible supply of support, patience, guidance and wisdom. He will always have my most heartfelt respect and my most sincere apologies.

I would like to thank my lab manager, Florian Schoeggl for his guidance and training in the lab, his willingness to share his vast wealth of experience, and also for all the hilarious stories.

I appreciate and thank Dr. Shawn Taylor for his good humour, insightful input and invaluable assistance in the development new experimental methods.

I would like to thank Elaine Baydak for the support, guidance and chocolate.

I owe a most profound debt of gratitude to my friend and colleague, Dr. William Daniel Loty Richardson, for all the feelings, all the science, all the late nights, all the comic books and all the Scotch that we shared over the years. I probably could have done it without him, but it would not have been anywhere near as much fun.

I'm thankful to the members of the HOPP research group, past and present, that helped along the way; Pawan Agrawal, Catalina Sanchez, Orlando Castellanos-Diaz, Diana Powers, Francisco Ramos Pallares, Adel Mancilla Polanco, Mahdieh Shafiee.

Thank you to the NSERC Industrial Research Chair in Heavy Oil Properties and Processing, Schlumberger, Virtual Materials Group, Shell Canada, Suncor Energy, Petrobas, Nexen Energy

This thesis is dedicated to Dr. Marco Satyro; a good teacher, a great mentor and an all-around fantastic dude. You left us too soon, Marco. You are loved and you will be missed.

Table of Contents

List of Tables

List of Figures

List of Symbols and Abbreviations

a	Attractive parameter in Equation of State, subscript *i* denotes *i*th component value, subscript *m* denotes mixture value
a_{ij}	Adjustable constant to capture temperature dependence
A	Helmholtz Energy
A^{chain}	Helmholtz energy contribution from covalent bonds in SAFT
A^{res}	Residual Helmholtz energy
A^{CEoS}	Helmholtz energy contribution from CEoS
A^{assoc}	Helmholtz energy contribution from association
A^{seg}	Helmholtz energy contribution from hard spheres in SAFT
b	Exclusive volume in Equation of State, subscript *i* denotes *i*th component value, subscript *m* denotes mixture value
b_{ij}	Adjustable constant to capture temperature dependence
c	Volume translation
c_{ij}	Adjustable constant to capture temperature dependence
C	Adjustable constant for an empirical fitting equation
D	Adjustable constant for an empirical fitting equation
g	Radial distribution function used in SAFT EoS
g^E	Gibbs excess energy
g_∞^E	Limiting value of Gibbs excess energy as pressure approaches infinity
g_{ij}	Interaction energy between molecules of components *i* and *j*
H	Henry's constant
H/F	Heavy phase split ratio
ΔH^{vap}	Enthalpy of vaporization
k_{ij}	Adjustable interaction parameter
k_{ij}^0, k_{ij}^1,and k_{ij}^2	interaction parameters in temperature dependent estimation of k_{ij}
k_b	Boltzman constant
K	Equilibrium constant

l_{ij}	Adjustable interaction parameter
m_{ij}	Adjustable interaction parameter
m	mass
M_i	Number of association sites in SAFT EoS
MW	Molecular weight
MW_{avg}	Average molecular weight
MW_m	Monomer molecular weight
n	Number of moles
n_c	Number of components
n_{ij}	Adjustable parameter
P	Pressure
P_c	Critical Pressure
P_{sat}	Saturation Pressure
P_v	Vapor Pressure
R	Universal Gas Constant, 8.314 J/mol.K.
T	Temperature
T_R	Reduced Temperature
T_c	Critical Temperature
v	Molar Volume
V	Volume
ΔV_{pump}	Volume of fluid displaced by pump
ΔV_{PVT}	Change in volume measured in PVT cell using cathetometer
w	Mass fraction
x_i	Mole fraction of component *i*
x_{ij}	Mole fraction of component *i* in the vicinity of component *j*
Y	Asphaltene Yield

Superscripts

H	Heavy Phase
L	Light Phase

Subscripts

asph	Asphaltene component
bit	Bitumen component
C5	*n*-pentane component
dil	Diluent component
i	Component i
j	Component j
m	mixture
malt	Maltene component
onset	Denotes mass fraction of diluent at onset of asphaltene precipitation
solv	Solvent component
tol	Toluene component

Greek symbols

α_{ij}	Non-randomness parameter
α	Alpha function in CEoS
β	Shape distribution factor
γ	Activity coefficient
Γ	Gamma function
δ	Solubility parameter
$\Delta_{ij}^{\alpha s}$	Association strength
ε	Association energy
κ	Association bonding volume
Λ	Constant in the Huron-Vidal mixing rules
ρ	Density
τ_{ij}	Interaction parameter between components *i* and *j*
ω	Acentric factor
σ	Constant in the general form of a CEoS
ψ	Constant in the general form of a CEoS

X	Mole fraction of unbonded molecules in CPA EoS

Abbreviations

AER	Alberta Energy Regulator
APR	Advanced Peng Robinson EoS
API	American Petroleum Institute
AvdW	Asymmetric van der Waals mixing rules
BPR	Back Pressure Regulator
CDvdW	Compositionally Dependent van der Waals mixing rules
CEoS	Cubic Equation of State
CPA	Cubic Plus Association EoS
CSS	Cyclic Steam Stimulation
DSC	Differential Scanning Calorimetry
EoS	Equation of State
ES-SAGD	Expanding Solvent SAGD
GC	Gas Chromatograph
HPM	High Pressure Microscope
HV	Huron Vidal mixing rules
LLE	Liquid-Liquid Equilibrium
MRS	Modified Regular Solution
MW	Molecular Weight
NBP	Normal Boiling Point
NRTL	Non-Random Two Liquid
PC-SAFT	Perturbed Chain Statistical Associating Fluid Theory
PNA	Paraffins-Napthenes-Aromatics
PR	Peng-Robinson EoS
PVT	Pressure, Volume, Temperatue
SAFT	Statistical Associating Fluid Theory EoS
SAGD	Steam Assisted Gravity Drainage
SANS	Small Angle Neutron Scattering
SARA	Saturates-Aromatics-Resins-Asphaltenes

SAXS	Small Angle X-Ray Scattering
SG	Specific Gravity
SRK	Soave-Redlich-Kwong EoS
SvdW	Symmetric van der Waals mixing rules
SWV	Sandoval, Wilczek-Vera, Vera mixing rules
TBP	True Boiling Point
VAPEX	Vapor Extraction
VLE	Vapor-Liquid Equilibrium

Chapter One - INTRODUCTION

Canada has an estimated 2 trillion barrels of heavy oil and bitumen reserves [AER 2015]. In Alberta, the shallow deposits are mined but deeper deposits are produced mainly with thermal recovery methods, such as SAGD (steam assisted gravity drainage) or CSS (cyclic steam stimulation). In these recovery methods, steam is injected into the reservoir to reduce the oil viscosity so that the bitumen can flow to a producing well. However, steam-based methods are energy intensive, costly, and draw heavily on the available water supply. Therefore, alternative recovery methods are being investigated including solvent-based processes, such as VAPEX, and solvent-assisted processes, such as ES-SAGD. To succeed, these methods must achieve similar oil recovery as thermal methods as well as high solvent recovery, while reducing water requirements and operating costs.

Solvent based and solvent-assisted processes involve a complex combination of heat transfer, mass transfer, and phase equilibrium as well as the usual fluid flow through a porous medium. Hence, reservoir (and process) simulations that include accurate phase behavior and fluid property models are required. This thesis focuses on the phase behavior (data and modeling) for bitumen/solvent systems.

Bitumen/solvent systems are asymmetric and can exhibit multiphase behavior including vapor-liquid (VL), liquid-liquid (LL), VLL, and possibly VLLL regions. The heavy phase that forms in the LL region can strongly affect fluid flow and therefore the amount and composition of this phase is of particular interest. The phase behavior of these mixtures depends on temperature, pressure, composition, and the carbon number of the *n*-alkane.

In methane-bitumen systems, only VL regions have been observed [Mehrotra and Svrcek, 1985] likely because the solubility of methane in bitumen is relatively low. For ethane diluted bitumen, VL and VLL boundaries have been observed [Mehrotra and Svrcek, 1985]. In this case, the two liquid phases are a solvent-rich (L_1) and a bitumen-rich (L_2) phase. Several phases have been observed in mixtures of propane and bitumen including vapor and up to two liquid phases [Badamchi-zadeh *et al.*, 2009; Jossy *et al.*, 2009].

It is well known that asphaltenes separate from heavy oils diluted with *n*-pentane or higher carbon number *n*-alkanes [Speight, 1999]. Bitumens are rich in asphaltenes, the densest, highest molecular weight fraction of crude oils. Asphaltenes are defined as the fraction of crude oil that is soluble in toluene and insoluble in either *n*-pentane or *n*-heptane. They are a mixture of polynuclear aromatic species with the highest density, molecular weight, polarity, and heteroatom content of the crude oil.

Most research on bitumen phase behavior has focused on the onset of asphaltene precipitation and the amount of separated asphaltenes (*i.e*. their solubility) because asphaltene precipitation has a significant impact on deposition and flow assurance. "Asphaltene precipitation" is the commonly used term to describe the formation of an asphaltene-rich heavy phase. The onset refers to the conditions (temperature, pressure, and composition) at which the heavy phase appears. The mass of the asphaltene partitioning to the heavy phase relative to the original mass of asphaltene in the oil is referred to as the asphaltene yield.

For *n*-alkane diluted bitumen, asphaltene solubility increases as the carbon number of the *n*-alkane increases from 3 to 7 and decreases slightly at carbon numbers above 10 [Hu and Guo, 2001; Andersen and Birdi, 1990; Mannistu *et al*., 1997; Ali and Al-Ghannam, 1981; Wiehe *et al*., 2005]. The increase in solubility means that more solvent is required to initiate precipitation and there is less asphaltene precipitation at a given composition above the onset of precipitation.

Most researchers [Akbarzadeh *et al*., 2005; Ali and Al-Ghannam, 1981; Hu and Guo, 2001] have found that asphaltene solubility in crude oil and hydrocarbon solvents increases with temperature up to 100°C. Andersen and Birdi [1990] reported an initial decrease in solubility as temperature increased from 4 to 25 °C, then an increase in solubility from 25 to 100°C. Based on a small amount of data [Andersen 1994, Andersen *et al.* 1998], C7-asphaltenes (asphaltenes precipitated with *n*-heptane) may become less soluble at temperatures above 100°C.

Asphaltene solubility tends to increase with increased pressure. For example, asphaltenes solubilized in an undersaturated live oil at reservoir pressure can precipitate when the oil is depressurized [Joshi *et al.*, 2001; Tharanivasan *et al.*, 2011]. Akbarzadeh *et al.* [2005] found that asphaltene solubility in heavy oils also increased with increased pressure. Overall, while trends in

asphaltene solubility with temperature and pressure have been reported, the data are too sparse to accurately assess these trends.

Data on the composition of the asphaltene-rich heavy phase is even sparser because it is challenging to measure. Yarranton *et al.* [2011] conducted drying experiments on asphaltene sediments to determine the solvent content of the precipitated asphaltene phase at ambient conditions. At these conditions, they reported the *n*-pentane content of the asphaltene phase from *n*-pentane diluted bitumen to be <4 mass % at ambient conditions.

At temperatures below approximately 100°C, the asphaltenes appear to separate as a glass-like phase of micron-scale primary particles that rapidly flocculate [Rastegari *et al.,* 2004; Luo *et al.,* 2010]. At higher temperatures, the mixture separates into two liquid phases: a solvent-rich and an asphaltene-rich phase [Agrawal *et al.,* 2012]. Asphaltenes appear to undergo a glass transition at higher temperatures which allows the formation of a liquid asphaltene-rich heavy phase. Several researchers have studied the glass transition temperature for asphaltenes [Zhang *et al.,* 2004; Gray *et al.*, 2004*;* Kriz *et al.,*2008]. Agrawal *et al*. [2012] measured the onset of asphaltene precipitation from *n*-pentane diluted bitumen at 180°C and 4820 kPa, and noted that the asphaltene-rich phase in solution forms a continuous liquid phase at these conditions. The formation of a continuous liquid asphaltene-rich phase at temperatures above 140°C makes it possible to separate this phase from the solvent-rich light phase and determine its composition.

A model that captures the full range of this phase behavior has proven elusive. To date, the most successful models for bitumen-solvent phase behavior treat all of the oil, including the asphaltenes, as a solution and treat all phase behavior, including asphaltene precipitation, as a chemical phase separation. These models include the modified regular solution (MRS) model, the perturbed-chain statistical associating fluid theory (PC-SAFT) EoS, and the cubic plus association (CPA) EoS. The MRS model can fit and, to some extent, predict asphaltene yield and onset points for various solvent-diluted bitumen systems [Tharanivasan *et al.,* 2011; Alboudwarej *et al.,* 2003; Wang and Buckley, 2001]. However, this version of regular solution theory is unable to accurately model component partitioning between an asphaltene-rich phase and a solvent-rich phase. In addition, it has not been applied to other phase transitions including VLE.

The CPA EoS can capture vapor-liquid equilibrium as well as asphaltene precipitation onsets in conventional oils and bitumen over a range of temperatures, pressures, and compositions [Li and Firoozabadi, 2010; Shirani *et al.*, 2012]. The PC-SAFT equation of state can also model both vapor-liquid equilibrium and the onset of asphaltene precipitation from a depressurized conventional crude oil [Panuganti *et al.*, 2012; Ting *et al.* 2003]. More recently, the PC-SAFT has been used to model asphaltene yield curves from solvent diluted bitumen and has been shown to capture the effects of asphaltene polydispersity [Tavakkoli *et al.*, 2014]. Both models were evaluated independently [AlHammadi *et al.*, 2015; Zhang *et al.*, 2012] for asphaltene precipitation from conventional oils and bitumens and were confirmed to give good predictions for phase boundaries and asphaltene precipitation amounts. A disadvantage of both the PC-SAFT and the CPA equation of state is that they can have more than three roots resulting in a more complex flash and longer computation time.

Cubic equations of state (CEoS) are used in most commercial reservoir and process simulation software due to their simplicity of application and relatively fast computation times. CEoS models and associated correlations have been developed and tuned for light hydrocarbon systems. While CEoS have been applied to bitumen systems, they have not yet been successfully tested on a broad range of phase behavior for bitumens and solvents. Mehrotra *et al.* [1988] successfully modeled solubility data for mixtures of Cold Lake bitumen and nitrogen, carbon dioxide, methane and ethane using the Peng-Robinson (PR) EoS. Jamaluddin *et al.* [1991] used the Martin EoS to fit solubility and saturated liquid density for systems of bitumen and carbon dioxide. Shaw and coworkers [Saber and Shaw, 2009; Saber and Shaw 2011; Saber *et al.*, 2012] have used a group contribution method in conjunction with the PR EoS to capture LLV phase behavior of Athabasca vacuum residue and solvent. Castellanos-Díaz *et al.* [2011] and Agrawal *et al.* [2012] modeled the phase behavior of bitumen-propane, bitumen-carbon dioxide and bitumen-pentane systems using the Advanced Peng-Robinson (APR) EoS. Their model correctly predicted saturation pressures and asphaltene onset points, but did not accurately predict asphaltene yields. The model predicted that the asphaltenes become soluble at high solvent dilutions while experimental data showed that the asphaltenes remain insoluble.

A possible remedy, recommended by Agrawal *et al.* [2012], is to apply asymmetric mixing rules rather than the symmetric van der Waals mixing rules used in the APR model. The first asymmetric

mixing rules proposed were empirically developed compositional dependent expressions for the binary interaction parametes (k_{ij}) used in the symmetric van der Waals mixing rules [Adachi and Sugie, 1986; Panagiotopoulos and Reid, 1986; Sandoval *et al.,* 1989; Stryjek and Vera, 1986]. Another class of asymmetric mixing rules are derived by equating the excess free energy (either Gibbs or Helmholtz) from an equation of state to the excess free energy from an activity coefficient model. The Huron-Vidal and Wong-Sandler mixing rules are well known examples of excess energy mixing rules [Huron and Vidal, 1979; Wong and Sandler, 1992]. The Huron-Vidal asymmetric mixing rules are theoretically applicable to mixtures of nonpolar and polar compounds [Pedersen and Christensen, 2007] and have been used to model mixtures of water and hydrocarbons [Kristensen and Christensen, 1993; Pedersen *et al.* 1996; Sørensen *et al.* 2007]. Gregorowicz and de Loos [2001] used the Wong-Sandler mixing rules to model LLV behavior in asymmetric hydrocarbon mixtures. To date, a CEoS with asymmetric mixing rules has not been applied to mixtures of bitumen and solvents.

1.1 Objectives

The solvents of potential interest for *in situ* recovery processes include *n*-alkanes, condensates, and naphtha. A program is underway under the NSERC IRC in Heavy Oil Properties and Processing to investigate the phase behavior of mixtures of bitumen with these solvents, and this thesis is part of that program. The main objectives of this thesis are to: 1) measure the phase behavior of mixtures of *n*-pentane and bitumen over the range of conditions that may be encountered in commercial in situ and surface processes; 2) evaluate the applicability of asymmetric mixing rules with a CEoS to model bitumen-solvent behavior.

Specific objectives of this thesis are to:

1. Map the phase behavior of *n*-pentane diluted bitumen over the conditions encountered in typical *in situ* and surface processes, including saturation pressures and asphaltene onset points (the compositions at which a separate asphaltene-rich heavy phases are formed) at temperatures up to 280°C and pressures up to 13.8 MPa
2. Develop and test an experimental procedure to measure the composition of the light and heavy phases formed in the liquid-liquid region.

3. Develop and commission a blind cell apparatus to measure asphaltene yields or saturation pressures at high temperature and pressure for up to 5 samples simultaneously.
4. Provide an assessment of the repeatability and uncertainty of heavy oil phase behavior measurements.
5. Evaluate the applicability of a cubic equation of state (CEoS) with several forms of asymmetric mixing rules to model the measured phase behavior. Identify the advantages and shortcomings of each set mixing rules tested.

A bitumen from Western Canada was used in this thesis and the phase behavior of the n-pentane diluted bitumen was investigated at temperatures from 20 to 280°C and pressures up to 14 MPa. The Advanced Peng-Robinson (APR) CEoS was used to model the measured data.

1.2 Organization of Thesis

This thesis is organized into seven chapters and the remaining chapters are outlined below.

Chapter 2 gives a brief review of petroleum chemistry, oil characterization, bitumen/solvent phase behavior, and successfully applied asphaltene precipitation models. Cubic equations of state, mixing rules and their application to petroleum systems are reviewed.

Chapter 3 summarizes the materials used in the experimental work; the experimental procedures for saturation pressures, asphaltene yields, asphaltene onsets, and phase composition measurements; and the techniques used to process the experimental data. A new PVT cell procedure is described that was developed to collect and assay the light and heavy phases for their phase volumes as well as solvent, maltene, and C5-asphaltene (pentane extracted asphaltene) contents. A new blind cell apparatus procedure is also described that was developed to measure only the light phase compositions and C5-asphaltene yields of up to 5 samples simultaneously. This procedure allowed data to be obtained more rapidly.

Chapter 4 describes the methodology used to model the experimental data including the oil characterization methodology, a description of the mixing rules tested, and a summary of the modeling workflow.

Chapter 5 presents the experimental results. The results are interpreted, uncertainties in the data are discussed, and the results are compared to related findings from the literature. Pressure-composition phase diagrams and pseudo-ternary phase diagrams of asphaltenes, maltenes, and *n*-pentane are presented.

Chapter 6 presents the modeling results for several sets of asymmetric mixing rules. First, the asymmetric van der Waals mixing rules ($k_{ij} \neq k_{ij}$) were evaluated. Then, the Sandoval *et al.* mixing rules [1989] were evaluated to test a composition-dependent type of mixing rule. Two forms of Huron-Vidal mixing rules [1979] were evaluated to test an excess energy type of mixing rule. Finally, the form of the compositional dependence required to fit asphaltene yield data was examined. The advantages and shortcomings of each type of model are discussed.

Chapter 7 summarizes the major findings of this thesis and provides recommendations for the developed experimental procedures and the tested modeling methodologies.

Chapter Two - LITERATURE REVIEW

This chapter explains the basics of crude oil characterization, including a discussion of asphaltene properties and characterization techniques. Phase behavior of bitumen and solvent mixtures is discussed as well as the thermodynamic models that have been used to model that phase behavior.

2.1 Oil Characterization

Crude oils are naturally occurring petroleum liquids. They consist primarily of hydrocarbons with variable amounts of compounds containing nitrogen, oxygen and sulfur together with small amounts of metals such as nickel and vanadium. Although oils contain few atomic species, they consist of hundreds of thousands, perhaps even millions, of different molecular species [Altgelt and Boduszynski, 1994; Rodgers and McKenna, 2011]. Crude oil is typically classified by its physical properties, such as boiling point, specific gravity or viscosity. The UNITAR classification of oils is given in Table 2.1 [Gray, 1994].

Table 2.1. UNITAR classification of oils by physical properties at 15.6°C [Gray, 1994].

Classification	Viscosity mPa.s	Density kg/m³	API Gravity
Conventional oil	$<10^2$	< 934	$>20^o$
Heavy oil	10^2 - 10^5	934 – 1000	$20^o – 10^o$
Bitumen	$>10^5$	>1000	$<10^o$

The molecular species in crude oils encompass a broad range of molecular weights (approximately 16 to 1200 g/mol) and actual/theoretical boiling points (approximately 20 to 800°C). The diversity and complexity of the molecules in the crude oil increases with boiling point and molecular weight, Figure 2.1. The molecules can be grouped into different chemical families including paraffins, naphthenes, and aromatics. The paraffins and napthenes together are termed saturates. The aromatics can be divided into aromatic, resin, and asphaltene fractions each with greater molecular weight, density, polarity, and heteroatom content.

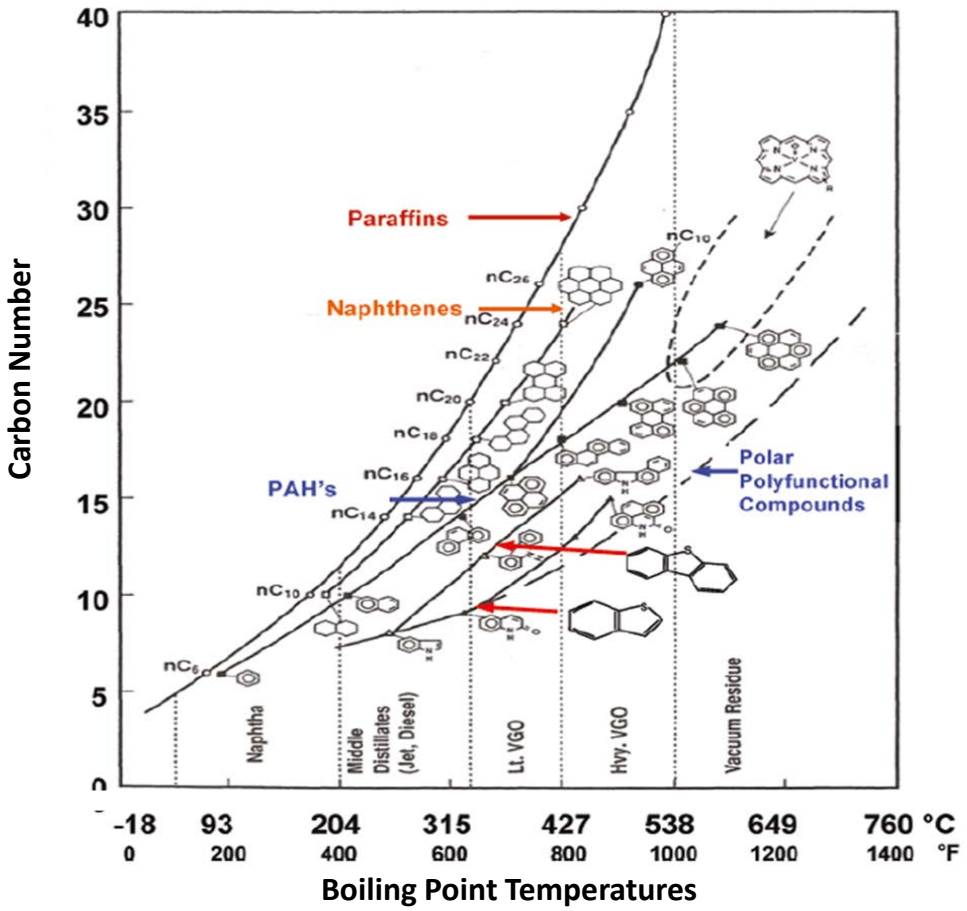

Figure 2.1 Relationship between molecular weight, structure, and boiling point [Altgelt and Boduszynsk, 1994].

To model the phase behavior and properties of crude oils and crude oil fractions for upstream and downstream processes, the oil must be characterized; that is, divided into a set of components and pseudo-components that represent the distribution of properties in the oil. It is currently impossible, and will likely always be impractical, to characterize a crude oil by its constituent molecular species. Instead, crude oils are typically represented by a set of pseudo-components assigned based on boiling point [Katz and Firoozabadi 1978, Castellanos-Diaz *et al.* 2011] or molecular weight distributions [Whitson, 1983]. These distributions are related to each other and can be constrained by the distribution of chemical families such as paraffins, naphthenes, and aromatics. Each pseudo-component is assigned the average properties of all the molecules in its boiling or molecular weight interval.

To create a set of pseudo-components, distillation or gas chromatography data are usually required. Typically, either the boiling point or molecular weight distributions are divided into mass fractions representing boiling or molecular weight ranges. Then, whatever properties are required for the phase behavior modeling are assigned to each pseudo-component using correlations such as the Riazi-Daubert [Riazi and Daubert, 1987], Lee-Kesler [Lee and Kesler, 1975] or Twu correlations [1984]. For equation of state models, the density, molecular weight, boiling point, critical temperature and critical pressure, and acentric factor must be estimated for each pseudo-component.

Additional data, such as paraffin-naphthene-aromatics (PNA) content or saturate-aromatics-resins-asphaltene (SARA) composition, can be used as a constraint when estimating pseudo-component properties. The PNA method uses refractive index data to determine the PNA content of the cuts [Pedersen and Christensen 2007, Riazi and Daubert 1986, Leelavanichkul *et al.* 2004]. SARA fractionation involves splitting the crude oil into solubility and absorption classes [Speight 1999]. Asphaltenes are separated by addition of excess *n*-pentane and saturates, aromatics and resins are separated by liquid chromatography. Pseudo-components can also be used to represent SARA fractions instead of, or as an extension to, a boiling point or molecular weight based characterization [Panuganti *et al.* 2012, Ting *et al.* 2003].

Conventional oils consist of relatively lower molecular weight compounds; hence, most of a conventional oil sample is distillable and can be eluted in a gas chromatograph. Bitumens, however, contain more of the larger and more complex molecular species, which makes characterization more challenging. Typically, boiling point distributions are determined from distillation or chromatography data; however, distillation assays are limited to temperatures below 300°C to avoid thermal cracking. Consequently, as little as 20-30% of a sample of bitumen can be distilled and the remainder of the boiling point or molecular weight distributions must be extrapolated. Bitumens also contain a significant amount of asphaltenes. Asphaltenes are known to self-associate and precipitate, and are more challenging to characterize than the other oil fractions.

2.2 Asphaltene Properties and Characterization

Asphaltenes are defined as the fraction of crude oil that is insoluble in *n*-pentane or *n*-heptane, but is soluble in aromatics such as toluene or benzene. Asphaltenes are the densest, highest molecular weight and most polar components of crude oil. Some properties of asphaltenes are summarized in Table 2.2 [Mullins 2011, Akbarzadeh *et al.* 2005, Sanchez 2013, Wang and Buckley 2001; Barrera *et al.*, 2013].

Table 2.2 Selected properties of asphaltenes.

Property	Values
Monomer Molecular Weight	400-1000 g/mol
Average Nano-aggregate Molecular Weight	1000-10000 g/mol
Density	1.1 – 1.2 g/cc
Solubility Parameter	20.1+

Asphaltenes are known to self-associate into larger structures, now often termed "nanoaggregates". Asphaltene self-association has been examined with a number of techniques including vapor pressure osmometry [Yarranton *et al.*, 2000], interfacial tension [Yarranton *et al.* 2000, Rogel *et al.* 2000], isothermal titration calorimetry [Merino-Garcia and Anderson, 2003], and small angle x-ray scattering measurements [Xu *et al.* 1995, Eyssautier *et al.*, 2012]. Average asphaltene molecular weight increases with asphaltene concentration in solvent, indicating the association of asphaltene monomers. Asphaltenes appear to associate into nanoaggregates of 2-6 monomers on average [Yarranton *et al.*, 2000].

It has been shown that the Gamma function is suitable for representing the molecular weight distribution of asphaltene monomers and nano-aggregates for the purposes of phase behavior modeling [Huang *et al.* 1991, Alboudwarej *et al.* 2003, Castellanos-Diaz *et al.* 2011, Agrawal *et al.* 2012]. The Gamma function is given by:

$$f(MW) = \frac{(MW - MW_m)^{\beta-1}}{\Gamma(\beta)} \left[\frac{\beta}{MW_{avg} - MW_m}\right]^{\beta} \exp\left[-\beta \frac{MW - MW_m}{MW_{avg} - MW_m}\right] \qquad 2.1$$

where MW_m is the monomer molecular weight, MW_{avg} is the average molecular weight of the asphaltenes and β is a parameter which determines the shape of the distribution. The average

molecular weight of the asphaltene nanoaggregates is not known with certainty and is therefore used as an adjustable parameter. A value of 2000 g/mol is suggested by Agrawal *et al.* (2012). A value of 2.5 for β is recommended by both Castellanos *et al.* (2011) and Agrawal *et al.* Figure 2.2 shows how the molecular weight distribution of asphaltenes can be divided into pseudo-components of equal mole fraction.

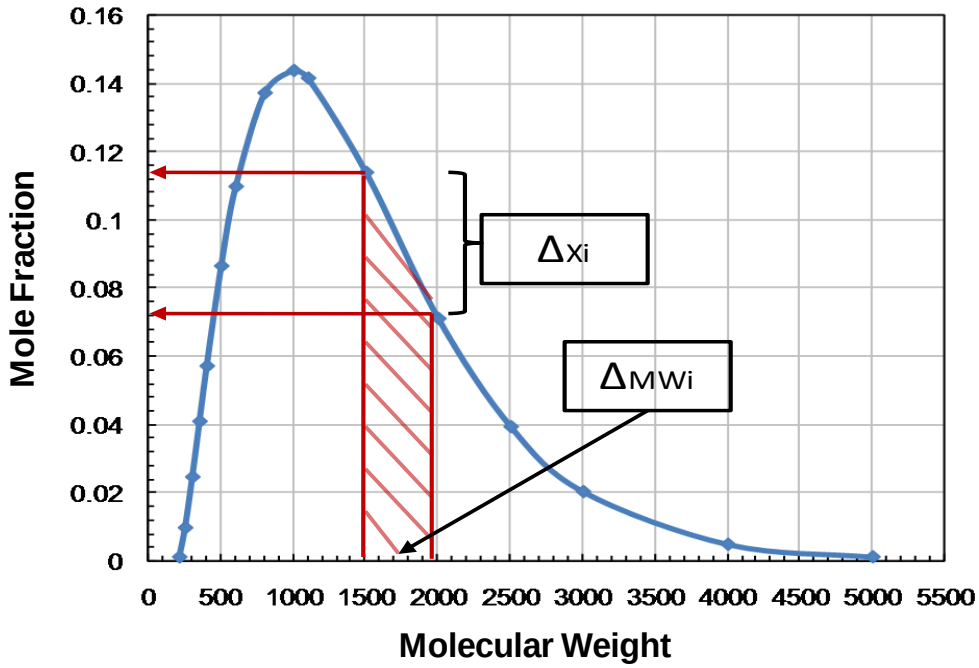

Figure 2.2 Gamma Distribution for Molecular Weight and the determination of the molecular weight and mole fraction of the i^{th} pseudo component [Castellanos-Diaz, 2012].

Density is also a required input for most correlations to determine pseudo-component properties. The density distributions of asphaltenes were recently measured in detail [Barrera *et al.*, 2013] and are compared with the density of maltene distillation cuts [Sanchez, 2013] in Figure 2.3. The asphaltene density deviates significantly from the observed for the maltene trend; therefore density correlations developed for maltene components are not applicable to asphaltene pseudo-components. Barrera *et al.* [2013] developed the following correlation for asphaltene density as a function of molecular weight:

$$\rho = 1100 + 100\left(1 - exp\left(-\frac{MW}{3850}\right)\right) \qquad 2.2$$

where ρ is the density in kg/m³.

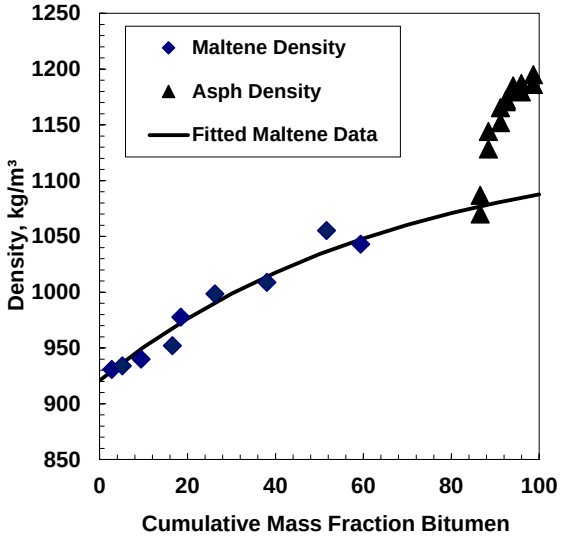

Figure 2.3 Density of maltene distillation cuts and asphaltene solubility cuts from a Western Canadian bitumen [Sanchez, 2013; Barrera *et al.*, 2013].

2.3 Bitumen/Solvent Phase Behavior

Bitumen-solvent systems are highly asymmetric mixtures and complex multiphase behavior has been observed for these systems including vapor-liquid (VL), liquid-liquid (LL), VLL, and possibly VLLL regions. The phase behavior depends on temperature, pressure, composition, and the carbon number of the *n*-alkane.

In methane-bitumen systems, only VL regions have been observed since the solubility of methane in bitumen is relatively low, Figure 2.4a [Mehrotra and Svrcek, 1985]. For ethane diluted bitumen, VL and VLL boundaries have been observed, Figure 2.4b [Mehrotra and Svrcek, 1985]. In this case, the two liquid phases are a solvent-rich (L_1) and a bitumen-rich (L_2) phase. Several phases have been observed in mixtures of propane and bitumen including vapor and up to two liquid phases [Badamchi-zadeh *et al.*, 2009; Jossy *et al.*, 2009]. Figure 2.5 shows a phase diagram for propane-bitumen with both LL and VLL regions, as predicted by an equation of state model based partly on Badamchizadeh *et al.*'s data [Castellanos-Diaz *et al.* 2011]. Recently, Dini *et al.* [2016] investigated the phase behavior of propane-bitumen systems more extensively. They observed VL

and LL boundaries but did not directly measure the compositions of the multiple liquid phases. They interpreted the two liquid phases as a bitumen-rich and a solvent-rich phase.

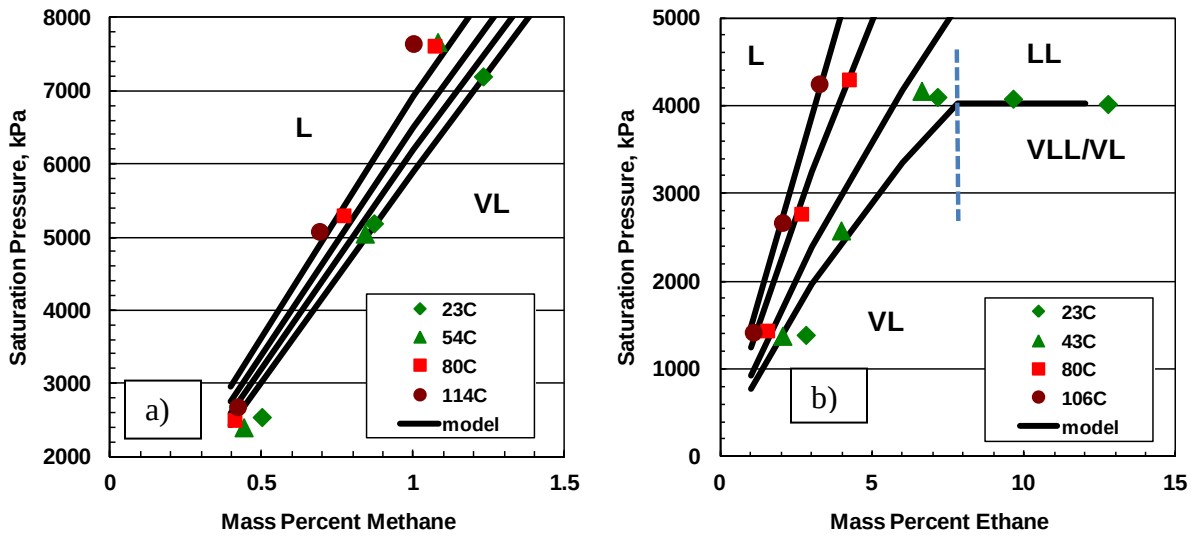

Figure 2.4 Pressure-composition phase diagram for mixtures of a) methane and Peace River bitumen and b) ethane and Peace River bitumen [Mehrotra and Svrcek, 1985].

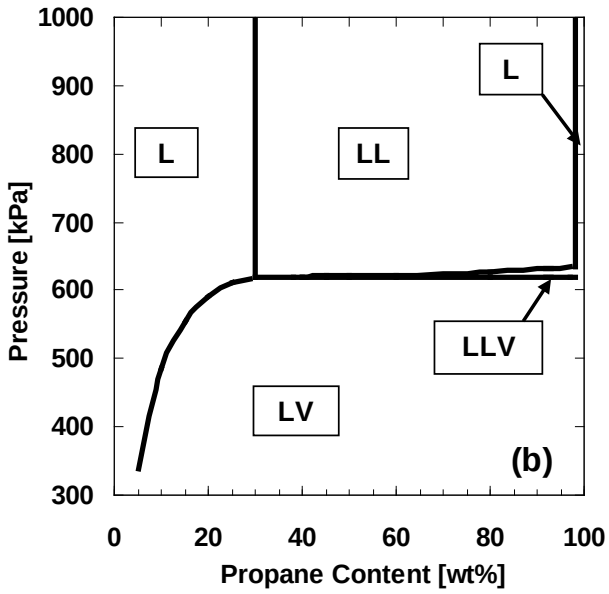

Figure 2.5 Pressure-composition phase diagram for mixtures of propane and Athabasca bitumen at 10°C [Castellanos-Diaz, 2011].

Zou *et al.* [2005] used x-ray transmission tomography to examine the phase behavior of mixtures of *n*-pentane and Athabasca vacuum residue (AVR), a 525+°C boiling fraction comprising 32 wt% C5-asphaltenes (asphaltenes insoluble in *n*-pentane). Depending on the overall composition, these mixtures were found to exhibit three and four phase equilibria including LLV and LLLV phase behavior. Figure 2.6a shows a diagram of the phase behavior for mixtures of AVR and pentane that the authors expect based on this work [Shaw and Zou, 2007]. In this case, the L_1 is a bitumen-rich phase, L_2 is a solvent-rich phase, and L_3 is likely an asphaltene-rich phase. Figure 2.6b shows the modeled and experimentally measured phase boundary data on a P-X plot for the same system [Saber *et al.*, 2012].

Asphaltenes can precipitate from crude oils due to changes in pressure, temperature, or composition. Typical examples are precipitation from relatively light oils with a drop in pressure [Panuganti *et al.* 2012] and precipitation from solvent-diluted bitumen [Akbarzadeh *et al.* 2004]. In general, crude oils become poorer solvents for asphaltenes as the pressure decreases and the fluid density decreases. Hence, asphaltenes tend to precipitate when the pressure drops. The trend will reverse if the fluid reaches its bubble point and light components evolve from the liquid [Tharanivasan *et al.* 2011, Ting *et al.* 2003, Pedersen 2007]. Experimental data suggest that asphaltenes become more soluble as temperature increases to a point [Akbarzadeh *et al.* 2005] and that they may become less soluble at temperatures above 100°C [Andersen 1994, Andersen *et al.* 1998].

Diluents can have a significant effect on asphaltene solubility. Most research has focused on paraffinic diluents. For *n*-alkane diluted heavy oils, asphaltene solubility increases as the carbon number of the *n*-alkane increases from 3 to 7 and decreases slightly at carbon numbers above 10 [Hu and Guo, 2001; Andersen and Birdi, 1990; Mannistu *et al*., 1997; Ali and Al-Ghannam, 1981; Wiehe *et al*., 2005, Mitchell and Speight, 1973]. The increase in solubility means that more solvent is required to initiate precipitation and there is less asphaltene precipitation at a given composition above the onset of precipitation.

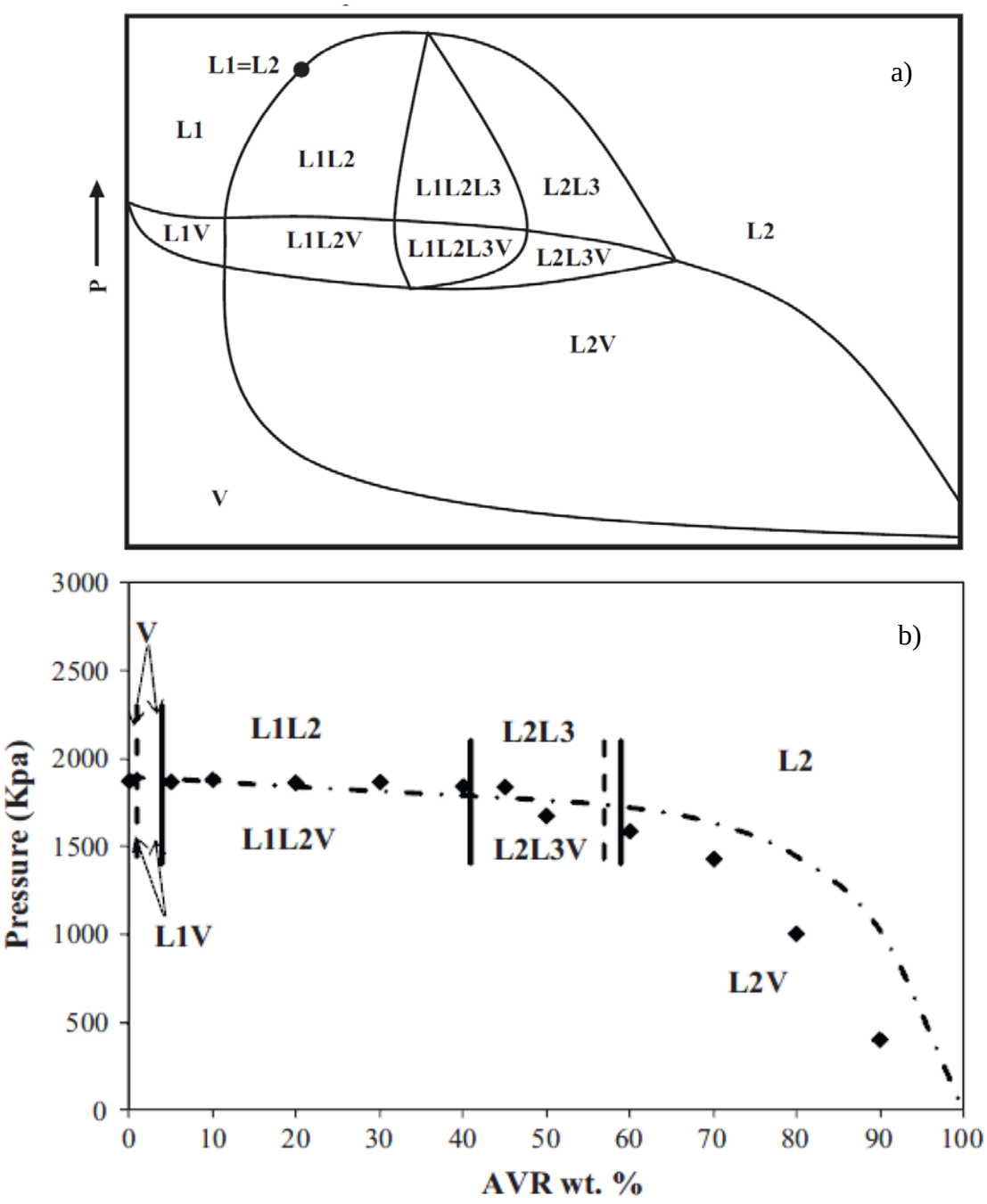

Figure 2.6 Pressure-Composition diagrams for AVR + pentane at 160°C: a) expected phase behaviors [Shaw and Zou, 2007]; b) experimentally measured (symbols) and simulated (dotted line) phase boundaries [Saber *et al.* 2012]. Note that the x-axis on these figures is reversed from all figures generated in this thesis (AVR wt% vs solvent wt%).

Most researchers [Akbarzadeh *et al.*, 2005; Ali and Al-Ghannam, 1981; Hu and Guo, 2001] have found that asphaltene solubility in crude oil and hydrocarbon solvents increases with temperature

up to 100°C. Andersen and Birdi [1990] reported an initial decrease in solubility as temperature increased from 4 to 25°C, then an increase in solubility from 25 to 100°C. Based on a small amount of data [Andersen 1994, Andersen *et al.* 1998], C7-asphaltenes (asphaltenes precipitated with *n*-heptane) may become less soluble at temperatures above 100°C.

Asphaltene solubility tends to increase with increased pressure. For example, asphaltenes solubilized in an undersaturated live oil at reservoir pressure can precipitate when the oil is depressurized [Joshi *et al.*, 2001; Tharanivasan *et al.*, 2011]. Akbarzadeh *et al.* [2005] found that asphaltene solubility in heavy oils also increased with increased pressure. Overall, while trends in asphaltene solubility with temperature and pressure have been reported, the data are too sparse to accurately assess these trends.

The properties of the asphaltene-rich phase will depend on the amount of material "precipitated" and the solvent content of the precipitated phase. The first material to precipitate is the least soluble, densest, highest molecular weight, most polar, most heteratomic fraction of the asphaltenes [Speight, 1999]. This material has a relatively high glass transition temperature and will tend to form a solid-phase. As more asphaltenes precipitate, the precipitating material becomes more resinous with a lower glass transition and more affinity for solvent and will eventually tend to become a liquid phase. For example, Luo *et al.* [2010] observed that the heavy phase separated from crude oil by propane was a highly viscous liquid, much different from the glass-like asphaltene particles precipitated by dilution with pentane.

2.3.1 Solvent Content of Asphaltene-Rich Phases

In any process that involves asphaltene precipitation, it is useful to know the amounts of maltene and solvent that partition to asphaltene phase. The phase composition dictates the phase properties and therefore the performance of the process. Key factors such as solvent losses depend on the solvent content of the heavy phase. In addition, the composition of the precipitated asphaltene phase is useful for constraining a fluid model. However, there are very little data on composition of the precipitated asphaltene-rich phase available in the literature. Yarranton *et al.* [2011] conducted drying experiments on asphaltene sediments to determine the solvent content of the precipitated asphaltene phase at ambient conditions. At these conditions, the asphaltenes

precipitate as glassy particles and form a sediment which has a porosity of approximately 90%. The drying experiments were designed to differentiate between solvent in the asphaltene phase itself and solvent entrained in the pore space. However, this method could not distinguish between solvent content of the asphaltene phase and solvent content of a discontinuous film coating the asphaltene particles and therefore, the reported solvent contents are an upper limit to the solvent content. They found the *n*-pentane content of the asphaltene phase from *n*-pentane diluted bitumen to be less than 4 wt% at ambient conditions.

2.3.2 Glass Transition

Asphaltenes precipitate from pentane-diluted bitumen as glassy particles at room temperature [Rastegari *et al.,* 2004], but appear to be a continuous liquid phase in solution at 180°C [Agrawal *et al.,* 2012], indicating that asphaltenes in solution undergo a phase transition from a glass (or solid) to liquid at some temperature between 20 and 180°C. Sirota and Lin [2005, 2007] examined this phase transition using SAXS and SANS, concluding that the scattering of asphaltenes in solution is consistent with solution behavior and that the observed morphology of the asphaltenes in solution is consistent with a viscous glass close to its glass transition temperature. Zhang *et al.* [2004] studied the glass transition of neat asphaltenes (precipitated asphaltenes not in solution) using differential scanning calorimetry (DSC). They determined the glass transition temperature for four different oils (Iranian, Khagji, Kuwait and Maya) to be between 120°C and 130°C. These asphaltene samples were found to attain a completely liquid state at temperatures between 220°C and 240°C. Gray *et al.* [2004] observed the melting point of neat asphaltenes by rapidly heating thin films of asphaltene. They observed similar results for five different oils (Arab light, Arab heavy, Athabasca, Gudao, and Maya), reporting melting points of 214-311°C. Tran [2009] examined the reversibility of the phase transition in neat asphaltenes using DSC and found two overlapping phase transitions, the endothermic glass transition and an irreversible exothermic transition. He concludes that neat asphaltenes exhibit a minimum of two phases over the temperature interval 27-227°C (300 K to over 500 K). Lower glass transitions temperatures are to be expected with asphaltenes in an oil and solvent medium because a portion of lighter components will partition to the asphaltene-rich heavy phase.

2.4 Asphaltene Precipitation Models

The understanding of asphaltene stability is an important focus of current research because the mechanism which controls asphaltene stabilization in solution will dictate the theoretical applicability of any model. Two major types of theoretical models continue to be practiced and debated; colloidal and solubility models. The colloidal theory is based on the idea that asphaltenes are insoluble colloidal solids which are stabilized in oil by a surrounding layer of resins which sterically stabilizes the asphaltenes. In this theory, asphaltene precipitation is a result of partitioning of the resins to the bulk phase, allowing the colloidal asphaltenes to aggregate. This process is considered to be irreversible. Solution theory models are based on the idea that asphaltenes are macromolecules that are part of a non-ideal mixture. The precipitation of asphaltenes is a phase transition and is modeled as liquid-liquid equilibrium. The precipitation of asphaltenes is considered to be reversible.

There are indications that the colloidal theory does not accurately represent the behavior of asphaltenes in crude oils. Sedghi and Goual [2010] investigated the behavior of asphaltenes in the presence of resins using impedence analysis and concluded that resins are unlikely to provide a steric shell for asphaltenes. Sirota [2005] examined asphaltenes using SANS and SAXS and found their behavior to be consistent with solution theory, not colloidal theory. Several researchers have demonstrated that asphaltene precipitation is reversible [Hirshberg, 1984; Permanu *et al.*, 2001] although hysteresis effects have also been observed [Beck *et al.*, 2005].

Assuming that asphaltenes are part of a solution, asphaltene precipitation is modeled as a thermodynamic phase change using either an equation of state (EoS) or a regular solution approach. To date, the most successful models are the modified regular solution (MRS) model, the perturbed-chain statistical associating fluid theory (PC-SAFT) EoS, and the cubic plus association (CPA) EoS. In this thesis, a cubic equation of state (CEoS) is used to thermodynamically model asphaltene precipitation as a liquid-liquid phase split. The MRS, CPA, and PC-SAFT models and their applicability to modeling heavy oil and solvent systems are discussed below. CEoS are discussed in more detail afterwards because they are the focus of this thesis.

2.4.1 Modified Regular Solution Theory

Modified regular solution theory incorporates the enthalpy of mixing of regular solutions plus an added entropy of mixing. Hirschberg *et al.* [1984] used the Flory-Huggins [Flory, 1941; Huggins, 1941] lattice theory as a basis for their regular solution approach to modeling asphaltene precipitation. They included the entropy of mixing to develop an expression for activity coefficient as a function of volume fraction and solubility parameter. This methodology was further developed by Yarranton and coworkers [Alboudwarej *et al.*, 2003; Akbarzadeh *et al.*, 2005]. The form of the model presented by Akbarzadeh *et al.* is given below:

$$K_i^{HL} = \frac{x_i^H}{x_i^L} = exp\left\{\frac{V_i^H}{V^H} - \frac{V_i^L}{V^L} + \ln\left(\frac{V_i^L}{V^L}\right) - \ln\left(\frac{V_i^H}{V^H}\right) + \frac{V_i^L}{RT}\left(\delta_i^L - \delta^L\right)^2 - \frac{V_i^H}{RT}\left(\delta_i^H - \delta^H\right)^2\right\} \qquad 2.3$$

Where K_i^{HL} is the equilibrium constant for component *i*, x_i is the mole fraction of component *i*, *R* is the universal gas constant, *T* is temperature, v_i and δ_i are the molar volume and solubility parameter of component *i*, and the superscripts *H* and *L* denote the heavy and light phases. This form of the model is equivalent to that of an amorphous solid (or glass) with a negligible heat of fusion. When this model is applied to asphaltene precipitation, it is assumed that only asphaltenes and resins partition to the heavy phase. Usually, the heavy phase activity coefficients are assumed to be unity.

Regular solution theory has been shown to accurately predict asphaltene yield and onset points for various solvent-diluted bitumen systems [Tharanivasan *et al.* 2011, Alboudwarej *et al.* 2003, Wang and Buckley 2001]. However, the version of regular solution theory presented above is unable to accurately model component partitioning between an asphaltene-rich phase and a solvent-rich phase. This model constrains the solvent content of the asphaltene-rich phase to be zero; in effect, forcing an asymmetric solution. If this constraint were relaxed, it is likely that the MRS would provide poor predictions because it does not account for the asymmetry of the mixture. In addition, it has not been applied to other phase transitions including VLE.

2.4.2 Cubic Plus Association Equation of State

The cubic plus association (CPA) EoS is a thermodynamic model based on a CEoS with additional terms introduced to represent association between molecules with strong hydrogen bonding interactions [Kontogeorgis, 2009]. When used to model asphaltene precipitation, the association

term is used to describe self-association between asphaltene molecules and the cross-association between asphaltene and resin molecules [Li and Firoozabadi, 2010; Zhang *et al.*, 2012]. In the CPA approach, the reduced residual Helmholtz free energy is given by

$$\boldsymbol{A^{res} = A^{CEoS} + A^{assoc}} \qquad \textbf{2.4}$$

where A^{res} is the residual Helmholtz energy, A^{CEoS} is the contribution from the CEoS which relates to the short-range attraction and repulsion forces between molecules, and A^{assoc} is the contribution from hydrogen bonding forces between opposite partial charges in associating molecules. A^{assoc} is given by the following equations:

$$\boldsymbol{\frac{A^{assoc}}{nRT} = \sum_i x_i \left\{ \sum_s \left[ln\chi_i^s - \frac{1}{2}\chi_i^s \right] + \frac{1}{2} M_i \right\}} \qquad \textbf{2.5}$$

where x_i is the mole fraction of molecule *i* that forms association (or cross-association), χ_i^s is the mole fraction of molecule *i* not bonded at site *s* with other species and M_i is the number of association sites of molecule *i*. χ_i^s is given (for bonding site α) by:

$$\boldsymbol{\chi_i^\alpha = \left(1 + \sum_j \sum_s \frac{x_j}{v} \chi_j^s \Delta_{ij}^{\alpha s} \right)^{-1}} \qquad \textbf{2.6}$$

where $\Delta_{ij}^{\alpha s}$ between site α and β in the self-associating species is given by:

$$\boldsymbol{\Delta_{11}^{\alpha\beta} = g \kappa_{11}^{\alpha\beta} \left[\exp\left(\frac{\varepsilon_{11}^{\alpha\beta}}{k_B T} - 1 \right) \right]} \qquad \textbf{2.7}$$

where g is a radial distribution function used as a probabilistic measure of the presence of molecules in the vicinity of a reference molecule, k_B is the Boltzmann constant, κ is the association bonding volume, and ε is the association energy. When used to model asphaltene precipitation, the number of associating sites for asphaltene and resins are assumed to be 2, 3, 4, or 6 [Li and Firoozabadi, 2010; Zhang *et al.*, 2012] and association strength is assumed to be identical for all like association sites (i.e. $\Delta_{11}^{\alpha\beta} = \Delta_{11}^{\beta\gamma} = \Delta_{11}^{\gamma\delta} = \Delta_{11}$). In addition, k_{ij} is typically taken to be 0 to reduce the number of tuning parameters further. These assumptions result in a model for asphaltene precipitation with four parameters, $\varepsilon_{asph\text{-}asph}$, $\kappa_{asph\text{-}asph}$, $\varepsilon_{asph\text{-}resin}$, $\kappa_{asph\text{-}resin}$. Recommended values for association energy and association volume for aphaltenes are available in the literature [Zhang *et al.*,2012], which reduces the number of tuning parameters to two: the association energy and the volume for asphaltene-resin association.

The CPA EoS has been able to capture vapor-liquid equilibrium as well as asphaltene precipitation in conventional oils and bitumen from temperature, pressure and composition effects [Li and Firoozabadi 2010, Shirani *et al.* 2012]. The major shortcoming of the CPA equations of state is in computation time and a more complex flash.

2.4.3 Perturbed Chain Form of Statistical Associating Fluid Theory

The SAFT equation of state was developed by Chapman and coworkers [1988, 1990]. The perturbed chain form of the equation (PC-SAFT), developed by Gross and Sadowski [2002], has successfully been used to model phase behavior of high molecular weight associating polymers and hence has been applied to model the complex phase behavior of asphaltenes in crude oils. The physical basis for SAFT is that molecules are modeled as chains of hard spheres joined through covalent bonds. The chains can form associating molecules through hydrogen bonding forces. The effect of van der Waals attractions, chain formation, and polar interactions are added as perturbations. The residual Helmholtz free energy is calculated by summing the contributions from each of these interactions and is given by

$$\boldsymbol{A^{res} = A^{seg} + A^{chain} + A^{assoc}} \qquad \textbf{2.8}$$

where A^{res} is the residual Helmholz free energy, A^{seg} is the contribution from the hard spheres and dispersion forces, A^{chain} is the contribution as a result of the covalent bonds that form the chains, and A^{assoc} is the contribution from association.

When the PC-SAFT equation is applied to phase behavior of asphaltenes, the association term is dropped because it is believed that the phase stability of asphaltenes is dominated primarily by dispersion interactions (van der Waals forces) as opposed to polar interactions. For each non-associating species, three parameters are required as input into the model. These are the number of segments per molecule (m), the diameter of each molecular segment (σ), and the segment-segment interaction energy (ε/k). Correlations have been proposed and tested for these three parameters for resins and aromatics [Gonzalez *et al.*, 2007], reducing the number of parameters to just one, the aromaticity (γ). The Gonzalez *et al.* correlations were recently tested and successfully applied to asphaltene pseudo-components for the purposes of asphaltene precipitation modeling [Panuganti *et al.*, 2012].

The PC-SAFT equation of state has been shown to model both vapor-liquid equilibrium and the onset of asphaltene precipitation from a depressurized conventional crude oil [Panuganti *et al.* 2012, Ting *et al.* 2003]. More recently, the PC-SAFT has been used to model asphaltene yield curves from solvent diluted bitumen and has been demonstrated to capture the effects of asphaltene polydispersity [Tavakkoli *et al.* Zhang *et al.*].

Recently, several researchers have compared the PC-SAFT and CPA models for asphaltene precipitation from conventional oils and bitumens [AlHammadi *et al.*, 2015 and Zhang *et al.* 2011]. Both models have been found to give good predictions for phase boundaries and asphaltene precipitation amounts, with the PC-SAFT prediction for asphaltene precipitation being slightly closer to the experimental data. The major shortcoming of both the PC-SAFT and CPA equations of state is in computation time and the complex flash (more than three roots to the equation).

2.5 Cubic Equations of State for Bitumen Phase Behavior Modeling

Typically, petroleum phase behavior is modeled with simple black oil models for the vapor-liquid equilibrium of low volatility oils or K-values for more complex phase behavior over limited ranges of conditions. Cubic equations of state (CEoS) are used for more complex phase behavior. CEoS and their application to the phase behavior of bitumen/solvent systems are discussed below.

2.5.1 CEoS Background

The first form of a CEoS was proposed by van der Waals in 1873 and is given by:

$$\boldsymbol{P = \frac{RT}{v-b} - \frac{a}{v^2}} \qquad \textbf{2.9}$$

where *P*, *v*, *T* and *R* have their usual meaning; and *a* and *b* are constants specific to each substance. Many CEoS have since been proposed and are widely used. All are specific forms of the generic cubic equation of state, shown below.

$$\boldsymbol{P = \frac{RT}{v-b} - \frac{a(T)}{(v+\psi b)(v+\sigma b)}} \qquad \textbf{2.10}$$

where ψ and σ are constants specific to the CEoS and are the same for all substances. Fugacity coefficients are determined from derivatives of the CEoS, and then fluid phase equilibria

calculations can be performed using a two, three, or four phase flash calculation [Peng and Robinson, 1976].

2.5.1.1 Mixing Rules

Mixture values for the parameters *a* and *b* are required to use a cubic equation of state to model the phase behavior of a mixture. These are a function of the pure species values of *a* and *b* and the composition of the mixture, but there is no established theory that defines the form of this dependence. Rather, empirical mixing rules are developed and tested for their ability to model phase behavior of mixtures. Several forms of mixing rules are discussed below.

Classic van der Waals

One of the simplest forms of mixing rules is that proposed by van der Waals. The classical van der Waals mixing rules are given by:

$$\mathbf{a_m} = \sum_{\mathbf{i}} \sum_{\mathbf{j}} \mathbf{x_i x_j} \sqrt{\mathbf{a_i a_j}} \left(\mathbf{1} - \mathbf{k_{ij}}\right) \qquad \mathbf{2.11}$$

$$\mathbf{b_m} = \sum_{\mathbf{i}} \mathbf{x_i b_i} \qquad \mathbf{2.12}$$

where a_m and b_m are the EoS constants for the mixture, x_i is the mole fraction of the i^{th} component, and k_{ij} is a binary interaction parameter.

Binary interaction parameters represent the deviation from the geometric mean of the a-values of each binary pair used in Equation 2.10. They are generally determined by minimizing the difference between experimental data and model predictions. In effect, they are used as fitting parameters. Values for k_{ij} for binary combinations of well-known species are tabulated in the literature [Reid *et al.* 1989]. Several authors have developed correlations to predict k_{ij} values from properties of the pure species, such as critical properties or acentric factor [Chueh and Prausnitz 1968, Gao *et al.* 1992].

Symmetric and Asymmetric van der Waals

When $k_{ij} = k_{ji}$, the van der Waals mixing rules are said to be symmetric and the model has only one interaction parameter per binary pair. For non-ideal mixtures, such as mixtures of highly polar and non-polar components, the symmetric mixing rules are unable to accurately capture phase

behavior. If $k_{ij} \neq k_{ji,}$ the mixing rules are said to be asymmetric. The asymmetric van der Waals mixing rules have two interaction parameters per binary pair which can be used to better match phase behavior for highly non-ideal mixtures.

Compositionally Dependent Mixing Rules

It has been found that for systems with polar substances, the value of k_{ij} which matched experimental data is not a constant at a constant temperature, but is in fact variable with composition [Adachi and Sugie, 1986; Sandoval *et al.*, 1989; Panagiotopoulos and Reid, 1986]. This observation has led to the development of several forms of compositionally dependent asymmetric mixing rules, where k_{ij} is defined as a function of composition and several other fitting parameters. For example, Adachi and Sugie [1986] define k_{ij} as follows:

$$\mathbf{k_{ij} = l_{ij} + m_{ij}\left(x_i - x_j\right)} \qquad \textbf{2.13}$$

where l_{ij} and m_{ij} are fitting parameters.

Many proposed compositionally dependent mixing rules have the drawback of displaying the so-called Michelsen-Kistenmacher syndrome [Michelsen and Kistenmacher, 1990]. They are not invariant when dividing a component into a number of identical subcomponents. That is, two different values a_{mix} will be calculated for a binary and a ternary where the ternary is formed by dividing component 2 of the binary into two "new" identical components. Schwartzentruber and Renon [1991] proposed a modification to their mixing rules that rectifies this problem.

Gibbs Excess Based Mixing Rules

Several forms of mixing rules have been developed by setting the Gibbs free energy calculated using an activity coefficient model equal to the Gibbs (or Helmholtz) energy calculated by the CEoS at infinite or zero pressure. The Huron-Vidal mixing rules [Huron and Vidal, 1979] do this with Gibbs excess energy at infinite pressure. The Wong-Sandler mixing rules [Wong and Sandler, 1992] use the Helmholtz excess energy at infinite pressure and the Gibbs excess energy at zero pressure.

2.5.2 CEoS Application to Bitumen/Solvent Systems

CEoS models and associated correlations have been developed and tuned for light hydrocarbon systems. While some work has been done to adapt the methodology to bitumen systems, CEoS have not yet been successfully tested on a broad range of phase behavior for bitumens and solvents. Mehrotra and Svrcek [1988] successfully modeled gas-solubility data for mixtures of Cold Lake bitumen and nitrogen, carbon dioxide, methane and ethane using the Peng-Robinson (PR) EoS. Jamaluddin *et al.* [1991] used the Martin EoS to fit solubility and saturated liquid density for systems of bitumen and carbon dioxide. Saber and coworkers [Saber and Shaw, 2009; Saber and Shaw 2011; Saber *et al.,* 2012] have used a group contribution method in conjunction with the PR EoS to capture LLV phase behavior of Athabasca vacuum residue and solvent. Castellanos-Díaz *et al.* [2011] and Agrawal *et al.* [2012] modeled the phase behavior of bitumen-propane, bitumen-carbon dioxide and bitumen-pentane systems using the Advanced Peng-Robinson (APR) EoS. The EoS model was found to correctly predict saturation pressures and asphaltene onset points, but it failed to accurately predict asphaltene yields. The model predicted that the asphaltenes become soluble at high solvent dilutions while experimental data showed that the asphaltenes remain insoluble. A possible remedy recommended by Castellanos-Díaz *et al.* [2011] is to apply asymmetric mixing rules rather than the symmetric van der Waals mixing rules used in the APR model.

The asymmetric mixing rules discussed in the previous section have not been commonly applied to mixtures of bitumen and solvents. The Huron-Vidal asymmetric mixing rules are theoretically applicable to mixtures of nonpolar and polar compounds [Pedersen and Christensen, 2007] and have been used to model mixtures of water and hydrocarbons. Huron-Vidal mixing rules have been used with the SRK EoS to represent the distribution of methanol between a water phase, a hydrocarbon liquid phase, and a hydrocarbon gas phase [Kristensen and Christensen, 1993]. Pedersen *et al.* [1996] applied the Huron-Vidal mixing rules to model LLV phase boundaries and phase compositions for water-methanol and water-hydrocarbon pairs. Sørensen *et al.* [2002] found the SRK EoS with Huron-Vidal mixing rules gives a fair representation of gas solubility in salt water. Gregorowicz and de Loos [2001] used the Wong-Sandler mixing rules to model LLV behavior in asymmetric hydrocarbon mixtures. To date, a CEoS with asymmetric mixing rules has not been applied to mixtures of bitumen and solvents.

Chapter Three - EXPERIMENTAL METHODS

This chapter describes the experimental methods used to collect data in this thesis, including: saturation pressures for bitumen/solvent mixtures; the solvent content at which the asphaltene-rich phase appears (onset point), asphaltene yield and asphaltene-rich phase compositions in solvent diluted bitumen; and apparent glass transition temperatures of the asphaltene-rich phase in solution. The saturation pressure and onset point measurements are shown schematically by the arrows in Figure 3.1. The phase compositions and asphaltene yields are measured at a series of *n*-pentane concentrations within the L_1L_2 region, also shown in Figure 3.1.

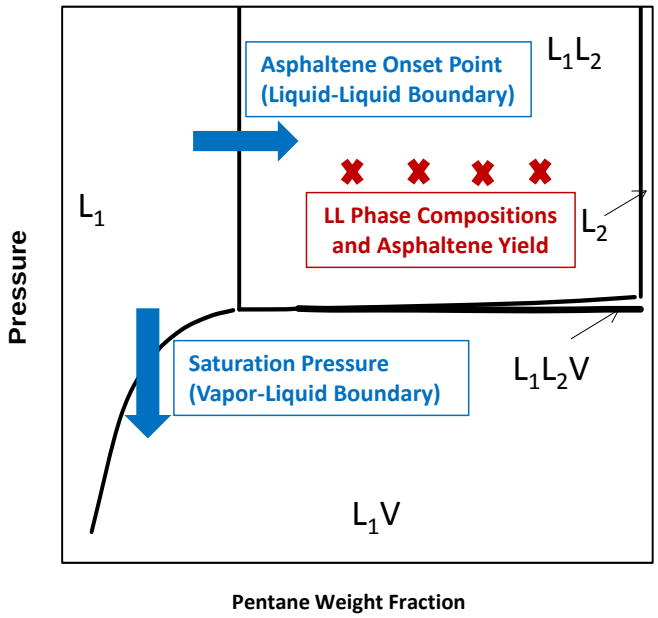

Figure 3.1 Schematic of the experiments performed in this work.

3.1 Materials

The bitumen samples used in this study, WC-B-B2 and WC-B-B3, are well-head samples from a SAGD process from the same reservoir and were provided by Shell Canada Ltd. The samples contained emulsified water. Prior to any measurements, the water was removed by sonicating the sample at ambient temperature for 24 h and then placed in a separatory funnel maintained at 60°C. After 2 weeks, the emulsion had broken and the water was drained from the funnel. The final water

content was less than 1 wt%. Selected properties of the water-free bitumens are provided in Table 3.1 and a spinning band distillation assay of the WC-B-B2 bitumen is provided in Table 3.2. The WC-B-B2 sample was used for the PVT experiments and the WC-B-B3 sample was used for the blind cell tests. Since the samples were from the same source and have similar properties, the SARA and distillation assays for WC-B-B2 were used for the characterization of both samples.

Table 3.1 Selected properties of WC-B-B2 and WC-B-B3 bitumen.

Property	WC-B-B2	WC-B-B3
Specific Gravity	1.015	1.020
Viscosity at 50°C, 1 atm, cP	2,900	3,100
Saturates, wt%	17	-
Aromatics, wt%	46.9	-
Resins, wt%	16.7	-
C5-asphaltenes, wt%	19.4	19.2

Table 3.2 Spinning band distillation assay of WC-B-B2 bitumen.

Volume % Distilled	Normal Boiling Point °C
1.7	218.0
3.4	237.4
5.0	252.4
6.7	267.9
8.4	278.6
10.1	289.4
11.8	301.7
13.4	313.5
15.1	324.0
18.5	339.8
20.2	349.6
21.8	358.0
23.5	367.3
25.2	375.2
26.9	380.0
28.57	382.5
30.25	384
31.93	385

3.2 Vapor-Liquid Boundary: Saturation Pressure Measurements

Saturation pressures were collected with a PVT cell and a blind cell apparatus. The PVT cell data were reported previously [Agrawal *et al.*, 2012] and the blind cell apparatus was designed as part of this thesis work. For the purpose of comparison, both the previous published PVT cell procedure and the blind cell apparatus procedure developed in this work are provided here.

3.2.1 PVT Procedure

Saturation pressure measurements were carried out in a DB Robinson Jefri PVT cell placed in an air-bath which controls the temperature to within ±0.1 ºC, Figure 3.2. The maximum pressure rating for the PVT Cell is 69 MPa and it can operate at temperatures from -15 to 200ºC. The maximum capacity of the PVT cell is 100 cm³. The main component of the PVT cell is a sight glass, a transparent Pyrex cylinder inside a steel shell. A magnetic mixer is installed at the bottom of the sight glass and a floating piston separates the sample fluid in the Pyrex cylinder from the hydraulic fluid. The volume of the sample fluid in the cell is determined using a calibrated cathetometer which is precise to $\pm 10^{-3}$ cm^3. The volume of cell, and hence the pressure of the sample fluid under investigation, are controlled by a variable volume computer-controlled positive displacement pump that allows for the injection or removal of hydraulic oil. The pressure in the PVT cell can also be maintained using a back pressure regulator (BPR).

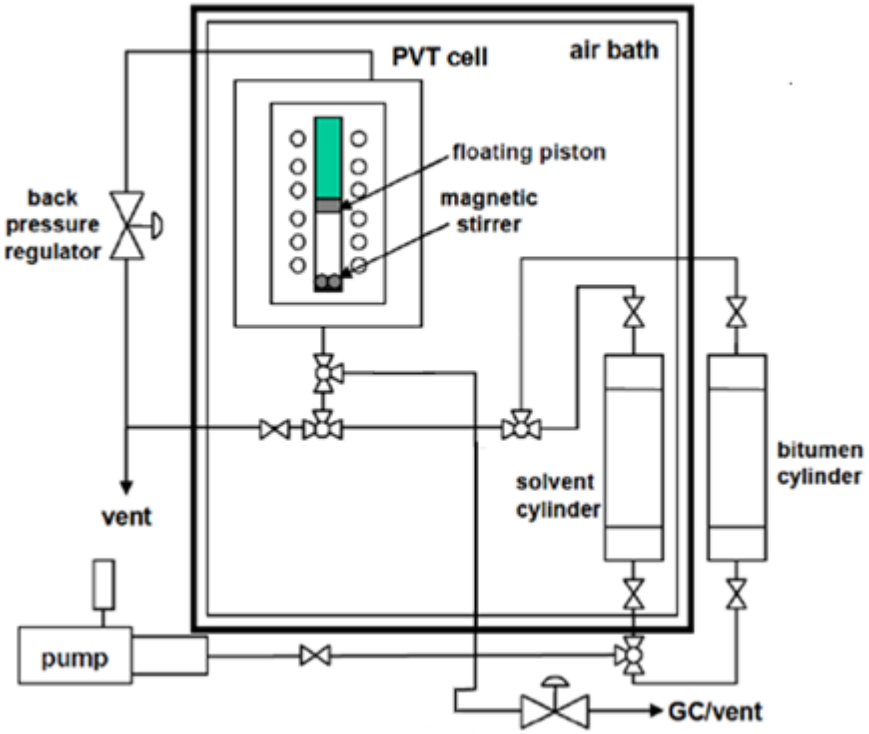

Figure 3.2 Schematic of PVT cell apparatus.

To begin an experiment, the PVT cell was first cleaned and placed under vacuum. Bitumen was transferred from a stainless steel injection cylinder equipped with a floating piston into the PVT cell at a constant temperature between 50 and 75°C to reduce the viscosity of bitumen for ease of injection. The injection volume was measured two ways: 1) directly from the PVT cell (ΔV_{PVT}), and; 2) indirectly from the volume of fluid displaced using the pump (ΔV_{pump}). In this case, the pump displacement was only used as a check on the direct measurement. The required diluent (in this case *n*-pentane) was injected in the same manner and the diluent volumes were determined in the same way. The masses of the bitumen and diluent feeds were determined from the measured volumes and fluid densities. While maintaining the pressure so that the fluid remained in the single phase region, the apparatus was then heated to experimental temperature. Once the planned test temperature and pressure were reached, the mixture was stirred using a magnetic mixer for about two hours and then was left to equilibrate until the PVT cell pressure was constant for at least four hours.

The saturation pressure was determined by step-wise isothermal expansion using the methodology described by Agrawal [2012]. At each pressure step, the system was given time to reach equilibrium and the total volume was recorded. The mixture was considered to have reached equilibrium when the pressure, temperature, and volume were all constant for a minimum of 2 hours. In general, the equilibration times required in the single liquid phase region and two-phase region were approximately 8 and 24 hours, respectively, at room temperature and 2 and 6 hours, respectively, at higher temperatures. The total volume after each step was measured using the cathetometer and the specific volume in the single phase region was determined using the known mass of the fluid in the cell. The saturation pressure was determined from the change in slope of the pressure-volume isotherm. The repeatability of the saturation pressure measurements will be discussed later.

3.2.2 Blind Cell Procedure

An apparatus was designed and commissioned to measure saturation pressures for several mixtures simultaneously. The apparatus is similar to the PVT cell apparatus described above, but is fitted with 5 blind cells (PVT cells without a sight glass) with floating pistons but no mixers, as shown in Figure 3.3. The maximum pressure rating for each blind cell is 100 MPa and it can operate at temperatures from 20 to 300ºC. The maximum capacity of each blind cell is 100 cm^3. The volume of each blind cell, and hence the pressure of the sample fluid under investigation, is controlled by a variable volume computer-controlled positive displacement pump which allows for the injection or removal of hydraulic oil.

To perform an experiment, the blind cells were first vacuumed out to remove any air present. Then, bitumen was injected into the blind cells through heated lines to reduce the viscosity for ease of flow. The injected mass of bitumen was determined by the difference between final and initial mass of the blind cell and displaced hydraulic oil. The diluent was injected and the diluent mass determined in the same way. Saturation pressures were again determined by the change in slope of a pressure-volume isotherm. However, since there is no sight glass in the blind cells, volumes of the mixtures at experimental conditions were not measured. Instead, the pressure was plotted against the volume of hydraulic oil displaced from the blind cell (measured by the pump). The displaced volume cannot provide the specific volume of the mixture but is sufficient to detect the

change in slope at the saturation condition. Additionally, there are no mixers installed in the blind cells, so equilibration times are longer than those in the PVT cell; up to 24 hours at high temperatures. The blind cell methodology was tested on pure pentane at 180°C. The measured vapor pressure was 2.58 MPa compared with 2.60 MPa from Linstrom and Mallard [2015].

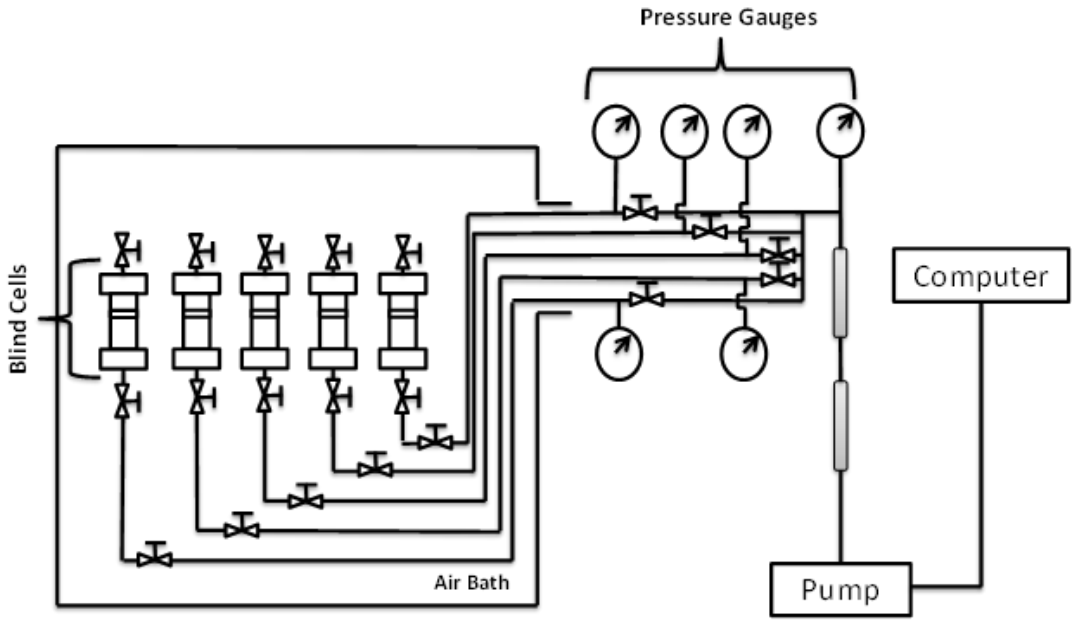

Figure 3.3 Schematic of the blind cell apparatus used for saturation pressure measurement.

3.3 Asphaltene Yield Determination

3.3.1 Bench Top Procedure at Ambient Conditions

To determine asphaltene yields at ambient conditions, a series of solutions of *n*-pentane and bitumen with different *n*-pentane contents were prepared in centrifuge tubes with known masses of bitumen and *n*-pentane. The solutions were sonicated for 1 hour and left to settle for 24 hours. Each mixture was then centrifuged at 4000 rpm for 5 minutes and a sample of the supernatant was collected. Supernatant samples were analyzed for *n*-pentane, maltene and asphaltene content; and asphaltene yield (the mass of C5-asphaltene partitioned to the heavy phase divided by the mass of feed bitumen) was determined from a mass balance as will be described later in Section 3.7. Yields measured using this methodology were compared to yields determined from the mass of precipitate at the same conditions and were found to be within the measurement error of ±1.0 wt% as will be discussed later.

3.3.2 Blind Cell Procedure

The blind cell apparatus described previously was also designed to determine light phase compositions and asphaltene yields at high temperature and pressure. The apparatus was configured to collect samples as shown in Figure 3.4. Known masses of bitumen and diluent were injected into the blind cells at ambient conditions. The samples were mixed on a roller at ambient conditions for 1 to 2 days to ensure complete mixing. The blind cells were installed in the oven and oriented so that the heavy phase settled on the floating piston. Once the samples reached the target temperature, the pressure and temperature were maintained for a minimum of 5 days to ensure equilibrium was reached. A sample of the light phase was displaced at experimental pressure and temperature into either constant volume pycnometers or a variable volume sample cylinder. The pycnometers were used to obtain a series of small samples so that their compositions could be compared. The sample cylinders were used to collect single large samples in order to minimize the experimental error in the sample collection. Both sample collection methodologies are described below.

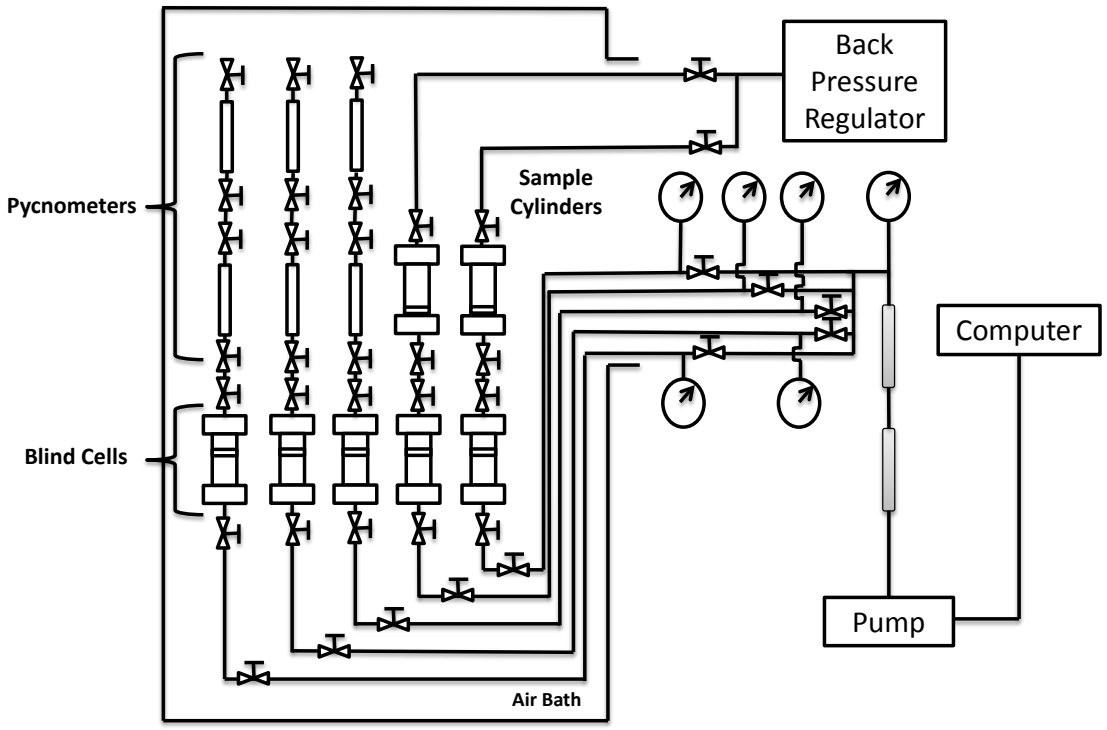

Figure 3.4 Schematic of blind cell apparatus used for asphaltene yield measurement.

Pycnometer Light Phase Sample Collection Methodology

Two or three calibrated pycnometers (5 to 10 cm^3) were vacuumed out at ambient conditions to remove any air present and were connected in series to the top valve of the blind cell. At experimental conditions, the valve connecting the blind cell to the pycnometers was opened with the pump set to maintain pressure. When the valve was initially opened, the sample expanded which causes some light ends to flash and the pressure to drop. The pump was then used to return the system to experimental pressure to ensure the flashed gas had re-dissolved into the light liquid phase. The system was held at experimental pressure for at least 4 hours to ensure the light liquid phase had reached equilibrium.

Sample Cylinder Light Phase Sample Collection Methodology

The sample cylinders used for collecting the light phase were identical to the blind cells used for the feed mixtures. The sample cylinders were assembled with the piston at the bottom to minimize dead volume and were vacuumed out at ambient conditions. Dead volumes from the blind cell to the sample cylinder were approximately 0.5 to 1.0 cm^3. The pump was used to displace approximately 30 cm^3 from the blind cell to the sample cylinder and a BPR was used to maintain pressure in the sample cylinder at experimental conditions.

The mass evaporation technique described in the previous section was used to determine the composition of the light phase samples for both the pycnometer and sample cylinder methodologies. The heavy phase could not be sampled with the blind cell procedure; only asphaltene yields were determined.

3.4 Liquid-Liquid Boundary: Onset of Asphaltene-Rich Phase Measurement

The asphaltene onset, the composition at which a separate asphaltene-rich heavy phase appears, is measured using two distinct methods. The first is by extrapolation of asphaltene yield data and the second is by direct observation using a high pressure microscope. Both methods are presented below.

3.4.1 Asphaltene Onset Extrapolated from Yields at Atmospheric Pressure

Figure 3.5 shows asphaltene yields measured with the previously described bench top method at 21°C and atmospheric pressure. To determine an *extrapolated onset* point (the *n*-pentane content at which an asphaltene-rich phase forms), the data were fit with the following empirical expression:

$$\boldsymbol{Y = C[1 - exp\{-D(w_{C5} - w_{onset})\}]} \qquad \textbf{3.1}$$

where Y is the asphaltene yield in wt%, w_{C5} is the *n*-pentane content, w_{onset} is the *n*-pentane content at the onset of the asphaltene-rich phase, and C and D are constants. The constants and the onset composition were adjusted to minimize the least square error. Based on all of the data collected in this study, extrapolated onsets are within ±1.5 wt% of the measured onsets.

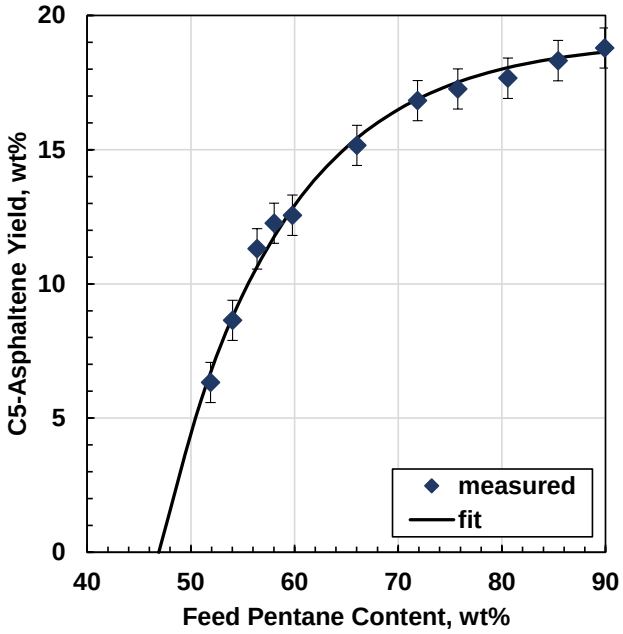

Figure 3.5 Yield and extrapolated onset of C5-asphaltene phase separation from *n*-pentane diluted WC-B-B3 bitumen at 23°C and 0.1 MPa. Data were fitted using Equation 3.1.

3.4.2 Asphaltene Onset from Yields at Elevated Temperatures and Pressures

Asphaltene yield curves were measured using both the blind cell apparatus and the PVT cell apparatus using the procedures described in Section 3.3. For both procedures, the mixture of pentane and bitumen were equilibrated and samples of the light phase were collected at experimental conditions. The mass evaporation technique, described later in Section 3.7, was used to determine the yield from the composition of the light phase and a mass balance. The extrapolated

onsets were determined as described previously and matched the measured onsets within the experimental error of ±1.5 wt%.

3.4.3 Measured Asphaltene Onsets above Atmospheric Pressure

The asphaltene onset point was measured directly using a high pressure microscope (HPM) coupled with the PVT cell, Figure 3.6. The HPM system consists of a cell with two sapphire windows, a light source, and a high focal length camera connected to a computer in order to capture digital images and video. The HPM has an adjustable gap of 100 to 400 μm between the two windows. To measure the asphaltene onset point of *n*-pentane diluted bitumen, the gap was set at 200 μm. The HPM system is placed in-line between two high pressure cylinders with floating pistons and magnetic stirrers, both of which are connected to a computer-controlled pump and a back pressure regulator. The pump and regulator are used to push fluid back and forth from one mixing cylinder, through the gap between windows in the HPM, to the second cylinder. The HPM is rated for temperatures up to 200°C and pressures up to 138 MPa.

The asphaltene onset point was measured by titrating the bitumen with diluent (in this case *n*-pentane), using the methodology described by Agrawal [2012] and summarized here. An initial amount of dewatered bitumen was injected into the HPM mixing cylinders and then diluent was injected in a step-wise fashion at a flow rate of 10-20 cm^3/h for each step. The magnetic stirrer in the mixer cylinders was turned on for injections. After each injection, the volume of injected diluent was determined from the cathetometer readings verified with pump displacements. The fluid was moved back and forth between the two cylinders until a uniform mixture was observed in the HPM cell and then an image was taken. This procedure was repeated for each incremental injection of diluent until an asphaltene-rich phase was observed. The diluent content at the onset of the asphaltene-rich phase (LL boundary) was taken to be the intermediate content between the highest content at which only one phase was observed and the lowest content at which the second phase was observed, Figure 3.7. Note that a small number of particulates are visible below the onset, Figure 3.7a. These are the toluene insoluble particles inherent in the bitumen. The onset of the asphaltene-rich phase is detected by a drastic increase in number of visible particles, Figure 3.7b. In most cases, the injection steps were set at intervals of 2 wt% diluent and the uncertainly of the diluent content was ±0.5 wt%; therefore, the uncertainty of the reported onset was ±1.5 wt%.

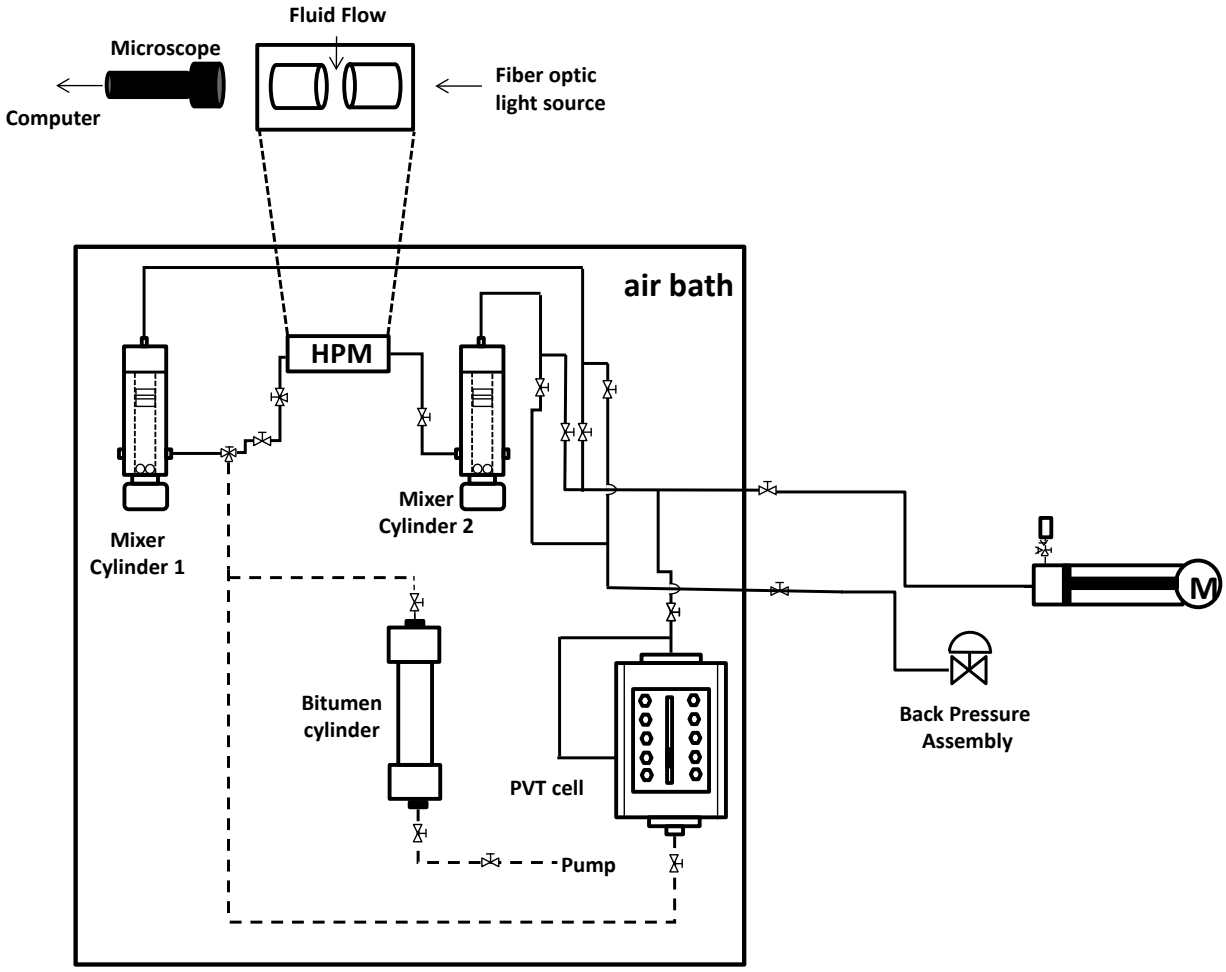

Figure 3.6 Schematic of HPM and supporting PVT apparatus.

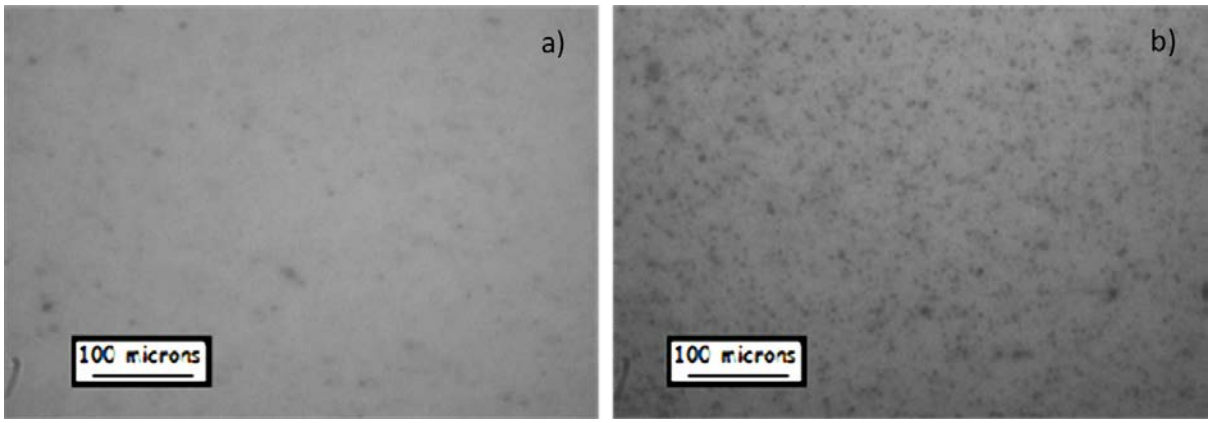

Figure 3.7. HPM images of *n*-pentane diluted bitumen at 180°C and 4800kPa at 50 wt% (a) and 52 wt% (b) *n*-pentane. The reported onset is 51 ±1.5 wt%.

3.5 PVT Cell Procedure for Asphaltene-Rich Phase Amount and Composition

The phase volume measurements were carried out in a DB Robinson Jefri PVT cell described previously, Figure 3.2. However, in this procedure, the magnetic mixer was removed from the PVT cell end cap to create a less tortuous flow path for sample displacement which helps ensure a clean separation of the light phase from the heavy phase.

A feed composition was selected to meet two constraints: 1) that the overall mixture split into two phases, the diluent-rich light phase and asphaltene-rich heavy phase, and; 2) that a minimum of 3 cm^3 of heavy phase was formed as required to perform for compositional analysis. Bitumen was transferred from a stainless steel injection cylinder equipped with a floating piston into the PVT cell at a temperature between 50 to 75°C to reduce the viscosity of bitumen for ease of injection. The injection volume was measured two ways: 1) directly from the PVT cell (ΔV_{PVT}), and; 2) indirectly from the volume of fluid displaced using the pump (ΔV_{pump}). The apparatus was then heated to experimental temperature. Pressure was maintained at the experimental pressure using either the pump or the BPR. The required diluent was injected as described above. The bitumen and diluent were then mixed in the PVT cell by inverting the PVT cell several times daily for 1 to 2 weeks. It was assumed the system had reached equilibrium when no changes in pressure or volume were observed.

After equilibration, the PVT cell was rotated to allow the heavy phase to settle on the piston. The volume of the heavy phase was measured using the cathetometer while the interface between the phases was illuminated with a bright light so that it could be detected. Then, light phase samples were collected at pressure from the top of the cell by displacing the light phase into two or three 10 cm³ pycnometers. The remaining light phase was displaced until only the heavy phase remained in the PVT cell.

A known volume of toluene was injected into the PVT cell to dissolve the heavy phase and ensure the samples of heavy phase remained in a liquid state upon cooling. The PVT cell was inverted several times daily for 1 to 2 days to ensure proper mixing. The mixture of toluene and heavy phase was displaced into two 10 cm³ sample pycnometers. The sample collection methodology is summarized in Figure 3.8.

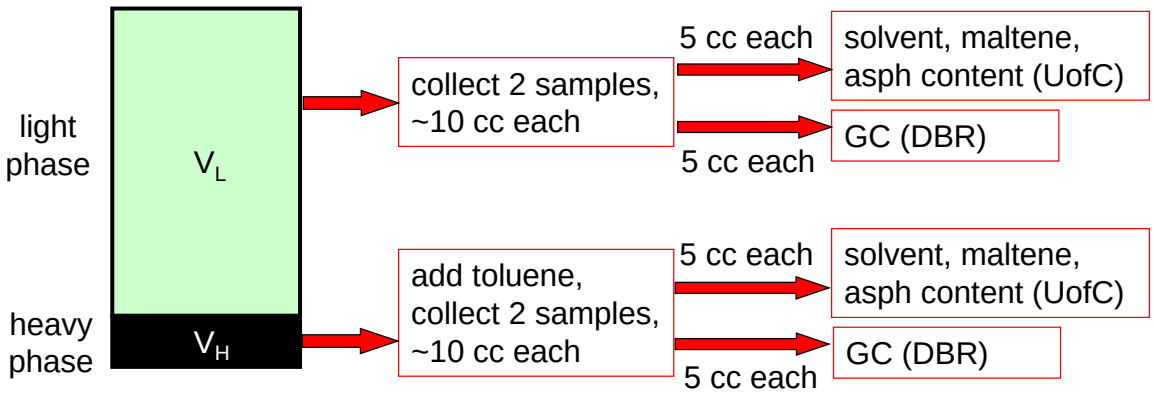

Figure 3.8. Schematic of sample collection methodology for asphaltene yield and phase composition determination.

3.6 Compositional Analysis

Four 10 cm^3 samples (2 samples of light phase and 2 samples of heavy phase+toluene) were available for compositional analysis. 5 cm^3 of each sample was placed in a glass centrifuge tube and analyzed for solvent, maltene, and asphaltene content using the Mass Evaporation method described below. The other half of each sample was placed in a vial and sent for a gas chromatographic (GC) assay. The heavy phase samples contained over 90 wt% toluene and the oil sample calibration used for these GC assays was not adequate to determine an accurate *n*-pentane

content with such a large toluene peak. There was no toluene in the light phase samples and the *n*-pentane peak was small enough to fall within the range of the standard calibration. Therefore, only the light phase assays were used in the analysis described below.

3.6.1 Mass Evaporation Method

The sample was allowed to dry in a vacuum oven at 60-70°C for up to 1 week. The initial and final (dried) masses were recorded. The solvent content was taken to be the fraction of overall mass that evaporated over the drying period. For the light phase samples, solvent content is simply the diluent (in this case, *n*-pentane) content of the phase. For the heavy phase samples, the solvent content is the sum of the diluent in the heavy phase and the added toluene. The uncertainty of the solvent content is 1.1 wt%; the determination of the uncertainty is discussed in Appendix A.

The remaining mass of sample was diluted with *n*-pentane at a 40:1 volume:mass ratio of diluent to bitumen. The mixture was sonicated for 1 hour and left to settle for 24 hours. After the settling period, the tube was centrifuged for 5 minutes at 4000 rpm. Then the supernatant was decanted leaving a mass of asphaltenes and solids with some residual maltenes. This mass was washed with the *n*-pentane, sonicated, and centrifuged twice as described above, leaving the asphaltenes, solids, and some *n*-pentane. At this point the tube and contents were dried in a vacuum oven and weighed to obtain the total mass of asphaltenes and solids in the sample. The asphaltene+solid content is the mass of dry asphaltene+solids divided by the mass of sample. The mass of maltenes is the difference between the initial and final mass of the sample. The repeatability of the asphaltene+solids content is ± 0.15 wt%.

3.6.2 GC Analysis

The GC assays were performed at the DBR Technology Center (Schlumberger Canada Ltd) in Edmonton. The GC assays of the light phase samples provided the total diluent content of the samples and was used to validate the mass evaporation results.

3.7 Data Processing

3.7.1 PVT Cell Data Analysis

The required outputs from the PVT cell experiments are the mass and composition of the feed, light phase, and heavy phase, and also the asphaltene yield. Note, in the following discussion, the term *solvent* indicates mixtures of diluent and toluene. The mass and composition of the feed were determined from the volumes and densities of the fluids injected into the PVT cell. The mass based composition of the light phase (in terms of solvent, maltenes, and asphaltenes) was measured as described in Section 3.5, Figure 3.8. In this case, the solvent is diluent only (*e.g. n*-pentane). The mass based composition of the heavy phase was measured but, in this case, the solvent content includes both diluent and added toluene. The composition prior to toluene addition must be calculated. While the volume of each phase was measured, the mass of each phase must also be calculated. The asphaltene yield was calculated once the masses and compositions of each phase were determined. The methodology for the calculations is outlined below.

3.7.1.1 Feed Composition

The feed composition is determined from the measured injection volume and calculated (or independently measured) densities. Recall that the injection volume is measured two ways: 1) directly from the PVT cell (ΔV_{PVT}), and; 2) indirectly from the volume of fluid displaced using the pump (ΔV_{pump}). The injected fluid volume is estimated from pump volume as follows:

$$\boldsymbol{V_{inj} = \Delta V_{pump} \frac{\rho_{hyd}(T_{amb})}{\rho_{hyd}(T_{oven})}} \qquad \textbf{3.2}$$

where ρ_{hyd} is density of the hydraulic oil, and T_{amb} and T_{oven} refer to the ambient temperature and the temperature in the oven. When a sample is injected at ambient temperature, V_{inj} is equal to ΔV_{pump}.

There are two injection periods to consider: 1) the initial low temperature injection of the bitumen, and; 2) the subsequent high temperature injection of diluent. For the initial injection of bitumen, ΔV_{PVT} and ΔV_{pump} are approximately equal. ΔV_{PVT} is considered to be a more accurate measurement and is used in the calculations, while ΔV_{pump} is used as a validation. The total mass of bitumen injected is simply the product of injected volume and the bitumen density.

When additional diluent is injected at high temperatures, a small but significant difference is observed between ΔV_{PVT} and ΔV_{pump} due to the excess volume of mixing. The mass of diluent injected at high temperature is calculated two ways: 1) using ΔV_{PVT} and the effective density of the diluent in the mixture, and; 2) using ΔV_{pump} and the density of liquid diluent. The mass of diluent injected is taken to be the average of these two values. The feed composition is calculated from the masses of bitumen and diluent. The densities used in these calculations are discussed later in Section 3.7.1.2 and summarized in Table 3.3.

3.7.1.2 Phase Compositions and Asphaltene Yield

Asphaltene yield can be calculated two ways: 1) directly from the mass of asphaltenes recovered from the heavy phase, and; 2) indirectly from the residual asphaltene content in the light phase data and a mass balance. Each method is described below.

Heavy Phase Method

The mass evaporation technique provides the total solvent content which is the sum of diluent in the heavy phase and the added toluene. The diluent content is determined by:

$$w_{dil}^{H} = \frac{w_{solv} - w_{tol}}{1 - w_{tol}} \qquad \textbf{3.3}$$

where superscript *H* denotes the heavy phase and the subscripts *dil, solv,* and *tol* refer to diluent, total solvent content from the evaporation technique, and toluene. The mass fractions of asphaltenes, w_A, and maltenes, w_M, are similarly determined from the original assay normalized to zero toluene content. The weight fraction of toluene is calculated from the fluid volumes measured in the PVT cell as follows:

$$w_{tol} = \frac{V_{tol}\rho_{tol}}{V^{H}\rho^{H} + V_{tol}\rho_{tol}} \qquad \textbf{3.4}$$

where V is the volume and ρ is the density. The phase density is unknown and is estimated assuming regular solution behavior as follows:

$$\rho^{H} = \frac{1}{\frac{w_{asph}^{H}}{\rho_{asph}} + \frac{w_{malt}^{H}}{\rho_{malt}} + \frac{w_{dil}^{H}}{\rho_{dil}}} \qquad \textbf{3.5}$$

where the subscripts *A* and *M* refer to asphaltenes and maltenes, respectively. The values used for asphaltene, maltene, and diluent density are discussed later. Equations 3.3 to 3.5 are solved simultaneously for w_{dil}, $w_{tol,}$ and ρ^{H}.

The samples provide compositions but not total masses of each phase. The total mass of the heavy phase is determined from the volume of the heavy phase measured directly in the PVT cell and the phase density calculated from Equation 3.5. Once the mass of the heavy phase is known, the mass of asphaltene in the heavy phase is determined from the product of the mass fraction of asphaltenes and the mass of the heavy phase. Asphaltene yield is mass of asphaltenes in the heavy phase divided by the mass of bitumen in the feed.

Light Phase Method

The light phase composition was measured as described in the experimental methods and no further data processing was required. To determine the asphaltene yield from the light phase composition, recall that asphaltene yield is the mass of asphaltenes in the heavy phase divided by the mass of bitumen in the feed. The mass of asphaltene in the heavy phase is calculated from the light phase data using a mass balance given by:

$$\boldsymbol{m^H_{asph} = m^F_{asph} - m^L_{asph} = m^F_{asph} - w^L_{asph} m^L} \qquad \textbf{3.6}$$

where the superscripts *L*, *H* and *F* denote the light phase, the heavy phase and the feed. The mass fraction of asphaltenes in the light phase, w^L_{asph}, is measured directly. The total mass of the light phase is calculated as follows:

$$\boldsymbol{m^L = {m^L_{dil}}/{w^L_{dil}}} \qquad \textbf{3.7}$$

The mass of diluent in the light phase is calculated from an overall mass balance as follows:

$$\boldsymbol{m^L_{dil} = m^F_{dil} - m^H_{dil}} \qquad \textbf{3.8}$$

The mass of diluent in the feed and the mass of diluent in the heavy phase are calculated as discussed previously in this section. The heavy phase split ratio, *H/F*, is given by:

$$\boldsymbol{{H}/{F} = \frac{m^H}{m^H + m^L}} \qquad \textbf{3.9}$$

Uncertainties

An error analysis is presented in Appendix A. The uncertainty of the light and heavy phase compositions were ±1.1 and ±2.9 wt%, respectively. The asphaltene yield was taken as the average

of the yields calculated with the light and heavy phase methods and its uncertainty was ±1.1 wt%. The material balance error, *MB error*, for each component (diluent, maltene and asphaltene) was calculated as follows:

$$\boldsymbol{MB\ error = \frac{(m^{L}_{component} + m^{H}_{component}) - m^{F}_{component}}{m^{F}_{component}} * 100} \qquad \textbf{3.10}$$

Densities used in Calculations

The densities used in this analysis are summarized in Table 3.3. Note, the effective density (used for *n*-pentane in bitumen) is the density of a component when dissolved in a liquid mixture. The effective density has been used mainly for dissolved gases but it also applies to components that are close to their critical point when not part of a liquid mixture [Saryazdi *et al.*, 2013]. The method is valid for liquid mixtures that are far from the mixture critical point, such as diluted bitumens.

Table 3.3 The densities used for the data processing.

Components	Temperature °C	Pressure MPa	Density g/cm³	Source
n-Pentane, liquid	180	4.8	0.429	Linstrom and Mallard [2015]
n-Pentane, effective	180	4.8	0.508	Saryazdi *et al.* [2013] correlation
Toluene	180	4.8	0.798	Linstrom and Mallard [2015]
Bitumen	50	1.4	0.9948	Interpolated from Motahhari *et al.* [2013] data
Asphaltenes	180	4.8	1.17	Barrera *et al.* [2013]
Maltenes	180	4.8	0.869	Calculated*

* maltene density calculated from extrapolated bitumen density and asphaltene density assuming regular solution behavior

Chapter Four - PHASE BEHAVIOR MODELING

One objective of this thesis is to evaluate the applicability of asymmetric mixing rules with a CEoS to model bitumen-solvent phase behavior. This chapter describes the Advanced Peng-Robinson (APR) CEoS model used in this thesis and summarizes the different set of mixing rules investigated for this model including: symmetric van der Waals mixing rules ($k_{ij} = k_{ij}$); asymmetric van der Waals mixing rules ($k_{ij} \neq k_{ij}$), the Sandoval *et al.* mixing rules [1989], and two forms of the Huron-Vidal mixing rules [1979]. The oil characterization methodology used for the CEoS model is also provided.

4.1 Advanced Peng Robinson CEoS

The model chosen for this study was the Advanced Peng Robinson cubic equation of state (APR EoS) [VMG 2015]. This EoS is well suited for petroleum fluids and is implemented in the VMGSim^{TM} software used for this study. The Peng-Robinson cubic EoS [Peng and Robinson, 1979] is given by:

$$\mathbf{P} = \frac{\mathbf{RT}}{\mathbf{v} - \mathbf{b}} - \frac{\mathbf{a}\alpha(\mathbf{T_R}, \omega)}{\mathbf{v(v+b)+b(v-b)}} \qquad \mathbf{4.1}$$

where P is pressure, v is the molar volume, a and b are constants related to the attractive and repulsive forces, $\alpha(T_R,\omega)$ is a function specific to the equation of state, T_R is the reduced temperature and ω is the acentric factor. The constants a and b for a pure component are related to its critical properties as follows:

$$\mathbf{a_i} = \mathbf{0.457235\ R^2 T_{ci}^2 / P_{ci}} \qquad \mathbf{4.2}$$

$$\mathbf{b_i} = \mathbf{0.0777969\ RT_{ci} / P_{ci}} \qquad \mathbf{4.3}$$

where T_c is the critical temperature, P_c is the critical pressure, and the subscript i denotes the component.

CEoS such as the Peng-Robinson EoS do not accurately predict liquid phase densities and are typically corrected using volume translation. The Peneloux volume translation [1982] was applied to the PR EoS by Jhaveri and Youngren [1988] as follows:

$$P = \frac{RT}{v-b} - \frac{a\alpha(T_r,\omega)}{(v+c)(v+b+2c)+(b+c)(v-b)} \quad \textbf{4.4}$$

where c is the volume translation. The APR EoS [VMG 2015] is the Peng Robinson EoS with volume translation implemented.

4.2 Mixing Rules

The mixing rules considered in this study are the asymmetric van der Waals (AvdW), compositionally dependent van der Waals (CDvdW), Sandoval *et al.* (SWV), and the Huron-Vidal (HV) mixing rules. The symmetric van der Waals mixing rules have been tested in previous studies [Agrawal *et al.* 2012] and are used as basis of comparison for this study. Each is described below.

4.2.1 Van Der Waals Mixing Rules

The classical van der Waals mixing rules are given by:

$$\mathbf{a_m} = \sum_{\mathbf{i}}\sum_{\mathbf{j}} \mathbf{x_i x_j}\sqrt{\mathbf{a_i a_j}}\left(\mathbf{1}-\mathbf{k_{ij}}\right) \quad \textbf{4.5}$$

$$\mathbf{b_m} = \sum_{\mathbf{i}} \mathbf{x_i b_i} \quad \textbf{4.6}$$

where a_m and b_m are the EoS constants for the mixture, x_i is the mole fraction of the i^{th} component, and k_{ij} is a binary interaction parameter.

Symmetric (SvdW): When $k_{ij} = k_{ji}$, the van der Waals mixing rules are symmetric and the model has only one interaction parameter per binary pair. For bitumen-solvent systems, Castellanos-Díaz *et al.* [2011] recommended that the symmetric binary interaction parameters be estimated using a modified Gao *et al.* correlation [Gao *et al.*, 1992] given by:

$$k_{ij} = 1 - \left(\frac{2\sqrt{T_{ci}T_{cj}}}{T_{ci}+T_{cj}}\right)^{n_{ij}} \quad \textbf{4.7}$$

where n_{ij} is an adjustable exponent with a default value of 0.27. Agrawal *et al.* [2012] recommended temperature dependent binary interaction parameters of the following form:

$$k_{ij} = k_{ij}^0\left(1 + \frac{k_{ij}^1}{T} + k_{ij}^2 ln(T)\right) \quad \textbf{4.8}$$

where k_{ij}^1 and k_{ij}^2 are constants and k_{ij}^0 is given by:

$$k_{ij}^{0} = 1 - \left[\frac{2\sqrt{T_{Ci}T_{Cj}}}{T_{Ci}+T_{Cj}}\right]^{n} \quad \textbf{4.9}$$

In this case, n, k_{ij}^{1}, and k_{ij}^{2} are adjusted to fit the data.

Asymmetric (AvdW): If $k_{ij} \neq k_{ji}$ in Equation 4.5, the mixing rules are asymmetric. The asymmetric van der Waals mixing rules have two interaction parameters per binary pair which can be used to better match phase behavior for highly non-ideal mixtures.

Compositionally Dependent (CDvdW): When k_{ij} in Equation 4.5 is defined as a function of composition, the mixing rules are asymmetric and compositionally dependent. The fitting of the asymmetric binary interaction parameters specifically for asphaltene-solvent binaries is discussed further in Section 4.3.

4.2.2 Sandoval, Wilczek-Vera and Vera Mixing Rules (SWV)

Sandoval *et al.* [1989] proposed several new forms of asymmetric, compositionally dependent mixing rules to better match data for asymmetric ternary systems. The Sandoval, Wilczek-Vera, and Vera form of mixing rule (SWV) tested in this study is expressed as follows:

$$\mathbf{a_m} = \sum_{\mathbf{i}}\sum_{\mathbf{j}} \mathbf{x_i x_j}\sqrt{\mathbf{a_i a_j}}\left(\mathbf{1} - \mathbf{l_{ij}}\right) \quad \textbf{4.10}$$

where l_{ij} is given by:

$$\boldsymbol{l_{ij}} = \bar{\boldsymbol{k}}_{\boldsymbol{ij}}\left(\mathbf{1} - \boldsymbol{x_i} - \boldsymbol{x_j}\right) + \boldsymbol{k_{ij}x_i} + \boldsymbol{k_{ji}x_j} \quad \textbf{4.11}$$

$$\bar{\boldsymbol{k}}_{\boldsymbol{ij}} = \frac{\boldsymbol{k_{ij}}+\boldsymbol{k_{ji}}}{\mathbf{2}} \quad \textbf{4.12}$$

The SWV model has two binary interaction parameters per binary pair, k_{ij} and k_{ji}. If $k_{ij} = k_{ji}$, the mixing rules reduce to the symmetric van der Waals mixing rules. This mixing rule can also be defined as a compositionally dependent van der Waals mixing rule but is labeled as *SWV* to distinguish it from the *CDvdW* mixing rule developed later.

4.2.3 Huron-Vidal Mixing Rules (HV)

For a CEoS, the limit of the Gibbs energy as pressure approaches infinity (g^{E}_{∞}) is defined as follows:

$$\mathbf{g}_{\infty}^{\mathbf{E}} = -\left(\frac{\mathbf{a_m(T)}}{\mathbf{b_m}} - \sum \mathbf{x_i} \frac{\mathbf{a_i(T)}}{\mathbf{b_i}} \right) \Lambda \qquad \textbf{4.13}$$

where Λ is a function of the equation of state and, for the Peng-Robinson EoS, is given by:

$$\Lambda = \frac{\mathbf{1}}{\mathbf{2\sqrt{2}}} \mathbf{ln} \left(\frac{\mathbf{2+\sqrt{2}}}{\mathbf{2-\sqrt{2}}} \right) \qquad \textbf{4.14}$$

Equation 4.13 can be rearranged to obtain the following expression for a_m as a function of g^E_∞ [Huron-Vidal 1979, VMG 2015]:

$$\mathbf{a_m} = \mathbf{b_m} \left(\sum \frac{\mathbf{a_i}}{\mathbf{b_i}} \mathbf{x_i} - \frac{\mathbf{g}_{\infty}^{\mathbf{E}}}{\Lambda} \right) \qquad \textbf{4.15}$$

The NRTL activity coefficient model can be used to calculate g^E_∞ in Equation 4.15. The NRTL model is used to represent strongly non-ideal mixtures where composition at a microscopic level deviates from the overall composition. Hence, it is referred to as a *local composition model*. The Gibbs excess energy at infinite pressure from the NRTL model is given by:

$$\mathbf{g}_{\infty}^{\mathbf{E}} = \sum_{\mathbf{i=1}}^{\mathbf{n}} \mathbf{x_i} \frac{\sum_{\mathbf{j=1}}^{\mathbf{n}} \mathbf{x_j} \exp\left(-\alpha_{\mathbf{ji}} \frac{\mathbf{g_{ji}} - \mathbf{g_{ii}}}{\mathbf{RT}} \right) \left(\mathbf{g_{ji}} - \mathbf{g_{ii}} \right)}{\sum_{\mathbf{k=1}}^{\mathbf{n}} \mathbf{x_k} \exp\left(-\alpha_{\mathbf{ki}} \frac{\mathbf{g_{ki}} - \mathbf{g_{ii}}}{\mathbf{RT}} \right)} \qquad \textbf{4.16}$$

where g_{ji} is the interaction energy between component j and i, and α_{ji} is a constant characteristic of the mixture called the non-randomness parameter. α_{ji} is analogous to the inverse of the coordination number of a lattice. In the NRTL model, there are three interaction parameters per binary pair that can be tuned to match experimental data: (g_{ji} - g_{ii}), (g_{ij} - g_{jj}), and α_{ij}.

Huron and Vidal introduced the component volume parameter, b_j, into the calculation of g^E_∞ as follows:

$$\mathbf{g}_{\infty}^{\mathbf{E}} = \sum_{\mathbf{i=1}}^{\mathbf{n}} \mathbf{x_i} \frac{\sum_{\mathbf{j=1}}^{\mathbf{n}} \mathbf{x_j b_j} \exp\left(-\alpha_{\mathbf{ji}} \frac{\mathbf{g_{ji}} - \mathbf{g_{ii}}}{\mathbf{RT}} \right) \left(\mathbf{g_{ji}} - \mathbf{g_{ii}} \right)}{\sum_{\mathbf{k=1}}^{\mathbf{n}} \mathbf{x_k b_k} \exp\left(-\alpha_{\mathbf{ki}} \frac{\mathbf{g_{ki}} - \mathbf{g_{ii}}}{\mathbf{RT}} \right)} \qquad \textbf{4.17}$$

This addition allows the Huron-Vidal mixing rules to be reduced to the classical van der Waals mixing rules by substituting the following values for α_{ij}, g_{ii}, and g_{jj}:

$$\boldsymbol{\alpha_{ij} = 0} \qquad \textbf{4.18}$$

$$g_{ii} = -(ln2)\frac{a_{ii}}{b_{ii}} \quad \textbf{4.19}$$

$$g_{ij} = -2\frac{\sqrt{b_{ii}b_{jj}}}{b_{ii}+b_{jj}}\sqrt{g_{ii}g_{jj}}(1-k_{ij}) \quad \textbf{4.20}$$

In this work, the mixing rules obtained by using Equation 4.16 with Equation 4.15 are referred to as the *mole-based Huron-Vidal* mixing rules and those obtained by using Equation 4.17 with Equation 4.15 as the *volume-based Huron-Vidal* mixing rules. Both the mole-based and volume-based Huron-Vidal mixing rules were evaluated. The *mole-based* Huron-Vidal mixing rules were tested using the VMGSim Gibbs Excess Peng Robinson (GEPR™) property package, which is commercially available [VMG 2015]. The *volume-based* Huron-Vidal mixing rules were tested using an unreleased beta version of VMGSim. In the VMGSim implementation of both versions of the Huron-Vidal mixing rules (mole-based and volume-based), the temperature dependence of the interaction energies is given by:

$$\frac{g_{ij}-g_{jj}}{RT} = a_{ij} + \frac{b_{ij}}{T} + c_{ij}lnT \quad \textbf{4.21}$$

where a_{ij}, b_{ij} and c_{ij} are tuning parameters. In this work, a_{ij}, a_{ji}, c_{ij}, and c_{ji} were all set to zero, and only b_{ij}, b_{ji}, and α_{ij} were tuned to fit experimental data.

4.3 Modeling Workflow

The overall modeling methodology is summarized in Figure 4.1. First the oil was characterized into pseudo-components (see Section 4.4) and initial values were input for binary interaction parameters. Flash calculations were performed using VMGSim™ Versions 8.0 to 9.5. VMGSim™ combines the Rachford-Rice algorithm to perform flash calculations with a stability test to minimize the Gibbs free energy. The binary interaction parameters were iteratively modified to obtain the best match to experimental data.

In particular, the interaction parameters between the pseudo-components were set to zero to simplify the comparison between different sets of mixing rules. In other words, the only non-zero interaction parameters were between the solvent and each oil component. This assumption had little effect on the model predictions. The effect of the temperature dependence on the saturation pressures considered in this study was negligible at temperatures up to 180°C (see Section 6.2)

and therefore the temperature dependence was also set to zero (k_{ij}^{1}=0 and k_{ij}^{2}=0) for preliminary fitting exercises to simplify the comparison between different types of mixing rule. Temperature dependent binary interaction parameters were only implemented in the most successful model (CDvdW) in order to generate P-X diagrams ranging from 23 – 280°C. The asphaltene/solvent binary interaction parameters were adjusted to match asphaltene onset and yield data. If a good match for asphaltene onset and yield data was found, the maltene/solvent binary interaction parameters were adjusted to match saturation pressure data.

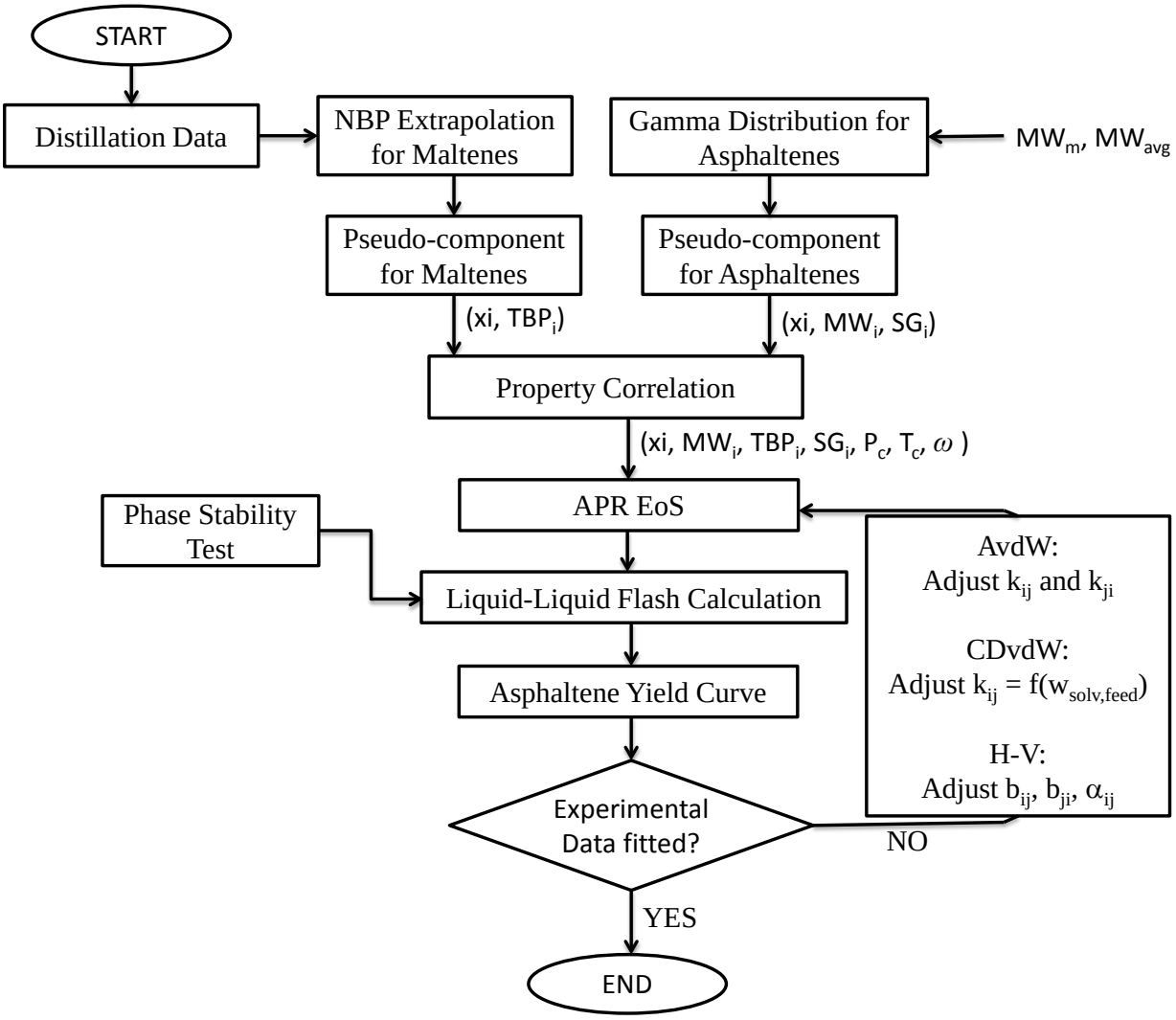

Figure 4.1 Modeling methodology algorithm.

4.4 Oil Characterization

In order to model bitumen/solvent systems using an EoS, the fluid was divided into components and pseudo-components, each with an assigned mole fraction, density, critical properties, and acentric factor. Each solvent was treated as an individual component with known properties. The maltene and C5-asphaltene (*n*-pentane extracted) fractions of the bitumen were characterized separately following the methodology recommended by Castellanos-Díaz *et al.* [2011] and Agrawal *et al.* [2012]. The maltene fraction was divided into pseudo-components based on a distillation assay. The asphaltene characterization was based on a gamma distribution of molecular weights. This characterization has been shown to match vapor-liquid and liquid-liquid equilibrium data for bitumens diluted with a variety of solvents at temperatures from 20 to 180°C and pressures up to 10 MPa [Agrawal *et al.* 2012]. The characterization of the maltenes and C5-asphaltenes are discussed in detail below.

4.4.1 Maltene Characterization

The bitumen examined in this work is WC-B-B2, from the Peace River region in Alberta. The C5-asphaltene content of this bitumen is 19.4 wt%. The remaining 80.6 wt% of the bitumen is defined as maltenes. The maltene characterization was based on distillation data, in this case, a spinning band distillation assay from Agrawal [2012]. The distillable fraction represents approximately 30% of the bitumen by volume. The remainder of the normal boiling point curve for the maltene fraction of the bitumen was extrapolated from the distillation data using a Gaussian distribution (linearly extrapolating on probability coordinates), Figure 4.2.

The next step was to divide the distillation curve into pseudo-components. Castellanos-Díaz *et al.* [2011] found that number of pseudo-components did not have a significant impact on the prediction of saturation pressures as long as there were are least two pseudo-components in the light oil section and two in the heavy oil section. In this work, ten maltene pseudo-components were used to ensure that the entire range of maltene properties is accurately represented when modeling liquid-liquid phase behavior: three in the light oil section (200°C – 375°C), five in the medium oil section (375°C- 515°C), and two in the heavy oil section (515°C – 585°C). The molecular weight and liquid density of each pseudo-component were constrained so that the mixture matched the average maltene molecular weight and liquid density of 450 g/mol and 1005

kg/m³, respectively. The Lee-Kesler correlations (summarized in Appendix C) were used to estimate the critical properties and acentric factor from the average boiling point of each pseudo-component. The pseudo-component properties are listed in Table 4.1 and shown in Figure 4.3.

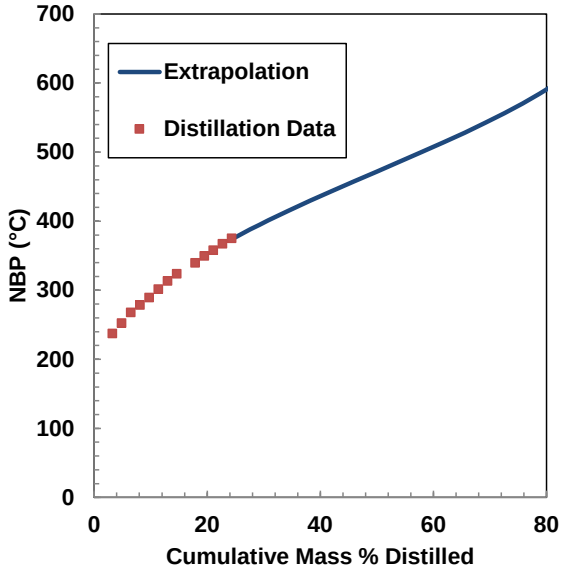

Figure 4.2 Extrapolated NBP data for the maltene fraction of the WC-B-B2 bitumen.

Table 4.1 Bitumen pseudo-components and their properties.

Name	Mass Fraction	Mole Fraction	MW	NBP (°C)	Density (kg/m^3)	P_c (kPa)	T_c (°C)
Malt1	0.059	0.127	246	236	901	2655	445
Malt2	0.082	0.140	308	295	934	2269	503
Malt3	0.098	0.136	382	355	967	1948	561
Malt4	0.085	0.102	439	397	988	1750	600
Malt5	0.075	0.083	479	425	1001	1633	625
Malt6	0.081	0.082	520	452	1015	1523	650
Malt7	0.082	0.077	563	480	1028	1421	675
Malt8	0.084	0.074	607	508	1040	1326	700
Malt9	0.085	0.068	658	540	1054	1227	727
Malt10	0.075	0.056	709	571	1067	1136	754
Asph1	0.025	0.011	1190	667	1070	758	817
Asph2	0.025	0.009	1491	706	1075	655	845
Asph3	0.031	0.010	1758	730	1080	603	863
Asph4	0.053	0.014	2084	751	1085	564	879
Asph5	0.060	0.011	2790	777	1090	515	897

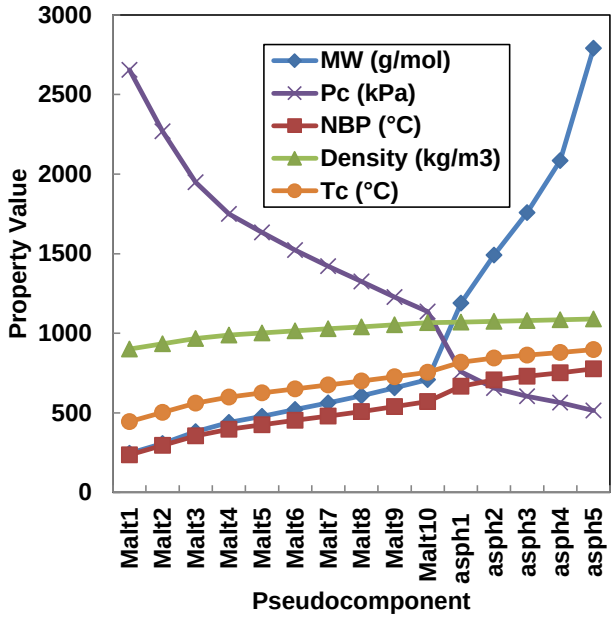

Figure 4.3 Bitumen pseudo-component properties.

4.4.2 Asphaltene Characterization

The C5-asphaltenes were characterized one of two ways; as a single lumped pseudo-component or based on a gamma distribution of molecular weights as recommended by Agrawal *et al.* [2012]. The gamma distribution characterization described below was used in the AvdW and HV models for consistency with previous studies. A single pseudo-component was used to represent the asphaltene fraction in the SWV and CDvdW models to simplify the tuning process for these two models. For all the asymmetric models investigated, similar model results can be generated with either one or five asphaltene pseudo-components although the k_{ij} values do need to be slightly adjusted for the different characterizations (see Section 6.1).

4.4.2.1 Gamma Distribution Characterization

To generate the molecular weight distribution, the gamma distribution parameters, MW_{avg} and β, were set to 2000 g/mol and 2.5, respectively, as recommended by Agrawal *et al.* [2012]. Once the MW distribution was generated, the asphaltenes were divided into five pseudo-components of approximately equal weight fraction.

The TBP of the asphaltene pseudo-components was calculated using the Søreide correlation [Søreide 1989], while critical properties and acentric factor were calculated using the Twu correlations [1984]. Both correlations are summarized in Appendix C. The characterizations reported by Agrawal *et al.* [2012] and Castellanos-Díaz *et al.*[2011] showed an increase in critical pressure with an increase in molecular weight for some pseudo-components, contrary to the overall trend in the maltene properties. To correct this problem, the critical properties and acentric factor were recalculated using the *aggregate* molecular weight and *monomer* density as inputs. The use of these values for molecular weight and density results in a continuously decreasing trend in critical pressure for the whole bitumen, Figure 4.3. Since the monomers in an asphaltene nano-aggregate are held together by van der Waals forces (which are very weak compared to the covalent bonds in the monomers), it is assumed that the properties of a pseudo-component representing a nano-aggregate will be closer to the monomer density than a density calculated based on the aggregate molecular weight.

4.4.2.2 Single Component Characterization

The single lumped pseudo component was characterized by defining molecular weight and density as 1800 g/mol and 1120 kg/m^3 respectively. TBP was calculated using the Søreide correlation [Søreide 1989], and critical properties and acentric factor calculated from Twu correlations. Table 4.2 compares the single component characterization with the range of properties in the Gamma distribution based characterization.

Table 4.2 Asphaltene pseudo-components and their properties for the Gamma distribution based and single component characterizations.

Property	Gamma Distribution Characterization	Single Component Characterization
MW	1190 - 2790	1800
NBP (°C)	667 - 777	721
Density (kg/m^3)	1070 - 1090	1120
T_c (°C)	817 - 897	906
P_c (kPa)	758 - 515	1057

Chapter Five - EXPERIMENTAL RESULTS AND DISCUSSION

This chapter summarizes the experimental data collected for this thesis. First, saturation pressure (VLE) data are presented. Asphaltene onset data collected using two different methods (extrapolation from yield data and observed through titration using the high pressure microscope apparatus) are also presented and discussed. Finally, the phase compositions of the asphaltene-rich heavy phase are reported. Uncertainties in all the experimental data are examined.

5.1 Vapor-Liquid Boundary: Saturation Pressures

The saturation pressures for *n*-pentane diluted bitumen measured in the PVT cell and the blind cell apparatuses are provided in Tables 5.1 and 5.2, respectively. Since the data encompass a broad temperature range, the uncertainty and repeatability in the measurement were first examined. The uncertainty in the *n*-pentane content is 0.1 wt% for the blind cell data (based on the error of the mass measurement) and 0.2 wt% for the PVT cell data (based on the propagated error of the volume and density measurements).

The main source of error in the saturation pressures is the variation in the differential pressure required to move the piston between the hydraulic oil and the sample. The piston can stick and jump and the magnitude of this error is difficult to quantify because it depends on the movement history of the piston and the temperature. Therefore, the repeatability of the measurements was determined rather than attempting to calculate a propagation of error. To determine the repeatability of the saturation pressures, the individual data points were compared with a Henry law model fitted to all of the data. The saturation pressure of a mixture of *n*-pentane and bitumen was modeled as follows:

$$\boldsymbol{P_{sat} = x_{C5} H_{C5} + x_{bit} \gamma_{bit} P_{v,bit}} \qquad \textbf{5.1}$$

with

$$\boldsymbol{H_{C5} = exp\left\{C_{C5} + \frac{D_{C5}}{T}\right\}} \qquad \textbf{5.2}$$

$$\boldsymbol{P_{v,bit} = exp\left\{C_{bit} + \frac{D_{bit}}{T}\right\}} \qquad \textbf{5.3}$$

where P_{sat} is the saturation pressure, x is the mole fraction, H is Henry's constant, P_v is the vapor pressure, γ is an activity coefficient, and subscripts *C5* and *bit* indicate *n*-pentane and bitumen,

respectively. Note, this model is only intended to provide a best-fit line with which to assess the repeatability of the data.

The mole fractions were calculated from the known mass fractions taking the bitumen molecular weight to be 520 g/mol. The activity coefficient was assumed to be unity. The vapor pressure constants for the bitumen were determined from a measured vapor pressure of 380 kPa at 180°C and an assumed vapor pressure of 90 kPa at 60°C (the barometric pressure at the temperature of the dewatering procedure). Note the contribution of the bitumen vapor pressure is not significant at most conditions. The Henry law constants were then determined by fitting the saturation pressure dataset to minimize the average relative deviation. The fitted constants are provided in Table 5.3 and the fit to the data is shown in Figure 5.1.

The uncertainty in the saturation pressures was determined from the deviations from the model to be 0.1, 0.4. 0.6, and ±0.8 MPa at temperatures of 90, 180, 230, and 280°C. The deviations appeared to be the same for both the PVT and blind cell methods. The saturation pressures measured for *n*-pentane with WC-B-B2 and WC-B-B3 bitumen were the same within experimental error.

Table 5.1 Saturation pressures of *n*-pentane diluted WC-B-B2 bitumen measured in the PVT cell. The uncertainty of the *n*-pentane content is 0.2 wt%. The uncertainties in the saturation pressures are 0.1, 0.4. 0.6, and ±0.8 MPa at temperatures of 90, 180, 230, and 280°C. Data from Agrawal *et al.* [2012].

Temperature (°C)	*n*-Pentane Content wt%	Saturation Pressure MPa
90	11.3	0.4
120	11.3	0.6
150	11.3	0.7
180	11.3	1.0
90	33.9	0.5
120	33.9	0.9
120	30.2	0.8
150	30.2	1.3
180	30.2	1.8

Table 5.2 Saturation pressures of *n*-pentane diluted bitumen measured in the blind cells. The uncertainty of the n-pentane content is ±0.1 wt%. The uncertainties in the saturation pressures are 0.1, 0.4. 0.6, and ±0.8 MPa at temperatures of 90, 180, 230, and 280°C.

Sample	Temperature (°C)	*n*-Pentane Content wt%	Saturation Pressure MPa
WC-B-B3	90	11.3	0.4
WC-B-B3	90	30.2	0.5
WC-B-B3	90	62.5	0.7
WC-B-B2	180	0.0	0.4
WC-B-B3	180	0.0	0.5
WC-B-B3	180	10.8	1.7
WC-B-B3	180	12.3	1.8
WC-B-B3	180	19.9	2.2
WC-B-B3	180	29.4	2.4
WC-B-B3	180	29.8	2.2
WC-B-B2	180	34.0	2.1
WC-B-B3	180	39.8	2.5
WC-B-B3	180	43.9	2.3
WC-B-B3	180	43.9	2.4
WC-B-B3	180	63.9	2.6
WC-B-B3	180	64.0	2.5
WC-B-B3	230	10.8	2.4
WC-B-B3	230	11.3	1.6
WC-B-B3	230	19.9	3.2
WC-B-B3	230	29.4	3.7
WC-B-B3	230	30.2	4.0
WC-B-B3	230	39.8	4.4
WC-B-B3	230	47.6	4.7
WC-B-B3	230	62.5	5.0
WC-B-B3	230	63.9	5.3
WC-B-B3	280	10.8	3.2
WC-B-B3	280	29.4	5.3
WC-B-B3	280	39.8	6.4
WC-B-B3	280	63.9	9.3

Table 5.3 Fitted constants for WC-B-B3 vapor pressure (Eq. 5.3) and Henry term (Eq. 5.2) for n-pentane in WC-B-B3 bitumen (based on T in K and pressures in kPa).

Constant	Value
C_{bit}	10.69
D_{bit}	-2061
C_{C5}	13.62
D_{C5}	-2599

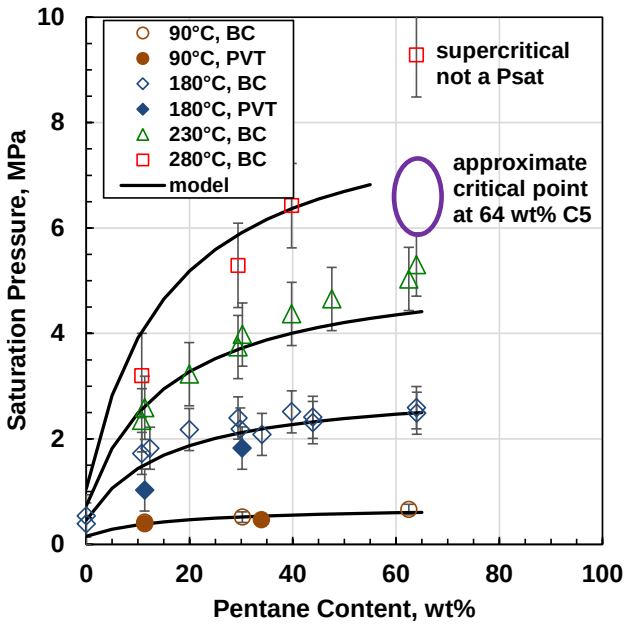

Figure 5.1 Saturation pressures for mixtures of *n*-pentane and bitumen at temperatures of 90, 180, 230, and 280°C. Legend notation: BC is the blind cell method, and PVT is the PVT cell method. The PVT data are from Agrawal *et al.* (2012).

Figure 5.1 shows an apparent critical point for the mixture 64 wt% *n*-pentane and 36 wt% bitumen in the vicinity of 280°C and 7 MPa. The evidence for near critical behavior is more apparent when examining the P-V isotherms, Figure 5.2. The P-V isotherms at 64 wt% *n*-pentane but lower temperatures have a distinct change in slope at the saturation pressure and nearly constant pressure in the two-phase region. Similarly, the P-V isotherms at 280°C but lower *n*-pentane contents exhibit a distinct change in slope. In contrast, the isotherm at 280°C has a significant slope at all the expanded volumes and no distinct change in slope. This shape in the P-V isotherm is characteristic of near critical behavior. A possible saturation pressure could be inferred at approximately 9 MPa but this pressure deviates greatly from the Henry Law model. Hence, we conclude there is a critical point near this condition. The proximity to the critical point may also explain the relatively high deviations from Henry's Law at 230°C and *n*-pentane contents above 40 wt%.

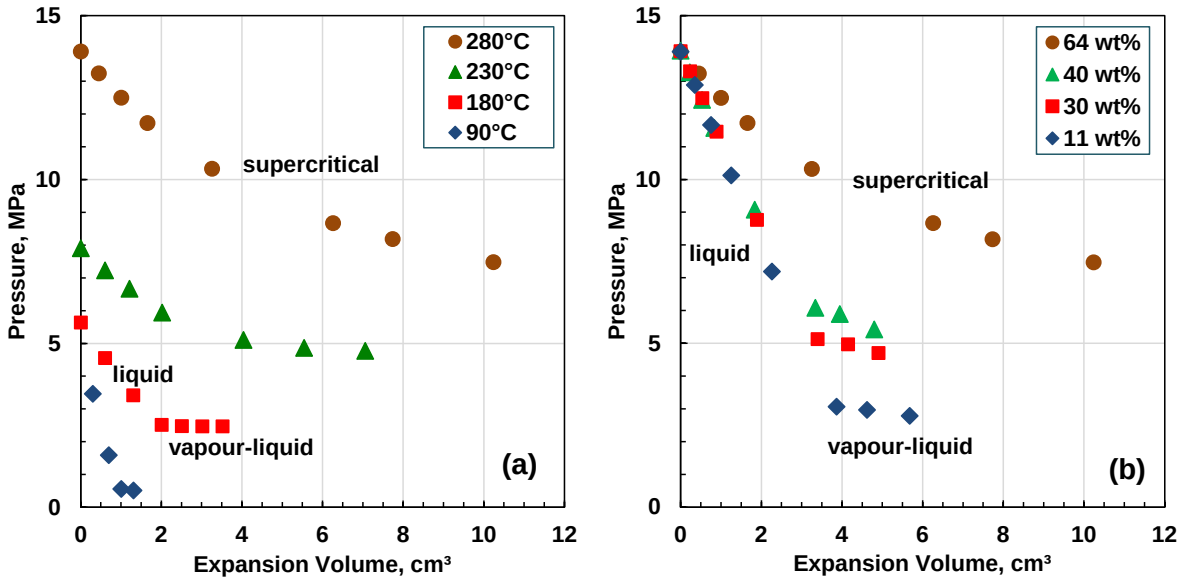

Figure 5.2 Pressure-volume isotherms for mixtures of *n*-pentane and WC-B-B2 bitumen: a) 64 wt% n-pentane at temperatures of 90, 180, 230, and 280°C; b) *n*-pentane contents of 11, 30, 40, and 64 wt% at 280°C.

5.2 Asphaltene Onsets and Yields

Figure 5.3 shows a typical dataset for asphaltene onset and yields measured with the HPM, PVT cell, and blind cell methods. The measured and extrapolated onsets of asphaltene phase formation are provided in Table 5.5. The extrapolated onsets are in exact agreement with the measured value in all but one case and within the experimental error of 1.5 wt% in the other case. This good agreement validates the extrapolation method for determining yields. Recall that the samples in the blind cell methodology were mixed at ambient temperature and then brought to experimental temperature, whereas the samples in the PVT cell were mixed at the experimental conditions. It is known that at ambient conditions, there is a hysteresis in the asphaltene yields when solvent is added versus removed [Beck *et al.*, 2005] and there may be hysteresis with temperature changes as well. However, the good agreement between the PVT and blind cell methods at both 90°C and 180°C, Table 5.4 and Figure 5.3a, indicates that the yields are independent of the temperature path. To assess error and determine an extrapolated onset condition, the asphaltene yield data were curve fit with the following empirical expression:

$$\boldsymbol{Y = C[1 - exp\{-D(w_{C5} - w_{onset})\}]} \qquad \textbf{5.4}$$

where Y is the asphaltene yield in wt%, w_{C5} is the *n*-pentane content, w_{onset} is the *n*-pentane content at the onset of the asphaltene-rich phase, and a and b are constants. The constants and the onset composition were adjusted to minimize the least square error. The onset condition determined with this method is termed the extrapolated onset condition. The repeatability of the yields was determined from the deviations between the curve fit and the data using all of the data collected in this study and was found to be ±1.5 wt% for the PVT cell and blind cell methods and ±0.75 wt% for the bench top method. Obvious outliers, such as the example shown in Figure 5.3, were screened out of the data. The screened asphaltene yield data for *n*-pentane diluted bitumen at temperatures up to 250°C and pressures up to 13.8 MPa are given in Table 5.4.

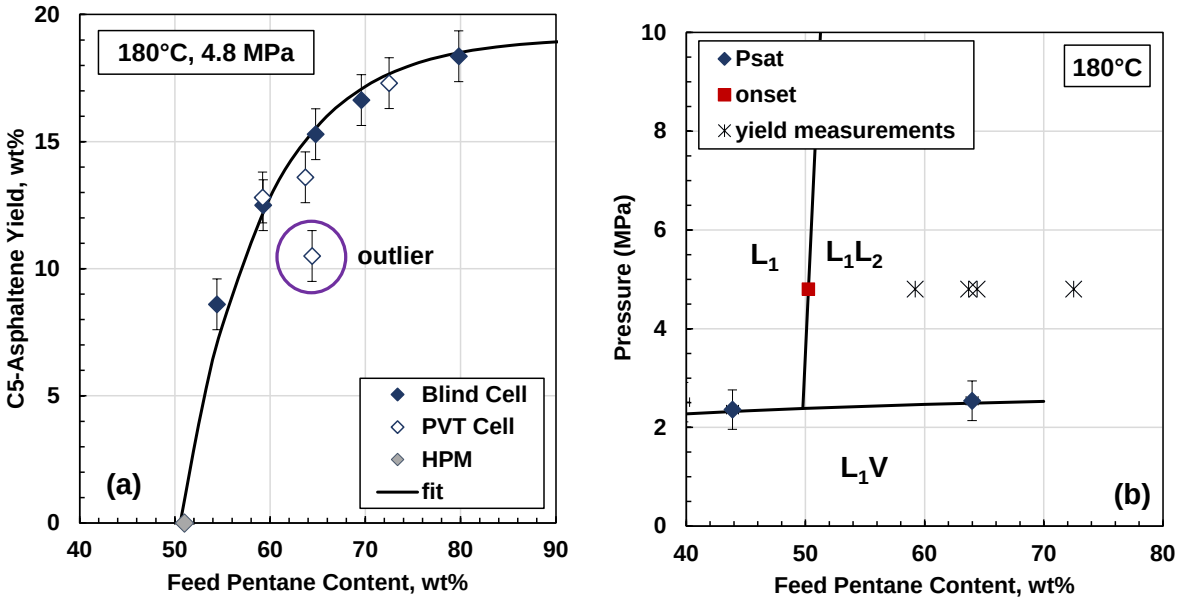

Figure 5.3 C5-asphaltene phase separation from n-pentane diluted WC-B-B3 bitumen at 180°C and 4.8 MPa: a) onset and yield; b) location on phase diagram at which the asphaltene-rich phase compositions were determined for the four PVT cell experiments.

Table 5.4 C5-asphaltene yield data from *n*-pentane diluted WC-B-B3 bitumen. The uncertainty in the yields are ±1.0 for the bench top method, +1 / -1.5 wt% for the pycnometer sample collection method, and 0.4 wt% for the blind cell sample collection method.

Method	Sample Collection Method	Temperature °C	Pressure MPa	*n*-Pentane Content wt%	Asphaltene Yield wt%
Benchtop	-	20	0.1	51.9	6.3
Benchtop	-	20	0.1	54.0	8.6
Benchtop	-	20	0.1	56.4	11.3
Benchtop	-	20	0.1	58.0	12.3
Benchtop	-	20	0.1	59.8	12.6
Benchtop	-	20	0.1	66.0	15.2
Benchtop	-	20	0.1	71.9	16.8
Benchtop	-	20	0.1	75.8	17.3
Benchtop	-	20	0.1	80.6	17.7
Benchtop	-	20	0.1	85.4	18.3
Benchtop	-	20	0.1	89.9	18.8
Benchtop	-	20	0.1	94.9	19.0
Benchtop	-	20	0.1	96.3	19.2
Blind Cell	Pycnometer	90	4.8	59.6	13.0
Blind Cell	Pycnometer	90	4.8	66.3	14.8
Blind Cell	Pycnometer	90	4.8	72.6	16.6
Blind Cell	Blind Cell	90	4.8	78.8	17.8
Blind Cell	Blind Cell	90	4.8	84.9	18.4
PVT	Pycnometer	90	4.8	64.8	11.5
PVT	Pycnometer	90	4.8	69.5	17.2
PVT	Blind Cell	90	4.8	74.6	17.1
PVT	Blind Cell	90	4.8	80.2	19.0
Blind Cell	Pycnometer	140	4.8	62.3	11.7
Blind Cell	Pycnometer	140	4.8	69.6	14.6
Blind Cell	Blind Cell	140	4.8	77.5	16.6
Blind Cell	Blind Cell	140	4.8	85.0	18.2
Blind Cell	Pycnometer	180	4.8	54.4	8.6
Blind Cell	Pycnometer	180	4.8	59.3	12.5
Blind Cell	Pycnometer	180	4.8	64.8	15.3
Blind Cell	Pycnometer	180	4.8	69.6	16.6
Blind Cell	Pycnometer	180	4.8	79.8	18.4

Method	Sample Collection Method	Temperature °C	Pressure MPa	*n*-Pentane Content wt%	Asphaltene Yield wt%
Blind Cell	Pycnometer	180	13.8	59.4	9.3
Blind Cell	Pycnometer	180	13.8	71.1	15.5
Blind Cell	Pycnometer	180	13.8	80.2	17.6
Blind Cell	Blind Cell	250	10.3	54.7	11.2
Blind Cell	Blind Cell	250	10.3	59.8	15.0
Blind Cell	Pycnometer	250	10.3	66.1	18.0
Blind Cell	Pycnometer	250	10.3	69.8	17.3

Table 5.5 Asphaltene onset points for *n*-pentane diluted WC-B-B2 bitumen (measured using HPM) and for *n*-pentane diluted WC-B-B3 bitumen (determined by extrapolating yield curves). The uncertainty of the onsets is ±1.5 wt%.

Pressure MPa	Temperature °C	WC-B-B2 Onset (Measured) wt% pentane	WC-B-B3 Onset (Extrapolated) wt% pentane
0.1	23	47	47
4.8	90	51	51
4.8	140	49	49
4.8	180	51	49.5
13.8	180	-	52
10.3	250	-	47

Figure 5.4 shows the yield data collected in this study and demonstrates that temperature and pressure have relatively little effect on C5-asphaltene yields compared with the effect of solvent content. Note, how all of the data converge at high solvent contents. This convergence is misleading because only the C5-asphaltenes are considered. The yield of all bitumen components partitioning into the heavy phase may well vary with temperature and pressure at high dilutions.

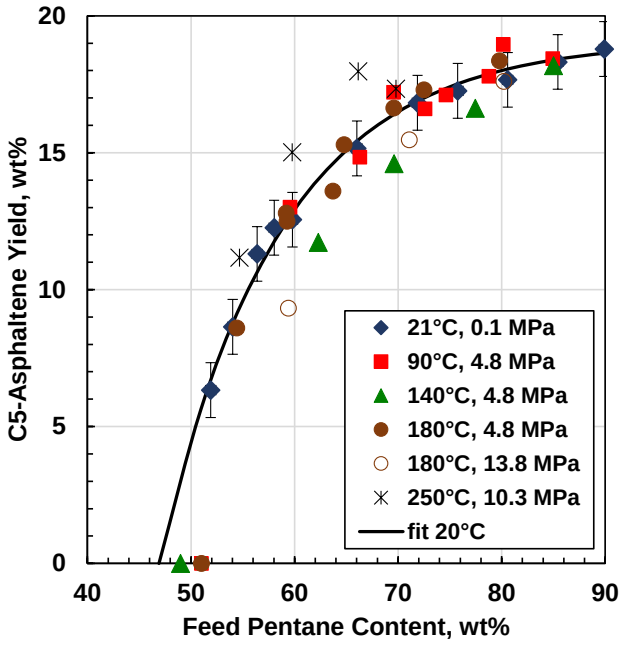

Figure 5.4 C5-asphaltene yield data from *n*-pentane diluted WC-B-B3 bitumen.

Figure 5.5 shows that asphaltene solubility increases (higher onset and lower yield) with pressure. This trend is consistent with the literature data for heavy oil diluted with *n*-alkanes (Akbarzadeh *et al.*, 2005) and with the observed precipitation of asphaltenes from depressurized live oils [Joshi *et al.*, 2001]. Figure 5.6 shows that the effect of temperature on asphaltene solubility. While there is some scatter in the data and not all of the data are at the same pressure, there appears to be a maximum in the C5-asphaltene solubility at approximately 140°C. The amount of solvent to initiate precipitation, Figure 5.6a, reaches a maximum between 100 and 200°C, and the yield at a fixed n-heptane content, Figure 5.6b, reaches a minimum at 140°C. Interestingly, the maximum occurs at approximately the same temperature as the asphaltenes in solution were observed to obtain a liquid state. It seems likely the two phenomena are connected but the nature of the connection is not yet known.

The literature data were examined for evidence of a maximum in asphaltene solubility. Most of the data were for *n*-heptane diluted bitumen, Figure 5.7. Almost all of the literature data show increasing solubility up to 100°C but, unfortunately, there are insufficient data at high temperatures

to verify a maximum in the solubility. The asphaltene yields from the Boscan and Kuwait oils are the only data above 100°C and appear to reach an asymptote at approximately 100°C.

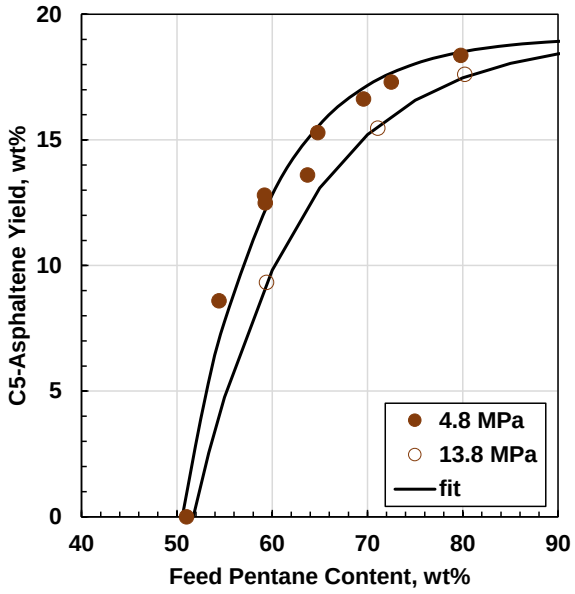

Figure 5.5 Effect of pressure on C5-asphaltene yields from *n*-pentane diluted WC-B-B3 bitumen.

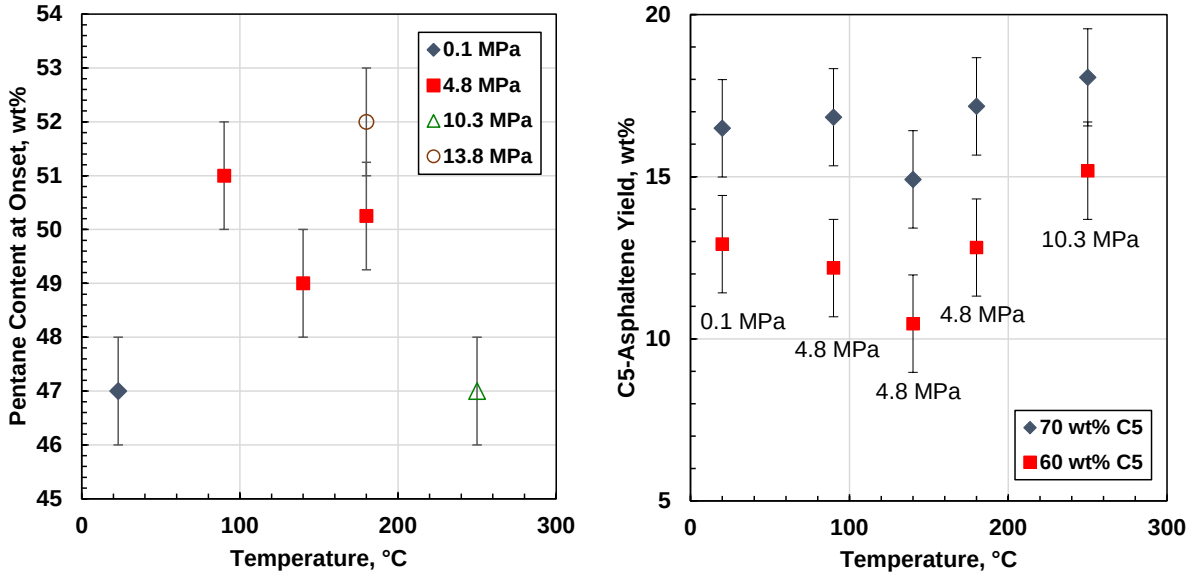

Figure 5.6 Effect of temperature on C5-asphaltene onsets and yields from *n*-pentane diluted WC-B-B3 bitumen: a) onset; b) yield.

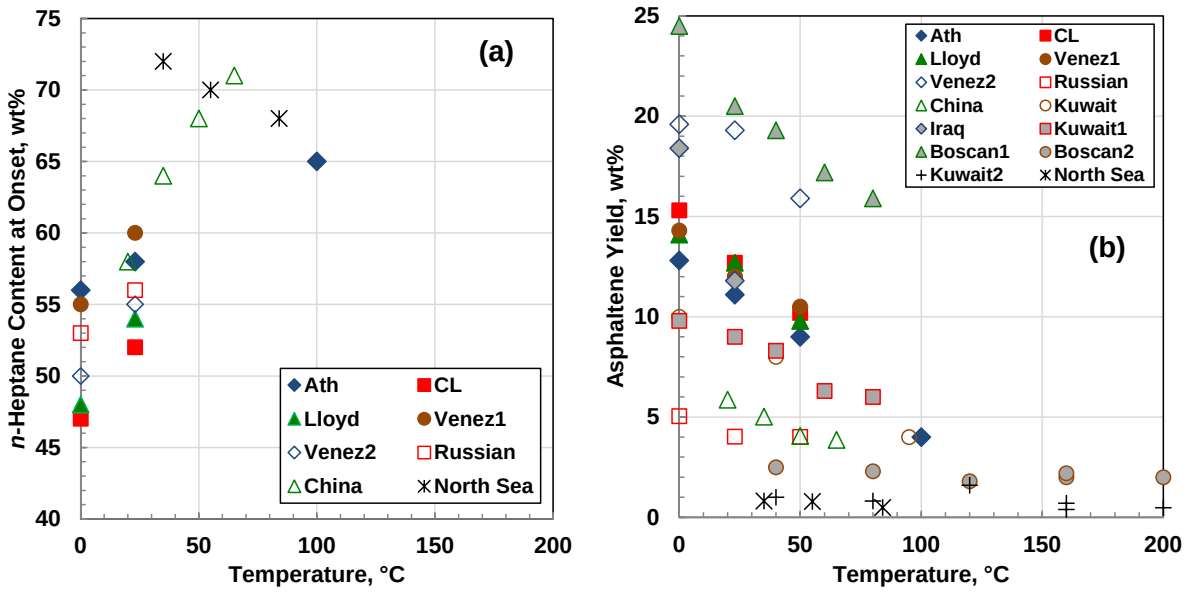

Figure 5.7 Effect of temperature on: a) the onset of asphaltene phase separation, and; b) asphaltene yields from *n*-heptane diluted crudes in the literature [Akbarzadeh *et al.*, 2005; Hu and Guo, 2001; Andersen and Birdi, 1990; Andersen *et al.*, 1994; Andersen *et al.* 1998; Ali and Al-Ghannam, 1981]. The legends indicates the source oils.

5.3 Nature of the Asphaltene-Rich Phase

Asphaltene-rich phases form at *n*-pentane contents above approximately 50 wt%. At temperatures below approximately 90°C, the asphaltene-rich phase appears as glassy particles, Figure 5.8a. Above 140°C, the phase appears as liquid droplets that coalescence into a continuous liquid phase, Figure 5.8b. This liquid phase is denser than the surrounding medium and flows like an extremely viscous fluid (stratified wavy flow was observed with slowly deforming wave crests). In between 90 and 140°C, the glassy-particles tend to stick on the HPM window and slowly and partially coalescence into irregular but smoother shapes, Figure 5.9. This behavior is interpreted as a gradual glass transition between 90 and 140°C. Similar glass transitions have been observed in asphalts and verified with differential scanning calorimetry (Kriz *et al.*, 2008).

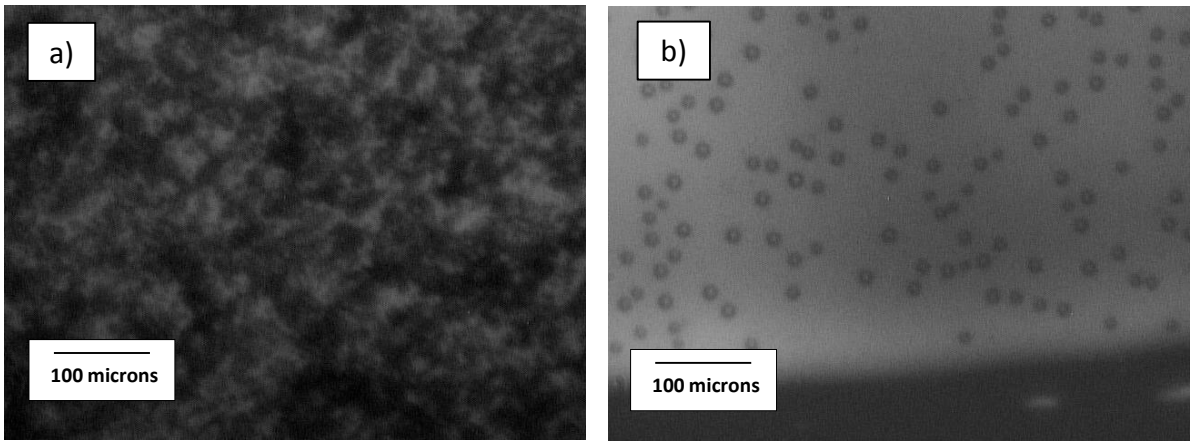

Figure 5.8 Images captured by the HPM of asphaltenes precipitated from *n*-pentane diluted bitumen at a) 23°C (glass-like particles) and b) 165°C (liquid droplets).

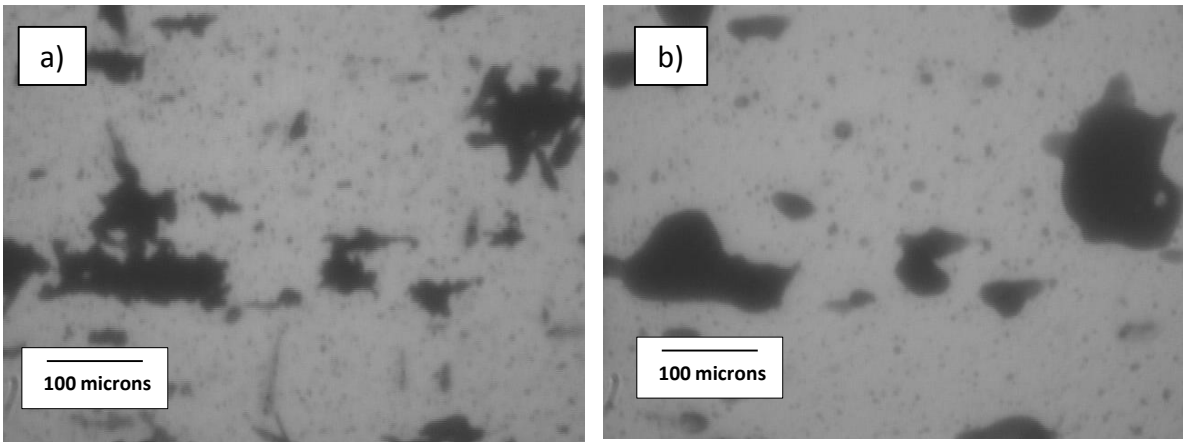

Figure 5.9 Images captured by the HPM of aphaltenes precipitated from *n*-pentane diluted bitumen at 90°C and 4.8 MPa at a) less than one hour after mixing and b) 20 hours after mixing.

5.4 Asphaltene-Rich Phase Compositions

The heavy phase composition method is limited to conditions where the asphaltene-rich heavy phase is a liquid (temperatures above 140°C and sufficient pressure) and by the PVT cell design limit of 200°C. Therefore, a series of four compositions were measured at 180°C and 4.8 MPa, as was shown in Figure 5.3b. The *n*-pentane content and C5-asphaltene yield at each condition are provided in Table 5.6. The feed, light phase, and heavy phase compositions for these mixtures are listed in Tables 5.7 to 5.10. One repeat was conducted at a composition of 64 wt% *n*-pentane. The results of the two trials (2A and 2B) are shown in in Tables 5.6, 5.8 and 5.9. The repeatability of the C5-asphaltene yield, light phase, and heavy phase compositions were ±1.6, ±2.4, and ±3.5

wt%, respectively. These values are slightly higher than the estimated experimental uncertainties of ±1.1, ±1.1 and ±2.9 wt%, respectively. Note, the component material balance errors are less than 16% in all but one case.

Table 5.6 C5-asphaltene yield from n-pentane diluted WC-B-B2 bitumen at 180°C and 4.8 MPa.

Run	*n*-Pentane Content wt%	C5-Asphaltene Yield wt%	Heavy Phase Split Ratio, H/F
1	59.2	12.8	0.118
2A	64.4	10.5	0.066
2B	63.7	13.6	0.091
3	72.5	17.3	0.085

Table 5.7 Composition of feed, light phase and heavy phase samples from mixtures of 41 wt% WC-B-B2 bitumen and 59 wt% *n*-pentane at 180°C and 4.8 MPa (Trial 1).

Sample	Feed wt%	Light Phase wt%	Heavy Phase wt%	MB Error %
n-Pentane	59.2	67.1	31.4	6.2
Maltenes	32.9	29.8	20.4	12.8
C5-Asphaltenes	8.0	3.1	48.2	5.3

Table 5.8 Composition of feed, light phase and heavy phase samples from mixtures of 36 wt% WC-B-B2 bitumen and 64 wt% *n*-pentane at 180°C and 4.8 MPa (Trial 2A).

Sample	Feed wt%	Light Phase wt%	Heavy Phase wt%	MB Error %
n-Pentane	64.4	68.0	26.0	1.3
Maltenes	28.7	29.0	22.0	0.6
C5-Asphaltenes	6.9	3.0	52	9.7

Table 5.9 Composition of feed, light phase and heavy phase samples from mixtures of 36 wt% WC-B-B2 bitumen and 64 wt% *n*-pentane at 180°C and 4.8 MPa (Trial 2B).

Sample	Feed wt%	Light Phase wt%	Heavy Phase wt%	MB Error %
n-Pentane	63.7	72.8	19.2	6.6
Maltenes	29.3	24.7	24.0	15.9
C5-Asphaltenes	7.0	2.6	56.8	7.6

Table 5.10 Composition of feed, light phase and heavy phase samples from mixtures of 27 wt% WC-B-B2 bitumen and 73 wt% *n*-pentane at 180°C and 4.8 MPa (Trial 3).

Sample	Feed wt%	Light Phase wt%	Heavy Phase wt%	MB Error %
n-Pentane	72.5	77.9	20.3	0.7
Maltenes	22.2	20.0	23.7	8.5
C5-Asphaltenes	5.4	2.1	56.0	23.7

There are no data with which to compare the solvent content of the heavy phase. However, as was shown in Figure 5.3a, all of the PVT cell method yields except for Trial 2B are within 1.1 wt% of the blind cell yields; that is, within the experimental error of 1.5%. The deviation of the Trial 2B yield is approximately 4.5 wt%, well beyond the expected error, and is taken to be an outlier. Due to the complexity of this experimental procedure, it is challenging to collect consistent, representative phase samples. Based on all of the data collected to date (not all shown here), approximately one out of every 4 or 5 samples collected is a non-representative sample. Therefore, it is recommended to collect multiple data points with this methodology so that outliers can be identified and discarded.

Tables 5.7 to 5.10 show that the *n*-pentane content of the heavy phase formed at 180°C range from 19 to 31 wt%. These *n*-pentane contents are significantly higher than the 4% reported by Yarranton *et al.* [2011] for glass-like asphaltene phases at 20°C. In other words, the solubility of the *n*-pentane in the heavy phase increases with temperature.

Tables 5.7 to 5.10 also show that, as the solvent content in the feed increases, the *n*-pentane content increases for the light liquid phase but decreases for the heavy phase. This type of component partitioning (where the asphaltene and diluent contents do not sum to unity) cannot be accurately represented on a pseudo-binary (diluent-bitumen) phase diagram but can be represented on a pseudo-ternary phase diagram. Figure 5.10 is a ternary phase diagram for *n*-pentane diluted bitumen at 180°C and 4.8 MPa (the bitumen is represented as a blend of asphaltenes and maltene). Point B is undiluted bitumen and Point O is the onset of asphaltene precipitation. Three tie-lines are shown for the three experimental feed compositions (59, 64, and 72 wt% *n*-pentane). While there is some scatter in the data points, a clear phase boundary can be identified. This diagram can

be used to find the compositions needed to predict the asphaltene-rich heavy and solvent-rich light phase properties and to tune phase behavior models for *n*-pentane diluted bitumen.

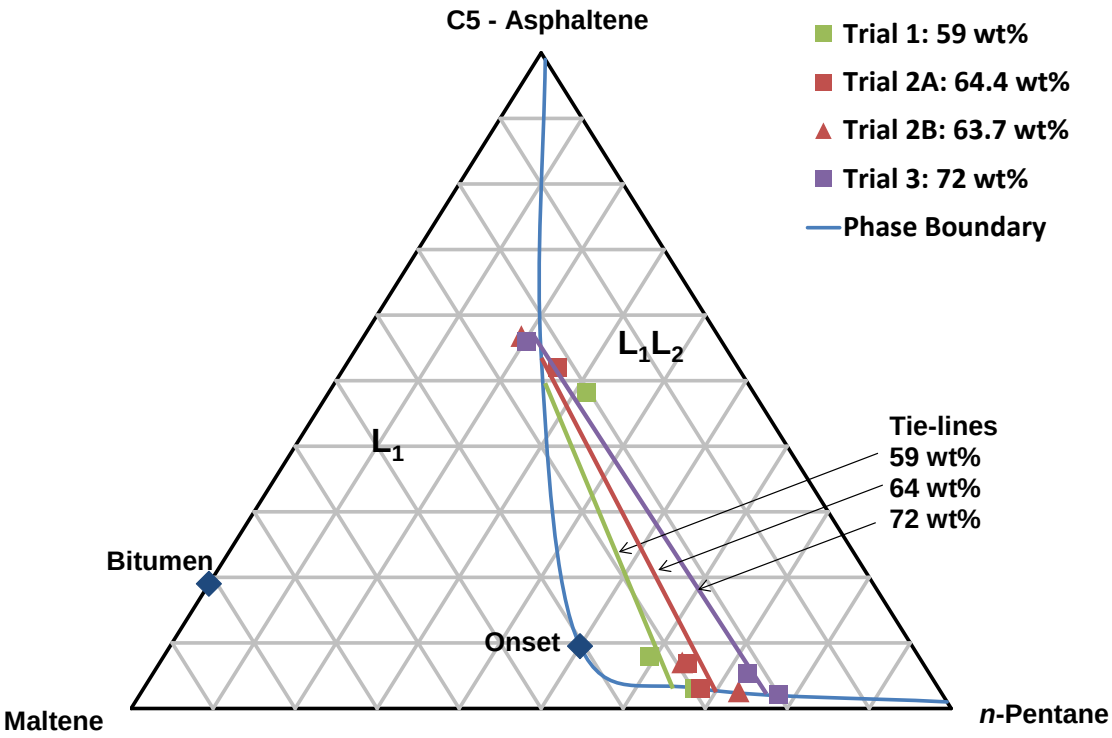

Figure 5.10 Ternary phase diagram for bitumen and *n*-pentane at 180°C and 4.8 MPa.

Chapter Six- MODELING RESULTS AND DISCUSSION

The modeling results and discussion begins with the symmetric (SvdW) and asymmetric van der Waals (AvdW) mixing rules. Next, the mole-based and volume-based Huron-Vidal (HV) excess energy mixing rules are examined. Then, the Sandoval *et al.* (SWV) compositional-dependent van der Waals mixing rules are evaluated and, finally, the compositional-dependence required to fit asphaltene yield with van der Waals mixing rules (CDvdW) data is investigated and an expression for k_{ij} is recommended.

In order to minimize the time required for the model evaluations, the mixing rules for most cases were first tested with a single component asphaltene and single component maltene characterization. The model with this simplified characterization gives similar results to the full characterization as will be shown in Section 6.1. If the model was able to fit asphaltene yield data, it was then evaluated on the ambient condition data with the full characterization summarized in Table 4.1. The interaction parameters were tuned to fit both the asphaltene yield curve and the saturation pressures. In addition, the effect of the temperature dependence on the saturation pressures considered in this study was negligible at temperatures up to 180°C (see Section 6.2) and therefore the temperature dependence was also set to zero (k_{ij}^1=0 and k_{ij}^2=0) for preliminary fitting exercises to simplify the comparison between the different types of mixing rule. Temperature dependent binary interaction parameters were only implemented in the most successful model (CDvdW) in order to generate P-X diagrams ranging from 23 to 280°C.

6.1 Model Sensitivity to Oil Characterization

Before modeling the data, the sensitivity of the model to the oil characterization was examined. The predicted asphaltene yield was found to be quite insensitive to the number of components in the characterization. For example, with the AvdW model, representing the maltene and asphaltene fraction each with one pseudo-component results in a very similar asphaltene yield curve to the curve modeled with the full 16 pseudo-component characterization, Figure 6.1. The binary interaction parameters must be tuned for each characterization to match the data, but similar fitted values are required for both cases, Table 6.1. While the one pseudo-component model is not recommended because the saturation pressure behavior cannot be modeled with only one maltene

pseudo-component, it is a straightforward starting point for tuning the model because the predicted yields and magnitudes of the k_{ij} are similar to the full characterization. Similar results were found with the other mixing rules. In all cases, when the characterization is changed, the model can be re-tuned to give similar results with small adjustments to the k_{ij} values.

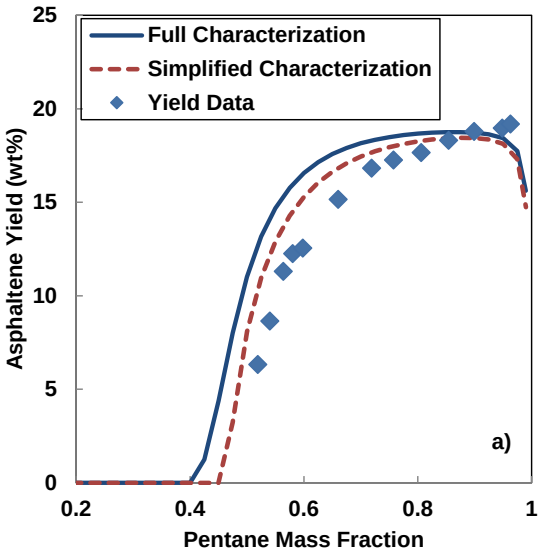

Figure 6.1 Measured and modeled asphaltene yield data for *n*-pentane diluted bitumen. Symbols are data and lines are the AvdW model with a) bitumen characterized as only two components (simplified characterization) and b) bitumen characterized as described in Table 4.1 (full characterization).

Table 6.1 Binary interaction parameters used in AvdW model with simplified and full characterizations.

Component Pair	Binary Interaction Parameter	
	Simplified Characterization	Full Characterization
Maltene-Solvent	0.02	0.030 - 0.046
Asphaltene-solvent	0.04	0.047 – 0.055
Solvent-Maltene	0.08	0.095 – 0.114
Solvent-Asphaltene	0.11	0.116 – 0.125

6.2 Temperature Dependence of Binary Interaction Parameters

Agrawal *et al.* [2012] recommended a temperature dependence for k_{ij} to match saturation pressures at high temperatures. The temperature dependence has relatively little effect on the predicted

saturation pressures up to 180°C but becomes significant at higher temperatures, Figure 6.2. For this reason and because the focus of this study was on modeling asphaltene yields, the temperature dependence for binary interaction parameters was neglected in all cases except the recommended CDvdW model.

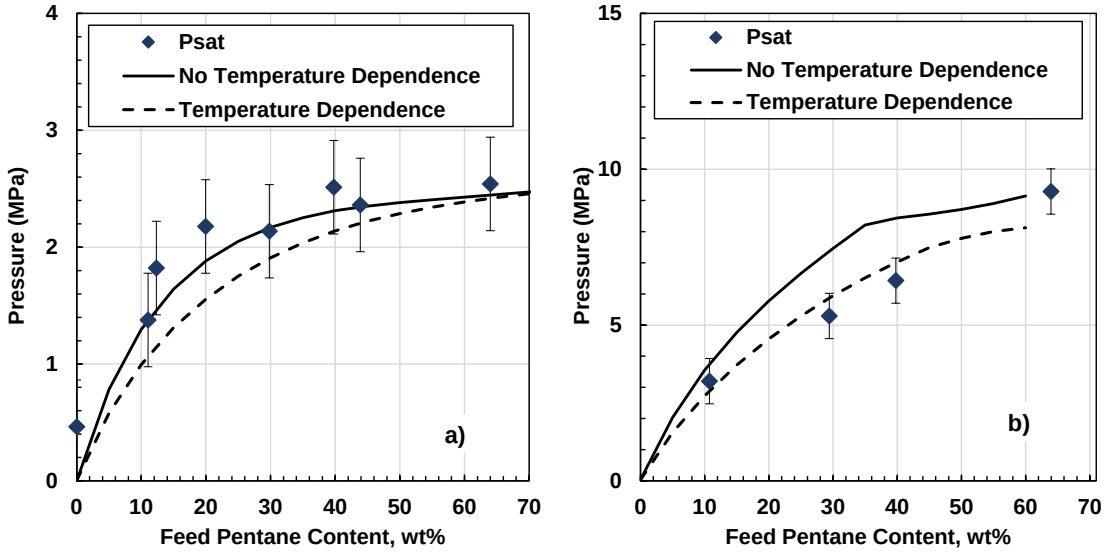

Figure 6.2 Measured and modeled saturation pressure data for *n*-pentane diluted bitumen at a) 180°C and b) 280°C. Symbols are data, and lines are the SvdW model with and without temperature dependence.

6.3 Van Der Waals Mixing Rules

6.3.1 Symmetric Van Der Waals Mixing Rules

Agrawal *et al.* [2012] demonstrated that the APR with symmetric van der Waals mixing rules ($k_{ij} = k_{ji}$) can be used to match asphaltene onset point for solvent diluted bitumen but severely under-predicts asphaltene yield at high dilution. Figure 6.3a confirms that the use of symmetric mixing rules (SvdW) under-predicts the asphaltene yields. Figure 6.3b shows that these mixing rules match the saturation pressures to within the accuracy of the measurement. Figure 6.3c demonstrates that the SvdW model over-predicts the pressure dependence of the onset point.

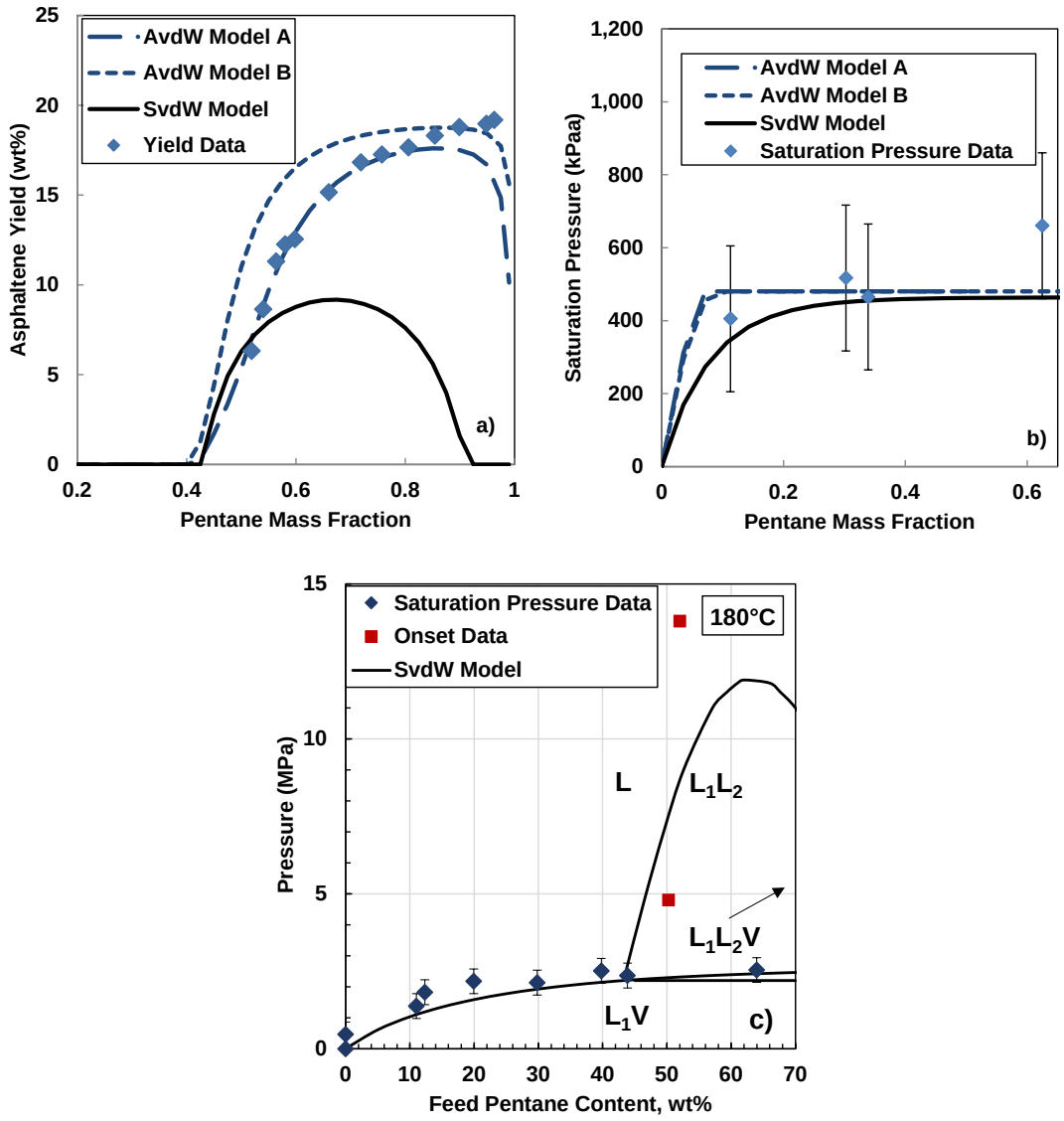

Figure 6.3 Measured and modeled (symmetric model and asymmetric Models A and B) phase behavior data for *n*-pentane diluted bitumen: a) asphaltene yield at 21°C and 0.1 MPa; b) saturation pressures of *n*-pentane diluted bitumen at 90°C; c) Pressure-Composition Phase Diagram at 180°C. SvdW and AvdW indicate symmetric and asymmetric van der Waals mixing rules, respectively.

6.3.1 Asymmetric Van Der Waals Mixing Rules

The use of asymmetric van der Waals mixing rules can improve the asphaltene yield match. Figure 6.3 shows the modeled yields and saturation pressures from the preliminary evaluation where the k_{ij} values for pseudo-component/pseudo-component binaries were set to zero and no temperature dependence was introduced into the other interaction parameters ($k_{ij} = k_{ij}^{o}$). Figure 6.3a shows the modeled yields at 21°C for two different sets of tuning parameters that illustrate the benefits and

limitations of the AvdW model (Models A and B). Both AvdW Model A and AvdW Model B have asymmetric interaction parameters for maltene-solvent and asphaltene-solvent binary pairs, Figure 6.4a. AvdW Model A has a step-change in k_{ij} values at the transition from maltene to asphaltene pseudo-components, whereas the k_{ij} values in AvdW Model B have a continuous trend from maltene to asphaltene pseudo components. AvdW Model A matches the shape of the asphaltene curve but does not predict the asphaltene components precipitating in the correct order; it predicts lighter pseudo-components precipitating before heavier pseudo-components. AvdW Model B predicts that the heaviest pseudo-components precipitate first and fits the ultimate yield, but over-predicts yields at intermediate dilutions.

Figure 6.3b shows the predicted saturation pressures for *n*-pentane diluted bitumen at 90°C. While the AvdW model predicts saturation pressures within the error bars of the reported data, the shape of the curve is not representative of the observed pressure trends; the AvdW model over-predicts the saturation pressures at low dilutions. Only the saturation pressure curve at 90°C is shown here, but the model was found to over-predict saturation pressures at low dilutions at temperatures up to 180°C, Appendix B. This shortcoming was observed in every case where asymmetry was introduced into the maltene-solvent interaction parameters.

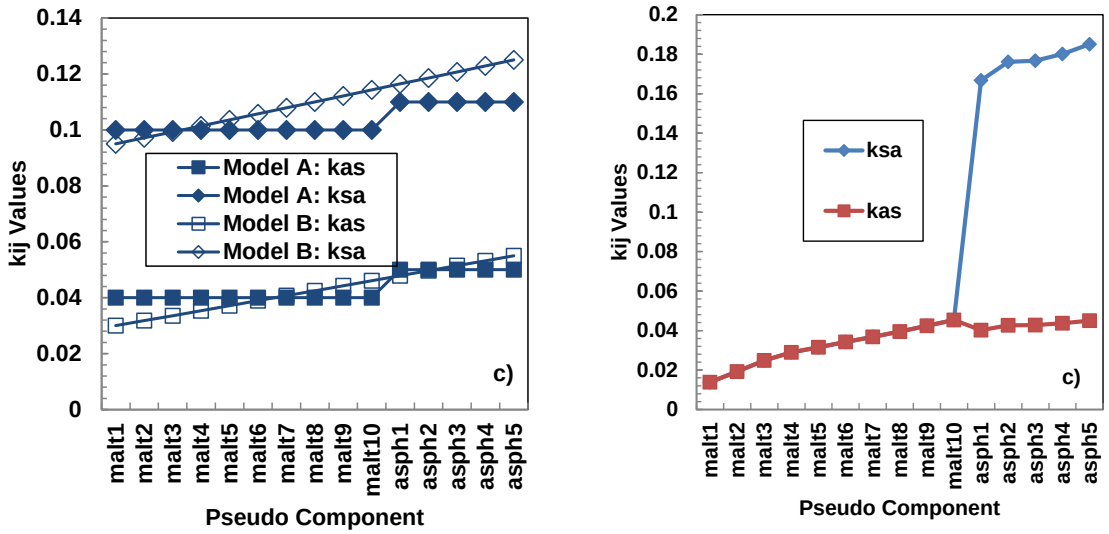

Figure 6.4 Binary interaction parameters at 21°C for solvent/pseudo-component binaries for *n*-pentane diluted bitumen: a) AvdW Models A and B; b) AvdW Model C.

The AvdW model with a third set of tuning parameters, AvdW Model C, is shown in Figure 6.5. In this model the interaction parameters between maltene-solvent binary pairs were kept symmetrical, and were generated using the modified Gao *et al.* correlation with $n = 0.62$. Asymmetry was introduced into the interaction parameters between asphaltene-solvent binaries only, Figure 6.4b. Asphaltene/solvent interaction parameters were also calculated from the modified Gao *et al.* correlation, using a fitted value of $n = 2$ to calculate k_{ij} and $n = 0.45$ to calculate k_{ji}. This model is an improvement over the AvdW model for asphaltene yield, and matches saturation pressures quite well at temperatures up to 180°C (only the saturation pressures at 90°C are shown here), but this model still under-predicts asphaltene yield at high dilutions because the AvdW model does not capture the asymmetry of system. Properties of the asphaltene components such as molecular mass and density change with the addition of *n*-pentane due to self-association. Simply setting $k_{ij} \neq k_{ji}$ in the AvdW does not fully account for this asymmetry. A significant disadvantage of this approach is the arbitrary division between the asphaltene-solvent and maltene-solvent binary interaction parameters. This means that this model is not predictive for asphaltene yields for other solvents or other temperatures; that is, the interaction parameters must be tuned for each condition. Note, as with any cubic equation of state based on an oil characterization, the exact values of the binary interaction parameters are sensitive to the number of pseudo-components and must be slightly retuned for each characterization (see Section 6.1).

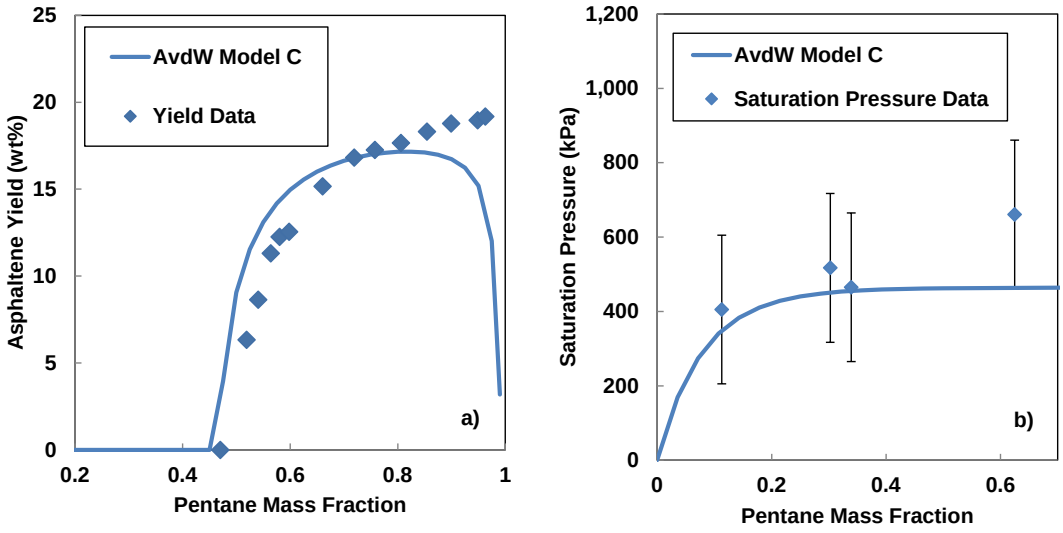

Figure 6.5 Measured and modeled (AvdW Model C) phase behavior data for *n*-pentane diluted bitumen: a) asphaltene yield at 21°C and 0.1 MPa; b) saturation pressures of *n*-pentane diluted bitumen at 90°C.

6.4 Compositionally Dependent Mixing Rules

6.4.1 Huron-Vidal Mixing Rules

Since the asymmetric van der Waals mixing rules were inadequate to match asphaltene yields, compositionally dependent mixing rules were considered. One way to introduce a composition dependence is via an excess energy mixing rule such as the Huron-Vidal mixing rules. In this case, the full bitumen characterization summarized in Table 4.1 was used. Several sets of tuning parameters for the Huron-Vidal mixing rules were evaluated for matching the onset and yield curve for asphaltene precipitation from *n*-pentane diluted bitumen. Figures 6.6 and 6.7 show the results for two different sets of tuning parameters that illustrate the benefits and limitations of this approach (HV Models A and B). HV Model A matches both the shape of the yield curve and the ultimate yield, Figure 6.6a. However, this model was tuned by introducing a significant step-change in b_{ij} and b_{ji} for precipitating components, Figure 6.6b. A step change is arbitrary and not easily correlated for other solvents, a major shortcoming. HV Model B preserves smooth trends in the interaction parameters, Figure 6.7b, but under-predicts yields, Figure 6.7a. Both models predict saturation pressures up to 180°C to within the measurement error, Figure 6.8. Only the saturation pressures at 90°C are presented here. The HV model results for the full dataset of saturation pressures is given in Appendix B.

The volume-based mixing rules were also examined (results not shown here) and yielded similar results. The model with volume-based HV mixing rules can better match asphaltene yields than the symmetric model, but it still under predicts asphaltene yield at high dilutions of *n*-pentane and requires tuning parameters that are not easily generalized. The HV models can better match asphaltene yields than the symmetric model because the effect of asphaltene association can somewhat be represented as a local variation in concentration. However, the local composition model does not fully capture the effect of asphaltene association.

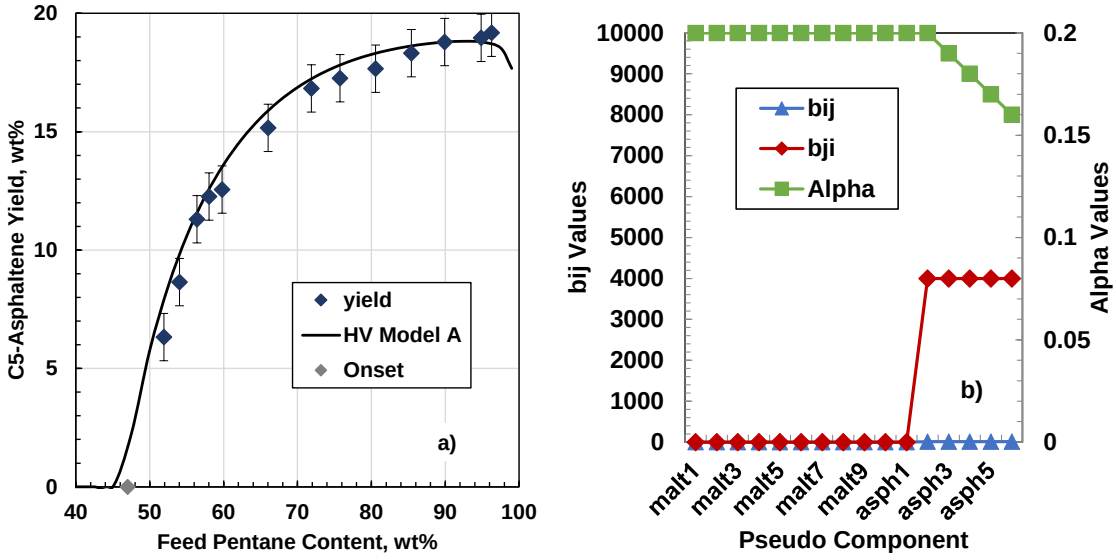

Figure 6.6 a) Measured and modeled asphaltene yield data from *n*-pentane diluted bitumen and b) tuning parameters used in HV Model A.

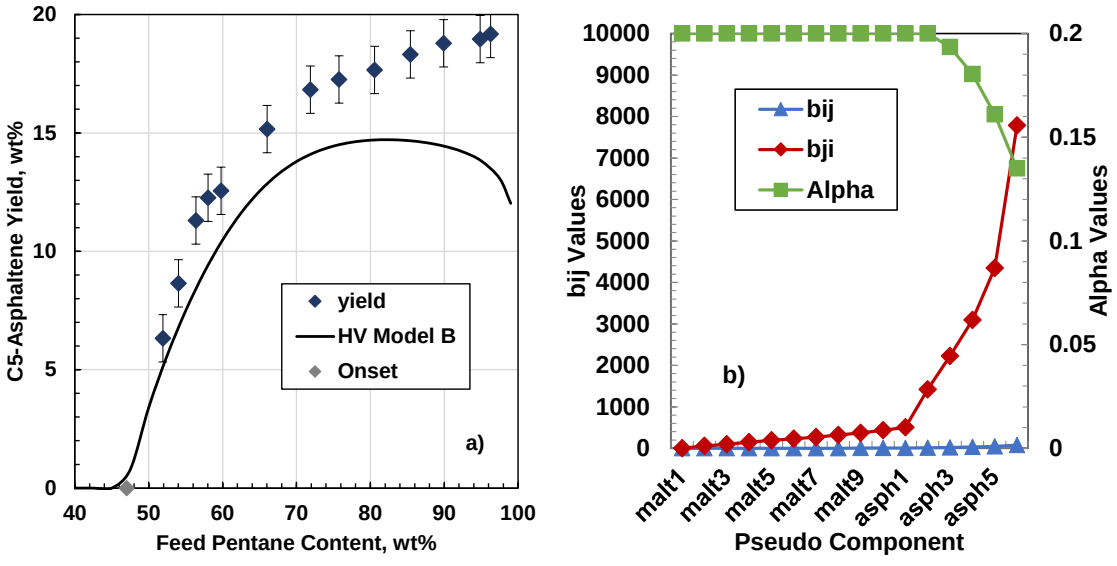

Figure 6.7 a) Measured and modeled asphaltene yield data from *n*-pentane diluted bitumen and b) tuning parameters used in HV Model B.

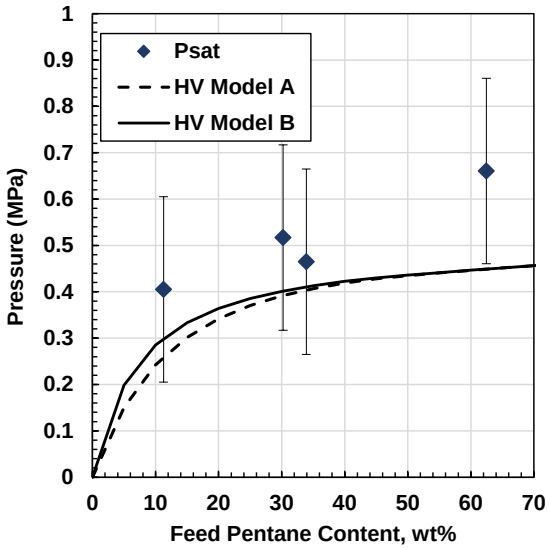

Figure 6.8 Saturations pressures for *n*-pentane diluted bitumen at 90°C. Symbols are experimental data and lines are modeled using HV Model A and HV Model B.

6.4.2 Sandoval *et al.* (SWV) Mixing Rules

Another way to introduce a compositional dependence to relate the asymmetric van der Waals binary interaction parameters to composition as was done with the Sandoval *et al.* mixing rules.

These mixing rules are the simplest of the compositionally dependent mixing rules with a linear relationship of the asymmetric binary interaction parameter to the mole fractions of the asymmetric pair of components. The Sandoval *et al.* mixing rules (SWV) were tested only with the simplified bitumen characterization with a single pseudo-component for each of the maltenes and the asphaltenes. The binary interaction parameters were set to zero for maltene/solvent and maltene/asphaltene binaries, and no temperature dependence was introduced. The solvent/asphaltene binary interaction parameters were tuned to match the yield data. The SWV mixing rules are an improvement over the symmetric mixing rules, but cannot match ultimate yield, Figure 6.9. Therefore, no further tests were performed. It appears that a linear relationship between k_{ij} and mixture composition is not sufficient to match asphaltene yields at high dilutions. The mathematical form of the compositional dependence required is explored below.

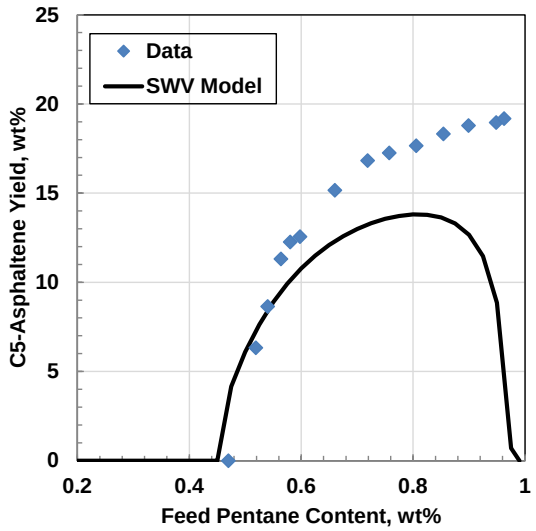

Figure 6.9 Asphaltene yield data for *n*-pentane diluted bitumen. Symbols are data, solid line is the SWV model with k_{as} = -0.05 and k_{sa} = 0.0015.

6.4.3 Compositionally Dependent van der Waals (CDvdW) Mixing Rules

Since the Sandoval *et al.* mixing rules could not adequately match asphaltene yield data for solvent diluted bitumen, the form of the compositional dependence necessary to capture asphaltene yield data was investigated. For the sake of simplicity, the asphaltene fraction of the oil was represented by only one asphaltene pseudo-component when determining the compositional dependence of the

asphaltene/solvent binary interaction parameters, $k_{asph\text{-}solv}$. The maltene fraction was represented by the ten pseudo-components summarized in Table 4.1. The values of k_{ij} for maltene/maltene and maltene/asphaltene binaries were set to zero. In order to accurately model saturation pressures at temperatures above 180°C, solvent/maltene k_{ij} were estimated using Equation 4.8 with k^1_{ij} = 2550 and k^2_{ij} = -1.50 as recommended by Agrawal *et al.* [2012].

The value of $k_{asph\text{-}solv}$ was adjusted at each temperature, pressure, and composition to fit asphaltene yields at temperatures from 20 to 250°C and pressures up to 13.8 MPa. The fitted $k_{asph\text{-}solv}$ are shown in Figure 6.10 as a function of the feed composition. Since the $k_{asph\text{-}solv}$ appear to be insensitive to pressure, they were correlated to temperature and feed composition as follows:

$$\boldsymbol{k_{asph-solv} = (0.00001T + 0.0345)e^{[(0.0059T+0.9125)w_{solv}]}} \qquad \textbf{6.1}$$

where w_{solv} is the mass fraction of solvent in the feed. The correlation is also shown in Figure 6.10.

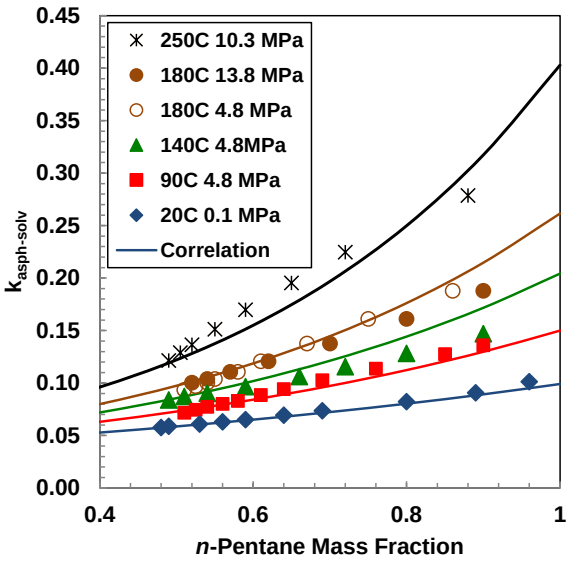

Figure 6.10 Values of $k_{asph\text{-}solv}$ used to fit asphaltene yield. Symbols are fitted $k_{asph\text{-}solv}$ and the lines are Equation 6.1.

The CDvdW model was used to generate PX phase diagrams and yield curves, Figures 6.11 and 6.12. The CDvdW model matches the saturation pressures and yield curves over the whole composition range. It also matches the pressure dependence of the LL boundary at high

temperatures, Figure 6.11, an improvement over the APR model with symmetric van der Waals interaction parameters. However, like all of the mixing rules evaluated in this study, the CDvdW model significantly under-predicted the solvent content in the asphaltene-rich phase at temperatures above 100°C Table 6.2. The low predicted solvent contents are consistent with the values below 6 wt% reported at ambient conditions [Yarranton *et al.* 2011].

Table 6.2 Heavy phase compositions of n-pentane diluted bitumen, measured and modeled using the CDvdW model at 180°C and 4.8 MPa.

Solvent Content in Feed (wt%)	**Measured**			**CvdW Model**		
	Solvent (wt%)	Maltene (wt%)	C5-Asph. (wt%)	Solvent (wt%)	Maltene (wt%)	C5-Asph. (wt%)
59.2	31.4	20.4	48.2	3.1	6.0	90.9
63.7	19.2	24.0	56.8	2.5	4.6	92.9
72.5	20.3	23.7	56.0	1.8	3.2	95.0

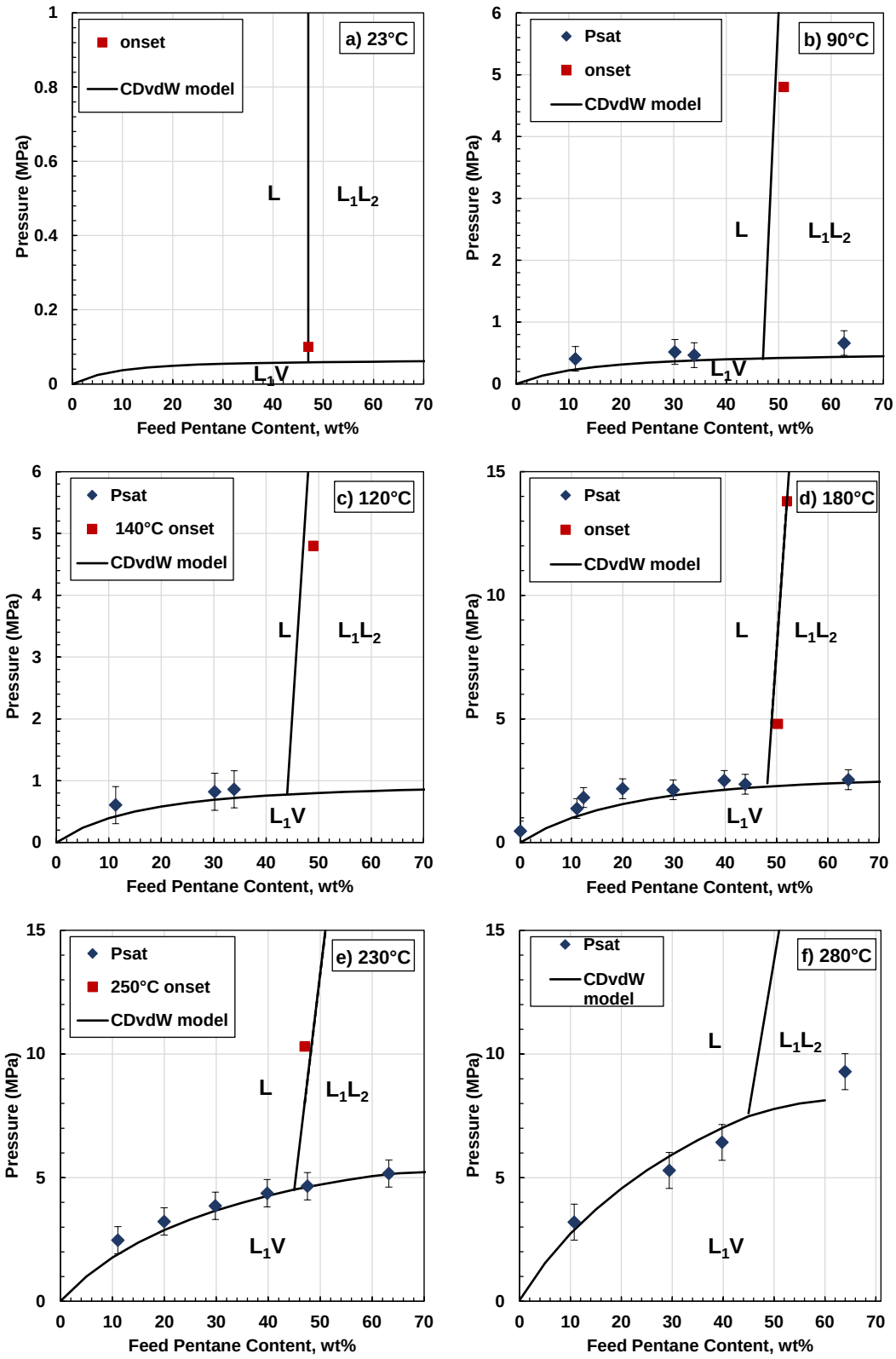

Figure 6.11 Pressure-Composition diagrams for *n*-pentane diluted bitumen at a) 23°C and b) 90°C c) 120°C d) 180°C e) 230°C f) 280°C. Symbols are experimental data and lines are CDvdW model.

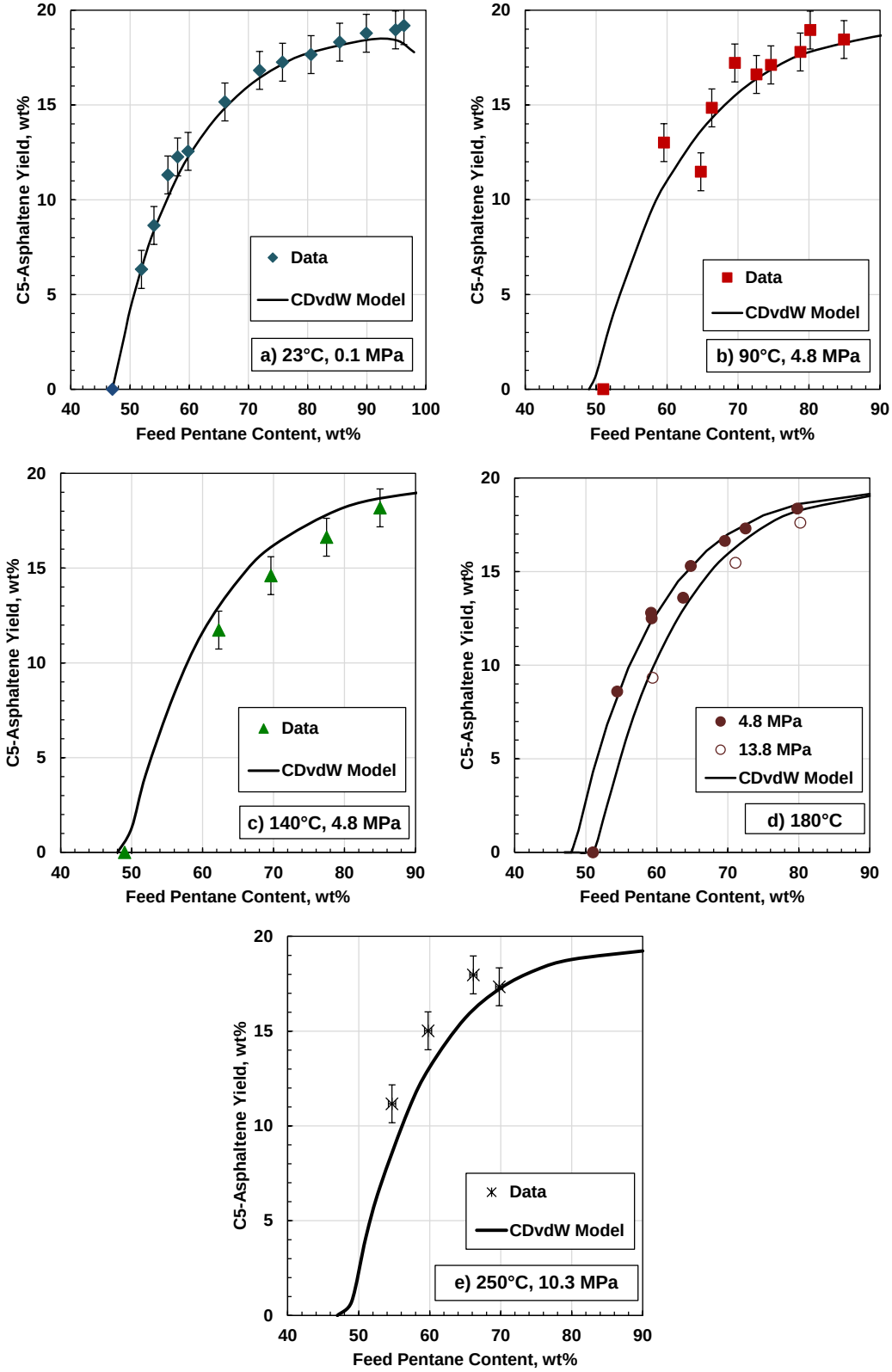

Figure 6.12 Asphaltene yields for *n*-pentane diluted bitumen at a) 23°C b) 90°C c) 140°C d) 180°C and e) 250°C. Symbols are experimental data and lines are the CDvdW model.

A similar fitting exercise was performed to match asphaltene yield data from *n*-heptane diluted WC-B-B2 bitumen data from Shafiee [2014], Figure 6.13 (data is tabulated in Appendix B). Similar trends are observed in the fitted *n*-pentane/asphaltene and *n*-heptane/asphaltene binary interaction parameters at ambient conditions, Figure 6.14. The similarity of the trends is promising for the development of a correlation to relate $k_{asph\text{-}solv}$ to solvent properties; however, more data are required before proceeding further.

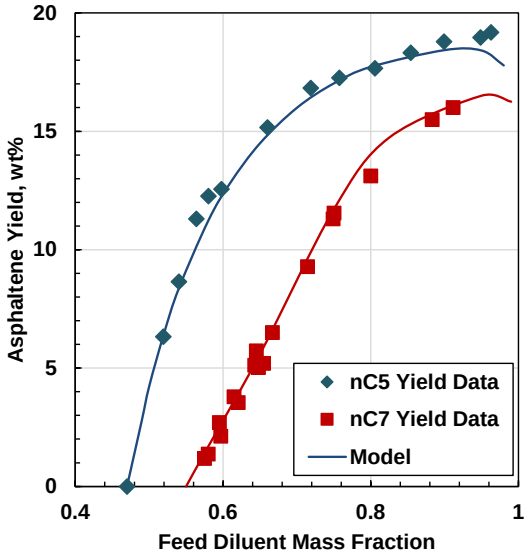

Figure 6.13 Asphaltene yields from *n*-pentane diluted bitumen (this work) and *n*-heptane diluted bitumen [Shafiee, 2014]. Symbols are experimental data and lines are CDvdW fitted model.

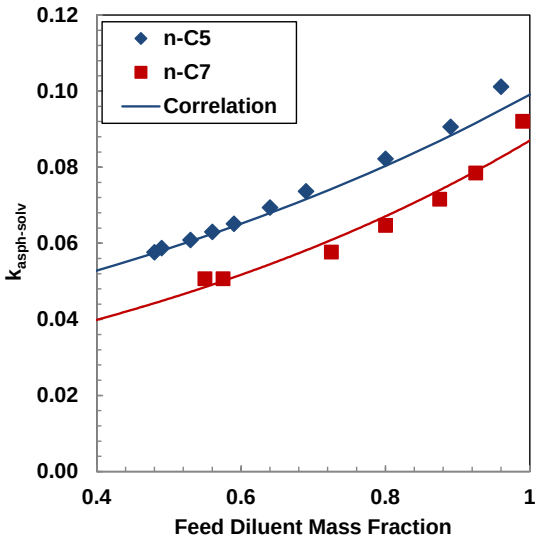

Figure 6.14 Values of $k_{asph\text{-}solv}$ used to fit asphaltene yield for *n*-pentane diluted bitumen and *n*-heptane diluted bitumen at ambient conditions. Symbols are fitted $k_{asph\text{-}solv}$ and the lines are lines of best fit.

Chapter Seven - CONCLUSIONS AND RECOMMENDATIONS

This thesis presented contributions for the phase behavior of mixtures bitumen and solvent (particularly *n*-pentane) including: the development of experimental methods, the collection of original data; and an assessment of the applicability cubic equations of state to these systems. The major conclusions and recommendations in each area are provided below.

7.1 Experimental Methods

A PVT cell based procedure to measure the composition of asphaltene-rich heavy phases was developed and tested. When outliers are eliminated, asphaltene yields and phase compositions were determined with an estimated uncertainty of ±1.1 and ±2.9 wt%, respectively. The repeatability of the C5-asphaltene yield, light phase, and heavy phase compositions were ±1.6, ±2.4, and ±3.5 wt%, respectively. The yields were within experimental error of independent blind cell measurements of asphaltene yields.

Asphaltene yields were measured at temperatures up to 250°C and pressures up to 13.8 MPa. When outliers are eliminated, asphaltene yields were determined with an estimated uncertainty of ±0.4 to ±1.5 wt%, depending on the methodology. To minimize uncertainties in yields, it is recommended to collect high temperature phase samples in variable volume blind cells rather than pycnometers. The reproducibility of the C5-asphaltene yields was within the estimated uncertainty. For both yield and composition measurements, it was challenging to collect representative samples and approximately 20% of the experiments were outliers. Therefore, it is recommended to collect multiple data points with this method so that outliers can be identified and discarded.

7.2 Experimental Results

Both vapor-liquid and liquid-liquid phase boundaries were observed for mixtures of *n*-pentane and bitumen. The second liquid phase is an asphaltene-rich phase that appears as glassy particles below 90°C and as a liquid above 140°C. There appears to be a gradual glass transition between 90 and 140°C.

Saturation pressures for these mixtures were measured at compositions up to 64 wt % *n*-pentane and temperatures up to 280°C with an estimated uncertainty of ± 0.1 MPa to ± 0.8 MPa. Asphaltene onset points were measured at temperatures up to 250°C using two methods; the high pressure microscope method and extrapolation of yield curve method. The two methods are in agreement within the uncertainty in the measured onset point of ±1.5 wt%.

Pressure-composition phase diagrams were constructed for mixtures of *n*-pentane and bitumen at temperatures from 90° to 280°C, pressures up to 10 MPa, and *n*-pentane contents up to 64 wt%. A possible critical point was observed for the mixture of 64 wt% *n*-pentane and 36 wt% bitumen at 280°C and approximately 6 MPa.

The C5-asphaltene solubility for WC-B-B2 and WC-B-B3 bitumen (Peace River) reaches a maximum with respect to temperature at approximately 140°C. The solubility increased with pressure. The *n*-pentane solvent content of asphaltene-rich heavy phases is significant (19 to 31 wt%) at 180°C and therefore must be accounted for when determining the phase properties. The phase compositions in terms of *n*-pentane, maltene, and C5-asphaltene content are better represented on a pseudo-ternary diagram rather than a pseudo-binary phase diagram.

This thesis presents an extensive set of phase behavior data for *n*-pentane diluted bitumen, which is only one solvent of interest for *in situ* recovery schemes. It is recommended to collect asphaltene yield and phase compositions at a range of conditions using other *n*-alkanes, such as propane, butane or *n*-heptane, to determine data trends with changing carbon numbers. It is also recommended to collect similar phase behavior data with mixtures of light hydrocarbons (eg. condensates) or members of other chemical families (eg. napthenes) to better model bitumen/diluent systems of interest.

7.3 Modeling

Several forms of mixing rules were evaluated with the APR CEoS to model asphaltene yields and phase boundaries of *n*-alkane diluted bitumen. While the asymmetric mixing rules are an improvement over the APR with symmetric mixing rules, each of these models still has several

limitations as noted in Table 7.1. None of the models could accurately predict phase compositions at temperatures above 90°C.

Table 7.1 Summary of limitations for mixing rules examined in this study.

Mixing Rule	Tunable to match asphaltene yield?	Tunable to match asphaltene yield and saturation pressures?	Tuning parameters easily correlated?
AvdW	Yes	No	-
SWV	No	-	-
HV	Yes	Yes	No
CDvdW	Yes	Yes	No

The use of asymmetric van der Waals mixing rules ($k_{ij} \neq k_{ji}$) adds more flexibility to the model and matches asphaltene yields. However, the tuning parameters that give the best match for asphaltene yields do not match VLE data with the same accuracy as symmetric mixing rules. The parameters that retain a good match to the saturation pressures require an arbitrary division between maltene/solvent and asphaltene/solvent binary interaction parameters and therefore are not predictive or easily correlated for other solvents. These models slightly over-predict asphaltene yields at intermediate dilutions and under-predict asphaltene yields at high dilutions.

The APR with Huron-Vidal excess energy based mixing rules can be tuned to match asphaltene yield. However, the tuning parameters that give the best match for asphaltene yield data require an arbitrary division between maltene/solvent and asphaltene/solvent binary interaction parameters and therefore are not predictive or easily correlated for other solvents. A model that can be predictive for other solvents cannot match the shape of the yield curve.

Mixing rules with compositionally dependent binary interaction parameters can successfully model asphaltene yield data but only with an appropriate mathematical form for the compositional dependence fits. For example, the Sandoval *et al.* mixing rules cannot be tuned to match asphaltene yields at high dilution, because the mixing rule includes a linear dependence of the binary interaction parameter on mole fraction. An exponential relationship to mass fraction provided better results and a correlation was found for the asphaltene/*n*-pentane binary interaction parameter as a function of the solvent mass fraction in the feed and absolute temperature. While the model is

not very sensitive to the characterization methodology, the binary interaction parameters must be slightly retuned if the characterization is changed; for example, when the number of pseudo-components is altered.

Overall, CEoS are not well suited to modeling asphaltene precipitation. CEoS with asymmetric mixing rules cannot account for the changing properties of the asphaltene components as they associate in the presence of an alkane like *n*-pentane. Data fitting is possible over a limited range of conditions using asymmetric or compositionally dependent binary interaction parameters but generalized correlations for a wide range of solvents and conditions is probably not possible. However, it is recommended to use the experimental methods presented in this thesis to collect asphaltene yield and phase composition data for propane diluted bitumen and to use the compositionally dependent binary interaction parameter model to fit the data. This method will determine if a correlation for binary interaction parameter can be developed for a small range of solvents.

The PC-SAFT and CPA equations of state have both been shown in the literature to match asphaltene yield trends and phase boundaries each in one internally consistent model. It is recommended to test both these models on the data measured in this thesis to determine if they can also accurately model the component partitioning between phases.

REFERENCES

Adachi, Y. and Sugie, H. “A New Mixing Rule – Modified Conventional Mixing Rule.” *Fluid Phase Equilibria* (28) pg. 103-118 (1986)

AER, Alberta’s Energy Reserves 2011 and Supply/Demand Outlook, ST98-2014

Agrawal, P., Schoeggl, F.F., Satyro, M.A., Taylor, S.D., Yarranton, H.W., “Measurement and Modeling of the Phase Behavior of Solvent Diluted Bitumens” *Fluid Phase Equilibria* (334) pg. 51-64 (2012)

Akbarzadeh, K., Alboudwarej, H., Svrcek, W.Y., Yarranton, H.W., “A Generalized Regular Solution Model For Asphaltene Precipiation from n-Alkane Diluted Heavy Oils and Bitumens” *Fluid Phase Equilibria* (232) pg. 159-170 (2005)

Akbarzadeh, K., Dhillon, A., Svrcek, W.Y., and Yarranton, H.Y., “Methodology for the Characterization and Modeling of Asphaltene Precipitation from Heavy Oils Diluted with n-Alkanes” *Energy & Fuels* (18) pg. 1434-1441 (2004)

Alboudwarej, H., Akbarzadeh, K., Beck, J., Svrcek, W.Y., and Yarranton, H.Y., “Regular Solution Model for Asphaltene Precipitation from Bitumens and Solvents” *AIChE Journal* (49) pg. 2948-2956 (2003)

AlHammadi, A.A., Vargas, F.M., Chapman, W.G., “Comparison of Cubic-Plus-Association and Perturbed-Chain_Statistical Associating Fluid Theory Methods for Modeling Asphaltene Phase Behavior and Pressure-Volume-Temperature Properties” *Energy&Fuels* (29) pg. 2864-2875 (2015)

Ali, L.H., and Al-Ghannam, K.A., “Investigations into Asphaltenes in Heavy Crude Oils. 1. Effect of Temperature on Precipitation by Alkane Solvents” *Fuel* (60) pg. 1043-1046 (1981)

Altgelt, K.H., Boduszynski, M.M., “Composition and Analysis of Heavy Petroleum Fractions” M. Dekker (1994)

Andersen, S.I., and Birdi, K.S., “Influence of Temperature and Solvent on the Precipitation of Asphaltenes” *Fuel Science and Technology International* (8) pg. 593-615 (1990)

Andersen, S.I., “Effect of Precipitation Temperature on the Composition of n-Heptane Asphaltenes” *Fuel Science and Technology International* (12) pg. 51-74 (1994)

Andersen, S.I., Lindeloff, N., Stenby, E.H., “Investigation of Asphaltene Precipiation at Elevated Temperature” *Petroleum Science and Technology* (16) pg. 323-334 (1998)

Badamchi-Zadeh, A., Yarranton, H.W., Svrcek, W.Y., Maini, B.B. “Phase Behaviour and Physical Property Measurments for VAPEX Solvents: Part 1. Propane and Athabasca Bitumen” *JCPT* (48) pg. 54-61 (2009)

Badamchi-Zadeh, A., Yarranton, H.W., Maini, B.B., Satyro, M.A., “Phase Behaviour and Physical Property Measurments for VAPEX Solvents: Part 2. Propane, Carbon Dioxide and Athabasca Bitumen” *JCPT* (48) pg. 57-65 (2009)

Barrera, D.M., Ortiz, D.P., Yarranton, H.W., “Molecular Weight and Density Distributions of Asphaltenes from Crude Oils” *Energy & Fuels* (27) pg. 2474-2487 (2013)

Beck, J., Svrcek, W.Y., Yarranton, H.W., “Hysteresis in Asphaltene Precipitation and Redissolution” *Energy Fuels* (19) pg. 944-947 (2005)

Castellanos-Díaz, O., Modaresghazani, J., Satyro, M.A., Yarranton, H.W., “Modeling the Phase Behavior of Heavy Oil and Solvent Mixtures” *Fluid Phase Equilibria* (304) pg. 74-85 (2011)

Chapman, W.G., Jackson, G., Gubbins, K.E., “Phase Equilibiria of Associating Fluids” *Molecular Physics* (65) pg. 1057-1079 (1988)

Chapman, W.G., Gubbins, K.E., Jackson, G., Radosz, M., “New Reference Equation of State for Associating Liquids” *Ind. Eng. Chem. Res.* (29) pg. 1709-1721 (1990)

Chueh, P.L., Prausnitz, J.M., “Calculations of High-Pressure Vapor-Liquid Equilibria” *Ind. Eng. Chem.* (60) (1968)

Dini, Y., Becerra, M., Shaw, J.M., “Phase Behavior and Thermophysical Properties of Peace River Bitumen + Propane Mixtures from 303K to 393K” *Journal of Chemical & Engineering Data* (61) pg. 2659-2668 (2016)

Eyssautier, J.; Hénaut, I.; Levitz, P.; Espinat, D.; Barré, L., “Organization of Asphaltenes in a Vacuum Residue: A Small-Angle X-ray Scattering (SAXS) - Viscosity Approach at High Temperatures” *Energy Fuels* (26) pg. 2696-2704 (2012)

Flory, P.J., “Thermodynamics of High Polymer Solutions” *Journal of Chem Physics* (9) pg.660 (1941)

Gao, G., Daridon, J.L., Saint-Guirons, H., Xans, P., “A Simple Correlation to Evaluate Binary Interaction Parameters of the Peng-Robinson Equation of State: Binary Light Hydrocarbon Systems” *Fluid Phase Equilibria* (74) pg. 85-93 (1992)

Gonzalez, D.L., Hirasaki, G.J., Creek, J., Chapman, W.G., “Modeling of Asphaltene Precipitation Due to Changes in Composition Using the Perturbed Chain Statistical Associating Fluid Theory Equation of State” *Energy Fuels* (21) pg. 1231-1242 (2007)

Gray M., “Upgrading Petroleum Residues and Heavy Oils” New York: Marcel Dekker (1994)

Gray, M.R., Assenheimer, G., Boddez, L., and McCaffrey, W.C., “Melting and Fluid Behavior of Asphaltene Films at 200-500°C” *Energy & Fuels* (18) pg. 1419-1423 (2004)

Gregorowicz, J., de Loos, T.W., “Prediction of Liquid-Liquid-Vapor Equilibria in Asymmetric Hydrocarbon Mixtures” *Ind. Eng. Chem. Res.* (40) pg. 444-451 (2001)

Gross, J., Sadowski, G., “Application of the Perturbed-Chain SAFT Equation of State to Associating Systems” *Ind. Eng. Chem. Res.* (41) pg. 5510-5515 (2002)

Hirschberg, A., DeJong, L.N.J., Schipper, B.A., Meijer, J.G., “Influence of Temperature and Pressure on Asphaltene Flocculation” *SPE Journal* (24) pg. 283-293 (1984)

Hu, Y-F, and Guo, T.-M., “Effect of Temperature and Molecular Weight of *n*-Alkane Precipitants on Asphaltene Precipitation” *Fluid Phase Equilibria*, (192) pg. 13-25 (2001)

Huang, S.H., Radosz, M., “Phase Behavior of Reservoir Fluids III: Molecular Lumping and Characterization” *Fluid Phase Equilibria* (66) pg. 1-21 (1991)

Huang, S.H., Radosz, M., “Phase Behavior of Reservoir Fluids IV: Molecular Weight Distributions for Thermodynamic Modeling” *Fluid Phase Equilibria* (66) pg. 23-40 (1991)

Huggins, M.L., “Solutions of Long Chain Compounds” *J. of Chem Physics* (9) pg.440 (1941)

Huron, M., Vidal, J., “New Mixing Rules in Simple Equations of State for Representing Vapour-Liquid Equilibria of Strongly Non-Ideal Mixtures” *Fluid Phase Equilibria* (3) pg. 255-271 (1979)

Jossy, C., Frauenfeld, T., Rajan, V., “Partitioning of Bitumen-Solvent Systems into Multiple Liquid Phases” *JCPT* (48) pg. 16-20 (2009)

Jamaluddin, A.K.M., Kalogerakis, N.E., and Chakma, A., “Predictions of CO_2 solubility and CO_2 saturated liquid density of heavy oils and bitumens using a cubic equation of state” *Fluid Phase Equilibria* (64) pg. 33-48 (1991)

Jhaveri, B.S., and Youngren, G.K., “Three Parameter Modification of the Peng Robinson Equation of State to Improve Volume Predictions” *SPE Res. Eng.* (3) pg. 1033-1040 (1988)

Joshi, N.B., Mullins, O.C., Jamaluddin, A., Creek, J., McFadden, J., “Asphaltene Precipitation from Live Crude Oil” *Energy & Fuels* (15) pg. 979-986 (2001)

Katz, D.L., Firoozabadi, A., “Predicting Phase Behavior of Condensate/Crude Oil Systems Using Methane Interaction Coefficients” *Journal of Pet. Technology* (30) pg. 1649-1655 (1978)

Kontogeorgis, G.M., Folas, G.K., “Thermodynamic Models for Industrial Applications” Johns Wiley and Sons, New York (2009)

Kristensen, J.N., and Christensen, P.L., "A Combined Soave-Redlich-Kwong and NRTL Equation for Calculating the Distribution of Methanol between Water and Hydrocarbon Phases" *Fluid Phase Equilibria* (82) pg. 199-206 (1993)

Kriz, P., Stastna, J., Zanzotto, L., "Glass Transition and Phase Stability in Asphalt Binders" *Road Materials and Pavement Design*, (9) pg. 37-65 (2008)

Lee, B.I., and Kesler, M.G., A Generalized Thermodynamic Correlation Based on Three-Parameter Corresponding States, *AIChE Journal* (22) pg. 510-527 (1975)

Leelavanichkul, P., Deo, M.D., and Hanson, F.V., "Crude Oil Characterization and Regular Solution Approach to Thermodynamic Modeling of Solid Precipitation at Low Pressure" *Petroleum Science and Technology* (22) pg. 973-990 (2004)

Li, Z., Firoozabadi, A., "Cubic-Plus-Association Equation of State for Asphaltene Precipitation in Live Oils" *Energy Fuels* (24) pg. 2956-2963 (2010)

Linstrom, P.J., Mallard, W.G., Eds., "NIST Chemistry WebBook, NIST Standard Reference Database Number 69", National Institute of Standards and Technology, Gaithersburg MD, 20899, http://webbook.nist.gov, (retrieved May 2015)

Luo, P., Wang, X., Gu, Y., "Characterization of Asphaltenes Precipitated with Three Light Alkanes Under Different Experimental Conditions" *Fluid Phase Equillibria* (291) pg. 103-110 (2010)

Mannistu, K.D., Yarranton, H.W., Masliyah, J.H., "Solubility Modeling of Asphaltenes in Organic Solvents" *Energy & Fuels* (11) pg. 615-622 (1997)

Mehrotra, A.K.; Svrcek, W.Y., "Viscosity, Density and Gas Solubility Data for Oil Sand Bitumens. Part II: Peace River Bitumen Saturated with N_2, CO, CH_4, CO_2, C_2H_6" *AOSTRA J.*, (4) pg. 269-279 (1985)

Mehrotra, A.K., Svrcek, W.Y., "Correlation and Prediction of Gas Solubility in Cold Lake Bitumen" *Canadian Journal of Chem. Eng.* (66) pg. 666-670 (1988)

Merino-Garcia, D., and Anderson, S., I., "Isothermal Titration Calorimetry and Fluorescence Spectroscopy Study of Asphaltene Self-Association in Toluene and Interaction with a Model Resin" *Pet. Science and Tech.* (21) pg. 507-525 (2003)

Michelsen, M.L., "The Isothermal Flash Problem Part 1. Stability" *Fluid Phase Equilibria* (9) (1982)

Michelsen, M.L., and Kistenmacher, H., "On Composition-Dependent Interaction Coefficients" *Fluid Phase Equilibria* (58) pg. 229-230 (1990)

Mitchell, D.L., Speight, J.G., “The Solubility of Asphaltenes in Hydrocarbon Solvents” *Fuel* (52) pg. 149-152 (1973)

Motahhari, H., Schoeggl, F.F., Satyro, M.A. Yarranton, H.W., “Viscosity Prediction for Solvent Diluted Live Bitumen and Heavy Oil at Temperatures up to 175°C” *J. Can. Petr. Technol.* (52) pg. 376-390 (2013)

Mullins, O.C., “Review of the Molecular Structure and Aggregation of Asphaltenes and Petroleomics” *SPE Journal* (2008) SPE Paper 95801

Mullins, O.C., “The Asphaltenes” *Annual Review of Analytical Chemisty* (4) pg. 393-418 (2011)

Panagiotopoulos, A.Z. and Reid, M.C., “A New Mixing Rule for Cubic Equations of State for Highly Polar, Asymmetric Mixtures” *ACS Symposium Series* (300) pg.571-582 (1986)

Panuganti, S.R., Vargas, F.M., Gonzalez, D.L., Kurup, A.S., and Chapman, W.G., “PC-SAFT Characterization of Crude Oils and Modeling of Asphaltene Phase Behaviour” *Fuel* (93) pg. 658-669 (2012)

Pedersen, K.S., Michelsen, M.L., Fredheim, A.O., “Phase Equilibrium Calculations for Unprocessed Well Streams Containing Hydrate Inhibitors” *Fluid Phase Equilibria* (126) pg. 13-28 (1996)

Pedersen, K.S., Christensen, P.L., “Phase Behavior of Petroleum Reservoir Fluids” Taylor & Francis Group, 2007

Péneloux, A., Rauzy, E., “A Consistent Correction for Redlich-Kwong-Soave Volumes” *Fluid Phase Equilibria* (8) pg. 7-23 (1982)

Peng, D., Robinson, D.B., “A New Two-Constant Equation of State” *Ind. Eng. Chem. Fundam.* (15) pg. 59-64 (1976)

Permanu, S., Singh, C., Agrawala, M., Yarranton, H.W., “Investigation on the Reversibility of Asphaltene Precipitation” *Energy and Fuels* (15) pg. 910-917 (2001)

Rachford, H.H., Rice, J.D., “Procedure to Use Electrical Digital Computers in Calculating Flash Vaporizing” *JPT* (4) (1952)

Rastegari, K., Svrcek, W.Y., Yarranton, H.W., “Kinetics of Asphaltene Flocculation” *Ind. Eng. Chem. Res.* (43) pg. 6861-6870 (2004)

Reid, R.C., Prausnitz, J.M., Poling, B.E., “The Properties of Gases and Liquids” McGraw-Hill, New York, (1989)

Renon, H., Prausnitz, J.M., “Local Compositions in Thermodynamic Excess Functions for Liquid Mixtures” *AIChE Journal* (14) pg. 135-144 (1968)

Riazi, M.R., and Daubert, T.E., “Prediction of Molecular-Type Analysis of Petroleum Fractions and Coal Liquids” *Ind. Eng. Chem. Process Des. Dev.*(25) pg. 1009-1015 (1986)

Riazi, M.R., and Daubert, T.E., “Characterization Parameters for Petroleum Fractions” *Ind. Eng. Chem. Res.* (26) pg755-759 (1987)

Rodgers, R.P., McKenna, A.M., “Petroleum Analysis” *Analytical Chemistry* (83) pg. 4665-4687 (2011)

Rogel, E., León, O., Torres, G., Espidel, J., “Aggregation of Asphaltenes in Organic Solvents Using Surface Tension Measurements” *Fuel* (79) pg. 1389-1394 (2000)

Saber, N., and Shaw, J.M., “Toward Multiphase Equilibrium Prediction for Ill-Defined Asymmetric Hydrocarbon Mixtures” *Fluid Phase Equilibria* (285) pg. 73-82 (2009)

Saber, N., and Shaw, J.M., “On the Phase Behavior of Athabasca Vacuum Residue + n-decane” *Fluid Phase Eqilibiria* (302) pg. 254-259 (2011)

Saber, N., Zhang, X., Zou, X., Shaw, J.M., “Simulation of the Phase Behavior of Athabasca Vacuum Residue + n-Alkane Mixtures” *Fluid Phase Equilibria* (312) pg. 25-31 (2012)

Sandoval, R., Wilczek-Vera, G., and Vera, J.H., “Prediction of Ternary Vapor-Liquid Equilibria with the PRSV Equation of State” *Fluid Phase Equilibria* (52) pg.119-126 (1989)

Saryazdi, F. Motahhari, H., Schoeggl, F.F., Yarranton, H.W., "Density of Hydrocarbon Mixtures and Bitumen Diluted with Solvents and Dissolved Gases," *Energy & Fuels*, (27) pg. 3666-3678 (2013)

Sanchez, C., Private Communication, *University of Calgary*, 2013

Schwartzentruber, J., and Renon, H., “Equations of State: How to Reconcile Flexible Mixing Rules, the Virial Coefficient Contraint and the ‘Michelsen-Kistenmacher syndrome’ for Multicomponent systems” *Fluid Phase Equilibira* (67) pg. 99-110 (1991)

Sedghi, M. and Goual, L., “Role of Resins on Asphaltene Stability” *Energy Fuels* (24) pg. 2275-2280 (2010)

Shafiee Neistanak, M., “Kinetics of Asphaltene Precipitation and Flocculation from Diluted Bitumen”, *University of Calgary*, Master’s Thesis (2014)

Shaw, J.M. and Zou, X., “Phase Behavior of Heavy Oils” In: Mullins, O.C., Sheu, E.Y., Hammani, A., Marshall, A.G., editors. *Asphaltenes, Heavy Oils, and Petroleomics*, New York: Springer, 2007, pg. 489-510

Shirani, B., Manouchehr, N., Mousavi-Dehghani, S.A., “Prediction of Asphaltene Phase Behavior in Live Oil with a CPA Equation of State” *Fuel* (97) pg. 89-96 (2012)

Sirota, E.B., “Physical Structure of Asphaltenes” *Energy & Fuels* (19) pg. 1290-1296 (2005)

Sirota, E.B., Lin, M.Y., “Physical Behavior of Asphaltenes” *Energ & Fuels* (21) pg. 2809-2815 (2007)

Smith, J.M., Van Ness, H.C., Abbott, M.M., “Chemical Engineering Thermodynamics” McGraw Hill, New York (2001)

Søreide, I., “Improved Phase Behavior Predictions of Petroleum Reservoir Fluids from a Cubic Equation of State” PhD Thesis, the Norwegian Institute of Technology and Applied Geophysics, Norway, 1989

Sørensen, H., Pedersen, K.S., Christensen, P.L., “Modeling of Gas Solubility in Brine” *Organic Geochemistry* (33) pg. 635-642 (2002)

Stryjek, R. and Vera, J.H., “PRSV – An improved Peng-Robinson Equation of State with New Mixing Rules for Strongly Nonideal Mixtures” *The Canadian Journal of Chemical Engineering* (64) pg. 334-340 (1986)

Speight, J.G., “The Chemistry and Technology of Petroleum” 3rd Edition, Marcel Dekker, Inc., New York (1999)

Tavakkoli, M., Panuganti, S.R., Taghikhani, V., Pishvaie, M.R., Chapman, W.G. “Understanding the Polydiverse Behavior of Asphaltenes During Precipitation” *Fuel* (117) pg. 206-217 (2014)

Tharanivasan, A.K., Yarranton, H.W., Taylor, S.D. “Application of a Regular Solution-Based Model to Asphaltene Precipitation from Live Oils” *Energy Fuels* (25) pg. 528-538 (2011)

Ting, P.D., Hirasaki, G.J., and Chapman, W.G., “Modeling of Asphaltene Phase Behavior with the SAFT Equation of State” *Petroleum Science and Technology* (21) pg. 647-661 (2003)

Tran, K.Q., “Reversing and Non-Reversing Phase Transitions in Athabasca Bitumen Asphaltenes” M.Sc. Thesis, University of Alberta (2009)

Twu, C.H., “An Internally Consistent Correlation for Predicting the Critical Properties and Molecular Weights of Petroleum and Coal-Tar Liquids” *Fluid Phase Equilibria* (16) pg. 137-150 (1984)

Virtual Materials Group Inc. VMG, VMGSim Version 9.5, “VMGSim User’s Manual” Calgary, Canada 2015

Wang, J.X., and Buckley, J.S., “A Two-Component Solubility Model of the Onset of Asphaltene Flocculation in Crude Oils” *Energy & Fuels* (15) pg. 1004-1012 (2001)

Whitson, C.H., “Characterizing Hydrocarbon Plus Fractions” *SPE Journal* (23) pg. 683-694 (1983)

Wiehe, I.A., Yarranton, H.W., Akbarzadeh, K., Rahimi, P.M., Teclemariam, A., "The Paradox of Asphaltene Precipitation with Normal Paraffins" *Energy & Fuels* (19) pg. 1261-1267 (2005)

Wong, D.S.H. and Sandler, S.I., "A Theoretically Correct Mixing Rule for Cubic Equations of State" *AIChE Journal* (38) pg. 671-680 (1992)

Xu, Y., Koga, Y., Strausz, P., "Characterization of Athabasca Asphaltenes by Small-Angle X-Ray Scattering" *Fuel* (74) pg. 960-964 (1995)

Yarranton, H.W., Alboudwarej, H., Jakher, R., "Investigation of Asphaltene Association with Vapour Pressure Osmometry and Interfacial Tension Measurements" *In. Eng. Chem. Res.* (39), pg. 2916-2924 (2000)

Yarranton, H.W., Fox, W.A., Svrcek, W.Y., "Effect of Resins on Asphaltene Self-Association and Solubility" *Canadian Journal of Chem. Eng.* (85) pg.635-642 (2007)

Yarranton, H.W., Schoeggl, F.S., George, S., and Taylor, S.D., "Asphaltene-rich Phase Compositions and Sediment Volumes from Drying Experiments" *Energy Fuels* (25) pg. 3624-3633 (2011)

Zhang, Y., Takanohashi, T., Sato, S., and Saito, I., "Observation of Glass Transition in Asphaltenes" *Energy Fuels* (18) pg. 283-284 (2004)

Zhang, X., Pedrosa, N., Moorwood, T., "Modeling Asphaltene Phase Behavior: Comparison of Methods for Flow Assurance Studies" *Energy&Fuels* (26) pg. 2611-2620 (2012)

Zou, X., Zhang, X., Shaw, J.M., "The Phase Behavior of Athabasca Vacuum Bottoms + n-Alkane Mixtures" *SPE International Thermal Operations and Heavy Oil Symposium* (2005)

APPENDIX A – ERROR ANALYSIS

A.1 PVT Cell Phase Composition and Yield Data

The major sources of error in the phase composition and asphaltene yield calculations are as follows:

1. Mass of Diluent in Feed: The mass of diluent injected at the experimental temperature was calculated in two ways (using either ΔV_{PVT} or ΔV_{pump}) as described in the *Feed Composition* section of Section 3.8. The reported mass of diluent was taken as the average of these two values. The deviation for a given run was taken to be half the difference between these two values. Considering the deviations of all data collected to date (not all shown here), the uncertainty was determined to be ±0.9 g based on a 90% confidence interval.
2. Phase Sample Composition: Two samples of each phase were collected and analyzed using the mass evaporation technique to determine the phase compositions. The reported phase compositions are the average of the two measured values and the deviation was taken to be half the difference between the two measured values. Considering the deviations of all data collected to date (not all shown here), the uncertainty was determined to be ±1.1 wt% based on a 90% confidence interval. The GC assays on each light phase sample were used as a validation of the measured compositions. The difference between the GC assays and the measured compositions from the mass evaporation technique was typically less than 2%.
3. Heavy Phase Density/Toluene Content: The heavy phase sample was diluted with toluene in the PVT cell before sample collection. Volumes of both the heavy phase and toluene were measured with a precision of 0.01 cm^3. However, in order to determine the mass fractions of each phase, densities are needed, and the uncertainty in the density is the main source of error. The density of the heavy phase is unknown and was estimated using a regular solution assumption. Saryazdi *et al*. [2013] reported errors of <1% when calculating densities of bitumen/alkane mixtures using regular solution theory and; therefore, an error of ± 1% was used in calculations.

The uncertainty in the light phase composition is then ±1.1 wt% as stated above in Point 2. The uncertainty in the heavy phase composition includes contributions from Points 2 and 3 and was determined from propagation of error to be ±2.9 wt%. The uncertainty in the yield calculation

includes all three contributions and was determined from the propagation of error. The final reported yield is the average of the yield calculated from the heavy phase data and the yield calculated from the light phase data. The deviation between the two yields was used to compute the uncertainty. Considering the deviations of all data collected to date (not all shown here), the uncertainty in the yield was determined to be ±1.1 wt% based on a 90% confidence interval.

A.2 Blind Cell Yield Data

The primary source of uncertainty is in the measured light phase sample compositions. In the blind cell apparatus, light phase samples were collected one of two ways. Either the sample was displaced into 3 constant volume (10 cm^3) pycnometers or the sample was displaced into an empty sample cylinder. The uncertainty analysis for each of these sample collection methodologies is discussed below.

Pycnometer Light Phase Sample Collection

Three samples of the light phase were collected from each blind cell and analyzed using the mass evaporation technique to determine the phase compositions. The uncertainty in the light phase compositions (see Point 2 above) was propagated through the mass balance calculations to determine the uncertainty of the asphaltene yields. The asphaltene yield is reported as the average of the calculated asphaltene yield from the three samples. The positive deviation is the difference between the highest calculated yield and the average yield. Similarly, the negative deviation is the difference between the lowest calculated yield and the average yield. Considering the deviations of the data collected to date, the positive and negative uncertainties were determined to be +1.0 wt% and -1.5 wt%, respectively, based on a 90% confidence interval, Table A.1. The negative uncertainty is higher than the positive. This is likely due to challenges in ensuring consistent washing of the asphaltenes in the light phase. Recall that asphaltene yield is determined from asphaltene content remaining in the light phase and a material balance. If the asphaltenes are poorly washed, asphaltene content remaining in the light phase will be over-estimated, resulting in underestimation of asphaltene yield.

Table A.1 Uncertainty in asphaltene yield propagated from uncertainties in measured light phase compositions (pycnometer sampling technique).

Experimental Method	Temp °C	Pressure Mpa	Solvent Content %	Asphaltene Yield %	Positive Uncertainty	Negative Uncertainty
blind cell	90	4.8	59.6	13.0	0.40	0.76
blind cell	90	4.8	66.3	14.8	0.83	0.89
blind cell	90	4.8	72.6	16.6	0.69	1.02
PVT	90	4.8	64.8	11.5	0.32	0.36
PVT	90	4.8	69.5	17.2	0.12	0.11
blind cell	140	4.8	62.3	11.7	1.42	1.91
blind cell	140	4.8	69.6	14.6	1.31	1.43
blind cell	180	4.8	59.3	12.5	0.94	0.95
blind cell	180	4.8	64.8	15.3	0.80	0.63
blind cell	180	4.8	69.6	16.6	0.56	0.95
blind cell	180	4.8	79.8	18.4	0.26	0.26
blind cell	180	13.8	59.4	9.3	1.64	1.64
blind cell	180	13.8	80.2	17.6	0.36	0.36
blind cell	250	10.3	66.1	18.0	0.97	4.07
blind cell	250	10.3	69.8	17.3	1.02	1.42
			Average Uncertainty		0.8	1.1
			Standard Deviation		0.5	1.0
			90^{th} Percentile		1.0	1.5

Sample Cylinder Light Phase Sample Collection

The volumes of the samples collected in the sample cylinder sampling methodology exceeded the volume of the centrifuge tubes, so the samples were divided into two centrifuge tubes and were analyzed as two samples. The reported asphaltene yields are the average of the yields calculated for the two samples. The deviation between the two yields was used to compute the uncertainty. Considering the deviations of all data collected to date, Table A.2, the uncertainty in the yield was determined to be ±0.4 wt% based on a 90% confidence interval.

Table A.2 Uncertainty in asphaltene yield propagated from uncertainties in measured light phase compositions (blind cell sampling technique).

Experimental Method	Temp °C	Pressure Mpa	Solvent Content %	Asphaltene Yield %	Positive Uncertainty	Negative Uncertainty
blind cell	90	4.8	78.8	17.8	0.28	0.28
blind cell	90	4.8	84.9	18.4	0.27	0.27
PVT	90	4.8	74.6	17.1	0.72	0.72
PVT	90	4.8	80.2	19.0	0.09	0.09
blind cell	140	4.8	77.5	16.6	0.38	0.38
blind cell	140	4.8	85.0	18.2	0.04	0.06
blind cell	250	10.3	54.7	11.2	0.09	0.09
blind cell	250	10.3	59.8	15.0	0.05	0.05
			Average Uncertainty		0.2	0.2
			Standard Deviation		0.2	0.2
			90^{th} Percentile		0.4	0.4

APPENDIX B – ADDITIONAL DATA

B.1 Additional Measured Data

This thesis presented the experimental results and modeling for a complete set of data for *n*-pentane diluted bitumen. Also of interest is creating similar data sets using other alkanes as solvents. The next solvent of interest chosen for follow up studies was propane and further research in this group will be targeted at mapping the phase behavior of propane diluted bitumen. In addition to the data presented in the body of this thesis, asphaltene onset points for propane diluted bitumen were measured up to 90°C and 10.3MPa, Table B.1, using the HPM methodology presented in Section 3.3.3 of this thesis

Table B1 Onset of second liquid phase for propane diluted bitumen.

Pressure (MPa)	Temperature (°C)	Onset Point (wt% propane)
2.1	20	21 ± 1.5
10.3	20	35 ± 1.5
6.9	50	31 ± 1.5
10.3	50	35 ± 1.5
10.3	90	33 ± 1.5

B.2 Supplemental Data

The focus of this work was primarily to test the modeling methodology on a dataset of *n*-pentane diluted phase behavior. The CDvdW model was also fitted to match asphaltene yield data for *n*-heptane data at ambient conditions, given in Table B1.

Table B1. Asphaltene yields for *n*-heptane diluted bitumen (WC-B-B2) at ambient conditions [Shafiee, 2014].

n-Heptane Content wt %	Asphaltene Yield wt %
57.5	1.2
58.0	1.4
59.5	2.7
59.7	2.1
61.5	3.8
62.0	3.5
64.5	5.7
65.5	5.2

n-Heptane Content wt %	Asphaltene Yield wt %
64.3	5.1
64.8	5.0
66.7	6.5
71.4	9.3
75.0	11.5
80.0	13.1
88.3	15.5
91.1	16.0

B.3 Additional Model Results

The body of this text includes the model results for saturation pressures at only one temperature to demonstrate the observed trends. The full model results for the AvdW model (saturation pressures up to 180°C, Figure B1) and the HV model (saturation pressures up to 280°C, Figure B2) are shown below. The AvdW model was run using a beta version of VMGSim™. When this software was made available, only saturation pressures for *n*-pentane diluted bitumen up to 180°C had been collected, so this model was not tested on data above 180°C. However,

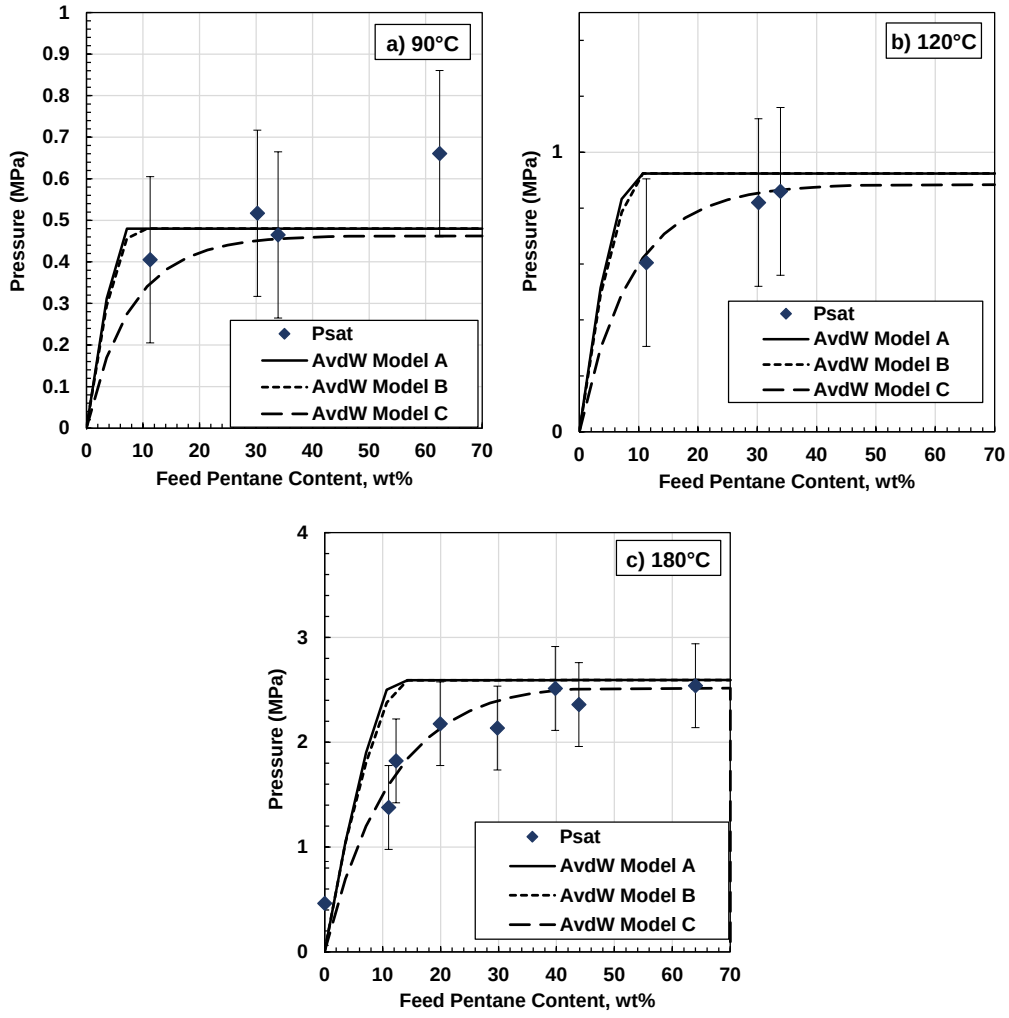

Figure B.1 Saturation pressures for *n*-pentane diluted bitumen at a) 90°C, b) 120°C and c)180°C. Symbols are experimental data, lines are the AvdW model with tuning parameters as presented in Section 6.3.

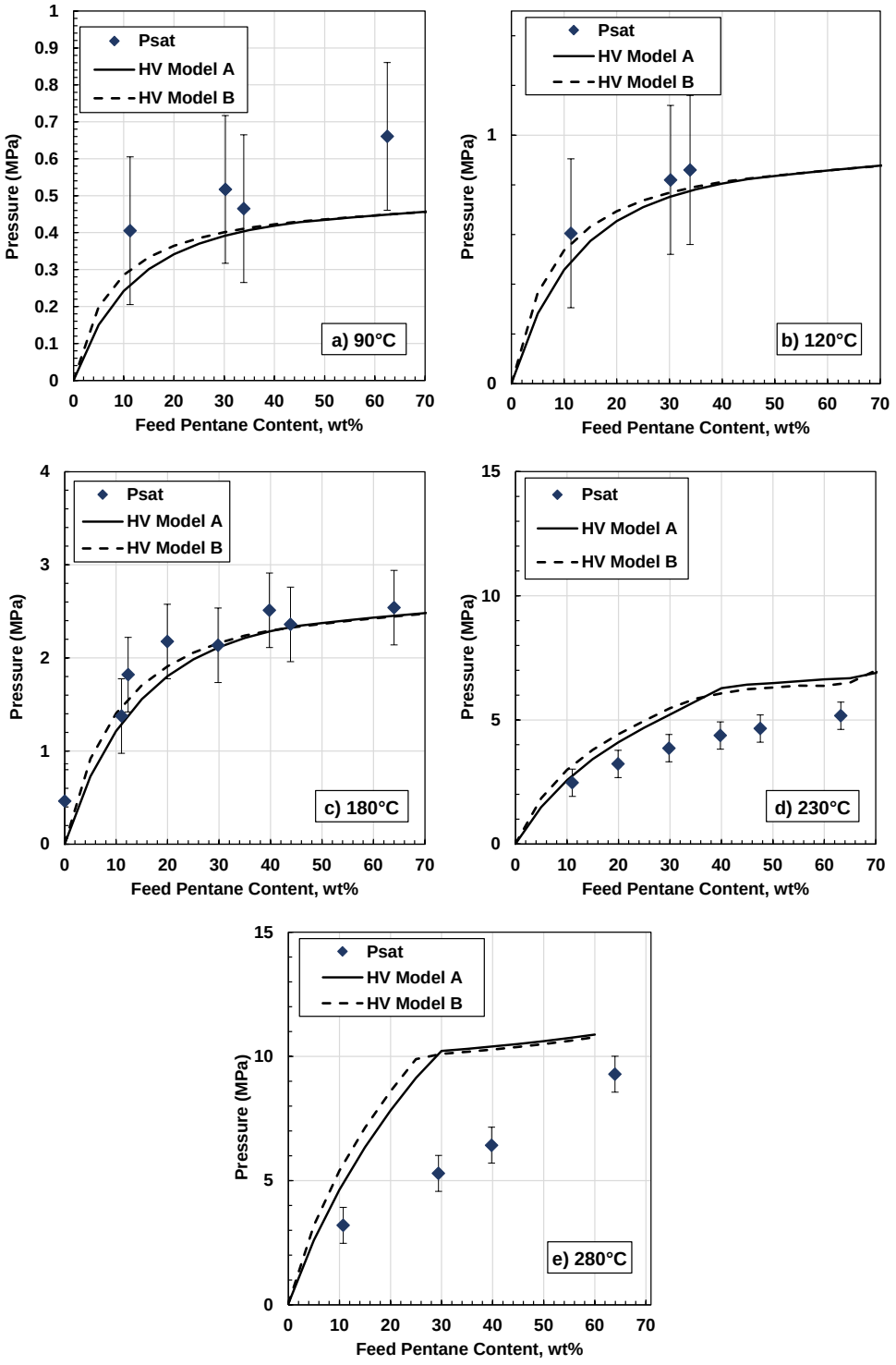

Figure B.2 Saturation pressures for *n*-pentane diluted bitumen at a) 90°C, b) 120°C, c)180°C, d) 230°C and e) 280°C. Symbols are experimental data, lines are the HV model with tuning parameters as presented in Section 6.4.

APPENDIX C – ADDITIONAL CORRELATIONS

Twu method

Reference Critical Temperature

$$T_C^O = T_b(0.533272 + 0.191017x10^{-3}T_b + 0.779681x10^{-7}T_b^2 - 0.284376x10^{-10}T_b^3 + 0.959468x10^{28}/T_b^{13})^{-1}$$

Reference Critical Pressure

$$P_C^0 = (3.83354 + 1.19629\eta^{0.5} + 34.8888\eta + 36.1952\eta^2 + 104.193\eta^4)^2$$

$$\eta = 1 - \frac{T_b}{T_C^0}$$

Reference Critical Volume

$$V_C^0 = [1 - (0.419869 - 0.505839\eta - 1.56436\eta^3 - 9481.7\eta^{14})]^{-8}$$

Reference Specific Gravity

$$SG^0 = 0.843593 - 0.128624\eta - 3.36159\eta^3 - 13749.5\eta^{12}$$

Deviation Parameters

$$\Delta SG_T = exp[5(SG^0 - SG)] - 1$$

$$\Delta SG_V = exp[4((SG^0)^2 - (SG)^2)] - 1$$

$$\Delta SG_P = exp[0.5(SG^0 - SG)] - 1$$

Perturbation Functions

$$g = g^0\left[\frac{1 + 2f_g}{1 - 2f_g}\right]^2, g = T_C, V_C$$

$$P_C = P_C^0 \left[\frac{1+2f_P}{1-2f_P}\right]^2 \left(\frac{T_C^0}{T_C}\right)\left(\frac{V_C}{V_C^0}\right)$$

$$f_T = \Delta SG_T\left[-0.352456T_b^{-0.5} + \left(0.0398285 - 0.948125T_b^{-0.5}\right)\Delta SG_T\right]$$

$$f_V = \Delta SG_V\left[0.466590T_b^{-0.5} + \left(-0.182421 + 3.01721T_b^{-0.5}\right)\Delta SG_V\right]$$

$$f_P = \Delta SG_P\left[\left(2.53262 - 46.1955T_b^{-0.5} - 0.00127885T_b\right) + \left(-11.4277 + 252.140T_b^{-0.5} + 0.00230535T_b\right)\Delta SG_P\right]$$

Lee Kesler method

Critical Pressure

$$lnP_C = 8.3634 - \frac{0.0566}{SG} - 1x10^{-3}T_b\left(0.24244 + \frac{2.2898}{SG} + \frac{0.11857}{SG^2}\right) + 1x10^{-7}T_b^2\left(1.46850 + \frac{3.6480}{SG} + \frac{0.47277}{SG^2}\right) - 1x10^{-10}T_b^3\left(0.42019 + \frac{1.69770}{SG^2}\right)$$

Critical Temperature

$$T_C = 341.7 + 8.11SG + T_b(0.4244 + 0.1174SG) + \frac{1x10^5}{T_b}(0.4669 - 3.2623SG)$$

Acentric Factor

$$\omega = \frac{ln\left(\frac{101.325}{P_C}\right) - 5.92714 + \frac{6.09648}{T_{br}} + 1.28862ln(T_{br}) - 0.169347T_{br}^6}{15.2518 - \frac{15.6875}{T_{br}} - 13.4721ln(T_{br}) + 0.43577T_{br}^6} \quad T_{br} < 0.8$$

$$\omega = -7.904 + 0.1352K_W - 0.007465K_W^2 + 8.359T_{br} + \frac{(1.408 - 0.01063K_W)}{T_{br}} \quad T_{br} \geq 0.8$$

$$K_W = \frac{1.8T_b^{1/3}}{SG}$$

Søreide Correlation

$$T_b = 1928.3 - (1.695 * 10^5)MW^{-0.03522}SG^{3.266}e^{[-0.004922*MW-4.7685*SG+0.003462*MW*SG]}$$